NEUTRINO OSCILLATIONS IN SUPERNOVAE

THESIS SUBMITTED TO

HOMI BHABHA NATIONAL INSTITUTE

FOR THE DEGREE OF

DOCTOR OF PHILOSOPHY (SCIENCE)

By

SOVAN CHAKRABORTY
SAHA INSTITUTE OF NUCLEAR PHYSICS
KOLKATA

NOVEMBER 2010

ACKNOWLEDGMENTS

It is customary to acknowledge contributions of people towards the completion of the thesis. In my case, the list is quite large.

Firstly, I express my gratitude towards my thesis supervisor Prof. Kamales Kar for extending his sincere help and guidance during the period of my research. He has always motivated me and has incessantly encouraged me to pursue my own line of thinking. I am grateful to him for his patience and boosting my confidence from time to time.

The next name come to my mind is Prof. Pijushpani Bhattacharjee, who helped me all the way through these last five years of learning at Saha Institute. In fact it was his teaching and influence that took me to the subject of astroparticle physics. I learned a lot from his valuable suggestions and guidance. My deep gratitude towards him for the stimulating discussions at many occasions which helped me to understand the intricate details of astroparticle physics.

Two persons without whom this thesis would remain incomplete are Dr. Sandhya Choubey and Dr. Srubabati Goswami. Sandhya-di always brought a fresh point of view and with it a better understanding of the subject. I was fortunate enough to discuss various physics issues with her. Apart from encouraging me to work in the new subject of collective oscillations Srubabati-di always influenced my way of thinking and my understanding . Her advice was always very sincere. In short, both of them have been true mentors.

I would also like to mention Dr.Basudeb Dasgupta, Prof. Debasish Majumdar, Prof. Ambar Ghosal, Dr. Abhijit Bandyopadhyay with whom working and learning was more than enjoyable.

I also thank all the members of the Theory Group of Saha Institute of Nuclear Physics for maintaining a cordial and comfortable working environment. My sincere thanks are due to Purnendu, Biswajit, Jyotirmoy, Subhrajyoti, Sayan, Pulak, Kumar, Kalyanbrata, Nilanjan, Lab, Raktim, Najmul, Somdev, Pratay and Arindam with whom I have shared my office at various stages and enjoyed a very warm and enjoyable ambiance. My thanks also to Bhramar, Srijit, Rana, Tirthasankar, Soumini, Susmita, Santanu and Susnata for making the environment enjoyable. I thank Srirupa Dasgupta for collaborating on some topics.

I would like to take this opportunity to thank my teachers who have inspired me to pursue a research career. I express my sincere gratitude for Prof. Narayan Banerjee who always inspired to read the masters and encouraged to cultivate an independent point of view. Thanks also to Prof. Ranjan Bhattacharya, Prof. Dhiranjan Roy, Prof. Amitava Datta, Prof. Soumitra Sen Gupta for their inspiring teaching. I must also thank Prof. Palash B. Pal, Prof. Parthasrathi Majumdar, Prof. Parthasarathi Mitra, Prof. Amit Ghosh, Prof. Gautam Bhattacharyya, Prof. Debades Bandyopadhyay and Prof. Asit K. De.

I am also grateful to my university classmates and friends Sumilan, Moitri, Baisakhi, Swastik and Basudeb for keeping a youthful company. Without their help and friendship this experience would have been incomplete.

I thank my family, my sister, my brother-in-law and particularly my parents for all the encouragement and also for keeping faith in my judgment. Finally, thanks are due to my wife Aparna for her patience.

TABLE OF CONTENTS

LIST OF FIGURES

Figure **Page**

LIST OF TABLES

CHAPTER 1

Introduction

1.1 Motivation

The resolutions of the solar neutrino problem and the atmospheric neutrino anomaly established non-zero neutrino mass and neutrino oscillations in a three flavor framework. It is also known that the neutrino oscillation phenomenon gets enhanced in the presence of matter, particularly for matter with a density gradient and this effect is known as the Mikheyev-Smirnov-Wolfenstein (MSW) mechanism [1]. The parameters involved in this three flavor oscillation are the two mass squared differences Δm^2_{32} and Δm^2_{21} ($\Delta m^2_{ij} = m^2_i - m^2_j$) with (m_1, m_2, m_3) the three mass eigenstates and the three mixing angles $\theta_{12}, \theta_{23}, \theta_{13}$. A number of accelerators and reactor experiments also gave independent support to the oscillation hypothesis.

On the other hand neutrinos emitted during the explosion of a core-collapse supernova (SN) turn out to be important in probing both neutrino properties and SN mechanism. Though only neutrinos from the SN 1987A explosions have been detected so far, one hopes to observe neutrinos in terrestrial detectors in future SN explosions at galactic distances. The neutrinos emitted during the explosions of core-collapse SN pass through a very large density gradient and undergo the MSW resonant flavor conversion. The flavor conversion can give information on neutrino mass hierarchy and the third mixing angle θ_{13} [2, 3].

In the last few years it was realized that a crucial feature in the study of SN neutrinos comes from the collective neutrino-neutrino interaction at very high densities of the core and this may change the emitted flux of different flavors substantially. Initial studies have shown that effectively the collective evolution of a three-flavor $(\nu_e, \nu_\mu, \nu_\tau)$ system can be treated like a two flavor (ν_e, ν_x) scenario, where ν_x can be ν_μ or ν_τ or a linear combination of ν_μ and ν_τ [4, 5]. The flavor evolution has been found to be driven by the effective mass squared difference Δm^2_{13} and the mixing angle θ_{13}, whereas the other ν_y remains unaffected by this collective effect. This two flavor scenario shows that for inverted hierarchy (IH, $\Delta m^2 < 0$), above a critical energy (split energy E_c), the spectrum in both the electron neutrino (ν_e) and antineutrino ($\bar{\nu}_e$) sectors end up with a complete exchange or swap with ν_x and $\bar{\nu}_x$ respectively, this is referred to as a 'spectral swap', whereas the Normal Hierarchy (NH, $\Delta m^2_{13} > 0$) is more stable under collective neutrino-neutrino interaction[6, 7, 8, 9]. Thereafter studies concerning the role of equipartion in energy and variation of luminosity in collective effect found interesting possibility of multiple splits in the supernova neutrino spectra for IH [10, 11, 12]. Single spectral split for Normal Hierarchy has been also reported for certain values of luminosities. Thus through detailed analysis of the luminosity variations one observes different spectral split scenario. One noteworthy characteristic of the collective effect is that it is felt only within a few hundred kilometers from the center of the core. However recent studies have shown that the solar mass squared difference Δm^2_{12} can also give rise to swap, which starts a little late than the Δ^2_{atm} driven one and hence the calculations are needed to be extended upto about a thousand kilometer [13, 14]. These three flavor analysis results showing the possible importance of both mass squared differences are very sensitive on the strength of the neutrino-neutrino interaction potential. For possible smaller values of the neutrino-neutrino interaction potential by one order will again give back the effective two flavor results [14] . Hence for studies with shallow neutrino-neutrino interaction potential the effective two flavor treatment seems a reasonable approximation.

This thesis studies mainly three aspects of SN neutrinos. The first aspect is regarding the effect of neutrino-neutrino interaction on the neutrino spectra. It has been seen that the number of split in the spectra and the split energy depend on the variation of initial relative luminosity or relative flux of different neutrino species. This dependence is extensively studied in the thesis. We analyzed the variation of split patterns with initial relative flux for different possible models of SN neutrino spectra.

Another aspect we discussed in this thesis is the prospect of SN as a r-process nucleosynthesis site in light of this variation of split patterns due to neutrino-neutrino interaction. Though the site for the mechanism of rapid capture of neutrons leading to synthesis of heavier element or r-process nucleosynthesis is not definitely known, supernovae are considered to be excellent candidates for it. One of the criteria for the rapid nucleosynthesis to take place is that it has to be in a neutron-rich region. With the two competing beta processes $n + \nu_e \to p + e^-$ and $p + \bar{\nu}_e \to n + e^+$ occurring in the hot bubble and neutrino driven wind region, the minimal condition is that the electron fraction (defined as the number of electrons divided by the total number of baryons), $Y_e < 0.5$.

The r-process in SN is expected to take place in the neutrino driven wind deep inside the supernova (within a few hundred kilometers). Since the collective flavor oscillations also happen very close to the neutrinosphere, it will definitely make an impact on the r-process nucleosynthesis. Hence we studied the effect of spectral splits on the electron fraction (Y_e) which is a diagnostic of successful r-process nucleosynthesis in supernova. We also considered the inverse problem i.e. to study the possibility of putting constraints on the initial relative fluxes by demanding the neutron rich condition of Y_e.

The other aspect studied in the thesis is the Diffuse Supernova Neutrino Background (DSNB) or the relic background of neutrinos emitted from all past SN. Our study included the fact that the DSNB can be affected by the collective as well as MSW oscillation. Since the two oscillation effects happen at two widely separated region, typically collective effect around a few 100 km and MSW around $10^4 - 10^5$ km, they are considered to be independent. In our analysis we considered the effect of these oscillations on the SN relic neutrinos. We also studied the variation of split patterns coming from the variation of initial relative flux and discussed how these split pattern variations can affect the DSNB flux. The important problem of mass hierarchy in neutrino physics is examined using the DSNB event rate and favorable situations where the inverted hierarchy can be distinguished from the normal one identified. The realistic situation of a distribution of supernovae as a function of the relative neutrino and antineutrino fluxes are also considered while investigating this issue.

1.2 Layout of Thesis

In this thesis we explore the implications of neutrino oscillations in the context of supernova neutrinos. We performed detailed analyses of the SN neutrino spectra considering neutrino-neutrino interaction or collective effects. We investigate the effect of variation of initial SN neutrino spectra models along with the variation of initial relative fluxes of different flavors. We found the consequences of this variation of split patterns on the process of heavy element nucleosynthesis inside SN and also on the relic background of neutrinos coming from past SNe.

We begin in chapter 2 with the presentation of the general structure of neutrino oscillation in vacuum and in matter. We analyse the adiabatic and non-adiabatic propagation of neutrinos in a medium where density is varying and also present the expressions for survival probability.

In chapter 3 we give a brief description of the core collapse SN mechanism and neutrino emission from such stellar collapse. We describe the different classification of SNe and show how a wide class of SNe can explode with the same core collapse mechanism. All these core collapse SNe (CCSNe) go through similar kind of stellar evolution. We describe the present status of our understanding of core collapse process briefly. This includes the neutrino emission mechanism of the CCSNe and we mention how these neutrinos can carry valuable information about SN.

The study of SN neutrinos is taken up in detail in chapter 4 describing the effect of neutrino-neutrino interaction or collective effect in the very high density region of the SN core. We give a general formalism of neutrino oscillation considering the collective effect. We describe how the difference in initial relative flux can give rise to difference in split patterns of the SN neutrino spectra. We discuss the possible split patterns for both normal and inverted hierarchy.

In chapter 5 we analyse the effect of the flux of oscillated neutrinos radiated out in core collapse supernovae on the electron fraction and discuss the possibility of getting allowed regions in the relative flux parameter space for r-process nucleosynthesis. The minimal criterion for r-process on which we focus is that the electron fraction Y_e is less than $\frac{1}{2}$.

We calculate the electron fraction (Y_e) as a function of the radius of the core and find the oscillatory behavior in the bipolar region due to collective effects, before saturating to a constant value which depends on the initial luminosities and the pattern of flavor swap. In the analysis different models of neutrino energy distributions are used. For each of the spectra initial fluxes of different flavors are varied and constraints on the initial neutrino fluxes consistent with successful r-process nucleosynthesis are found in form of the exclusion plots.

In chapter 6 we describe the general structure of diffuse Supernova Neutrino Background (DSNB) in the context of collective neutrino oscillation. Neutrinos accumulated in the universe from all past SN explosions form a cosmic background, known as the diffuse supernova neutrino background (DSNB) or supernova relic neutrinos. We discussed the estimation of DSNB with a simplified assumption of collective effects. In this chapter earlier considerations of matter induced resonances are followed by incorporating the 'collective' effects in the high density central regions of the core. Our studies on the effect of the collective flavor oscillations on DSNB fluxes and the corresponding predicted number of events in terrestrial detectors showed that the event rate can get substantially modified by collective effects. The detectors considered are water Cherenkov [like Super Kamiokande (SK), Hyper Kamiokande (HK) and both SK and HK with Gadolinium loaded (GDSK and GDHK)], Liquid Scintillator [like LENA] for antineutrinos and Liquid Argon detector [like GLACIER] for neutrinos. The results also show that observation of the DSNB fluxes at earth can shed light on the neutrino mass hierarchy for very small mixing angle $\theta_{13}(< 10^{-5})$.

In chapter 7 we analyse the fact that the DSNB flux comes from a superposition of the fluxes from all past SNe and since the initial flux conditions are expected to be sensitive to the properties of the progenitor star and since we have a whole distribution of stars which end as SN, realistically one should not take all supernovae to have the same relative neutrino and antineutrino flux. Thus a distribution of SN as function of the relative fluxes should be considered and event numbers averaged over the distributions are calculated. The main focus is to check the effect of the distribution of supernovae with initial flux on the possibility of distinguishing neutrino mass hierarchies through the observation of the

DSNB signal. Since the distribution of the initial fluxes over all past SNe are not available to us, we parameterise this by different distributions like log normal and uniform etc. In this chapter we calculate the DSNB event rate averaged over these distributions mainly for antineutrinos in both hierarchies and with very small mixing angle ($\theta_{13} < 10^{-5}$).

Our analysis in chapter 7 shows that if one assumes that all past SNe were to produce identical $\bar{\nu}_e$ fluxes, then it would be possible to distinguish the normal from the inverted hierarchy using the DSNB signal even for very small θ_{13} with megaton-class water Cherenkov detectors. However, once the distribution of the fluxes from all SNe are taken into account, the situation becomes more complicated. In the scenario of low mean values of the initial flux ratio distribution, the mass hierarchy determinability through DSNB is found to survive the averaging though the difference decreases significantly with respect to the one without the distribution. However for larger values of initial flux ratio it becomes impossible to distinguish hierarchy through DSNB once the distribution is taken into account.

BIBLIOGRAPHY

[1] L. Wolfenstein,*Phys. Rev.* **D17**, 2369 (1978); S.P. Mikheyev and A.Yu. Smirnov, *Sov. J. Nucl. Phys.* **42(6)**, 913 (1985); *Nuovo Cimento* **9c**, 17 (1986).

[2] G. Raffelt, *Stars as Laboratories for Fundamental Physics* (U. of Chicago Press, Chicago, 1996), 664 pp.

[3] A. Dighe, J. Phys. Conf. Ser. **136**, 022041 (2008).

[4] B. Dasgupta and A. Dighe, Phys. Rev. D **77**, 113002 (2008).

[5] G. Fogli, E. Lisi, A. Marrone and I. Tamborra, JCAP **0904**, 030 (2009) [arXiv:0812.3031 [hep-ph]].

[6] H. Duan, G. M. Fuller, J. Carlson and Y. Z. Qian, Phys. Rev. D **74**, 105014 (2006).

[7] G. G. Raffelt and A. Yu. Smirnov, Phys. Rev. D **76**, 081301 (2007); Erratum ibid. **77**, 029903 (2008).

[8] G. G. Raffelt and A. Yu. Smirnov, Phys. Rev. D **76**, 125008 (2007).

[9] G. L. Fogli, E. Lisi, A. Marrone and A. Mirizzi, JCAP **0712**, 010 (2007).

[10] B. Dasgupta, A. Dighe, G. G. Raffelt and A. Y. Smirnov, Phys. Rev. Lett. **103**, 051105 (2009) [arXiv:0904.3542 [hep-ph]].

[11] G. Fogli, E. Lisi, A. Marrone and I. Tamborra, arXiv:0907.5115 [hep-ph].

[12] S. Chakraborty, S. Choubey, S. Goswami and K. Kar, JCAP **1006**, 007 (2010) [arXiv:0911.1218 [hep-ph]].

[13] A. Friedland, Phys. Rev. Lett. **104**, 191102 (2010) [arXiv:1001.0996 [hep-ph]].

[14] B. Dasgupta *et al.* [arXiv:1002.2943 [hep-ph]]

CHAPTER 2

Basics of Neutrino Oscillation

In standard model neutrinos (ν) are considered to be massless. However the idea of neutrino oscillation involving neutrino mass was introduced by Pontecorvo [1] more than fifty years ago. In the last decades experiments involving atmospheric and solar neutrinos conclusively established non-zero neutrino mass and gave strong support to the oscillation hypothesis.

Neutrino oscillations are the most sensitive probe of ν's mass. Solar and supernova neutrino experiments are able to search for the ν-mass as small as 10^{-5} eV or even smaller far beyond the reach of the direct kinematic search experiments. Normally in ν-oscillation experiments, neutrinos are produced by the charged- current weak interactions and therefore are weak flavor eigenstate neutrinos ν_e, ν_τ, ν_μ. The neutrino mass matrix in this flavor basis is in general not diagonal. However the mass eigenstates ν_1, ν_2, ν_3 form a basis in which the neutrino mass matrix is diagonal and these eigenstates propagate in time. Thus the mass eigenstates are in general different from the flavor eigenstates. Therefore the probability of finding a neutrino created in a given flavor state to be in the same state (or any other flavor state) oscillates with time.

In this chapter we introduce the basics of neutrino oscillations. First we discuss vacuum oscillations in two and three flavor scenarios. After that we treat the matter interactions of neutrino, starting with a constant density medium and later consider the varying density case.

2.1 Vacuum Oscillation

Weak eigenstates ν_l's ($l = e, \mu, \tau$) are created in charged current interaction and neutrino mass matrix in this flavor basis is in general not diagonal. The flavor eigenstates

ν_l can be expressed as linear combination of physical mass eigenstates (ν_α) $(\alpha = 1, 2, 3)$ through the unitary transformation.

$$|\nu_l\rangle = u_{l\alpha}|\nu_\alpha\rangle, \tag{2.1}$$

, here the summing is over the repeated indexes and $u_{l\alpha}$ denotes the '$l\alpha$'th element of the unitary matrix U. The relation for antineutrinos is exactly the same but complex conjugating the elements in the mixing matrix $|\bar{\nu}_l\rangle = u^*_{l\alpha}|\bar{\nu}_\alpha\rangle$. The time evolution of the flavor eigenstate comes from the time evolution of the mass eigenstates, thus

$$|\nu_l(t)\rangle = u_{l\alpha}|\nu_\alpha\rangle e^{-iE_\alpha t}. \tag{2.2}$$

Thus amplitude of finding a $\nu_{l'}$ in the original beam of ν_l is

$$\begin{aligned} \langle\nu_{l'}|\nu_l(t)\rangle &= \langle\nu_\beta|u^\dagger_{\beta l'}e^{-iE_\alpha t}u_{l\alpha}|\nu_\alpha\rangle \\ &= e^{-iE_\alpha t}u_{l\alpha}u^*_{l'\alpha}. \end{aligned} \tag{2.3}$$

Therefore, the probability that a ν_l will be found in a original $\nu_{l'}$ after time t is

$$\begin{aligned} P_{\nu_l\nu_{l'}}(t) &= |\langle\nu_{l'}|\nu_l(t)\rangle|^2 \\ &= \sum_{\alpha,\beta} u_{l\alpha}u^*_{l'\alpha}u^*_{l\beta}u_{l'\beta}e^{-i[E_\alpha - E_\beta]t} \\ &= \sum_{\alpha,\beta} |u_{l\alpha}u^*_{l'\alpha}u^*_{l\beta}u_{l'\beta}|\cos[([E_\alpha - E_\beta)t - \phi_{ll'\alpha\beta}], \end{aligned} \tag{2.4}$$

where, $\phi_{ll'\alpha\beta} = \arg(u_{l\alpha}u^*_{l'\alpha}u^*_{l\beta}u_{l'\beta})$.

Now most of the practical cases of neutrino oscillation involve relativistic neutrinos where one can use the approximation
$E_\alpha \simeq |\mathbf{p}| + \frac{m^2_\alpha}{2|\mathbf{p}|} \simeq E + \frac{m^2_\alpha}{2E}$, and therefore, $E_\alpha - E_\beta = \frac{m^2_\alpha - m^2_\beta}{2E} = \frac{\Delta^2_{\alpha\beta}}{2E}$.

For this extremely relativistic case $x \equiv t$, thus

$$\begin{aligned} P_{\nu_l\nu_{l'}}(t) &\rightarrow P_{\nu_l\nu_{l'}}(x) \\ &= \sum_{\alpha\beta} |u_{l\alpha}u^*_{l'\alpha}u^*_{l\beta}u_{l'\beta}|\cos\left(\frac{2\pi x}{L_{\alpha\beta}} - \phi_{ll'\alpha\beta}\right). \end{aligned} \tag{2.5}$$

where, $L_{\alpha\beta}$ is defined as oscillation length $L_{\alpha\beta} = \frac{4\pi E}{m^2_\alpha - m^2_\beta} = \frac{4\pi E}{\Delta^2_{\alpha\beta}}$.

2.1.1 Two flavor vacuum oscillation

Consider the situation of oscillation between two neutrino flavors $|\nu_e\rangle$ and $|\nu_\mu\rangle$. Let the mass eigenstates be $|\nu_1\rangle$ and $|\nu_2\rangle$ having energies E_1 and E_2.

The transformation matrix between mass and flavor eigenstates U takes the form

$$U = \begin{pmatrix} \cos\theta & \sin\theta \\ -\sin\theta & \cos\theta \end{pmatrix}.$$

Thus U is now a real unitary matrix and therefore the conversion probability is,

$$P_{\nu_e\nu_\mu}(x) = \sin^2 2\theta \sin^2\left(\frac{\Delta_{21}^2 x}{4E}\right) = \sin^2 2\theta \sin^2\left(\frac{\pi x}{L_{21}}\right). \tag{2.6}$$

The above expression shows oscillatory behavior in $\frac{x}{E}$, explaining why we use the nomenclature neutrino oscillations. Moreover the amplitude $\sin^2 2\theta$ contains the constant mixing angle and only non zero mixing angles give rise to successful mixing. The other oscillatory term $\sin^2\left(\frac{\Delta_{21}^2 x}{4E}\right)$ shows the importance of non-zero mass square difference in neutrino oscillations. Thus existence of neutrino oscillation signifies the existence of at least one non-zero neutrino mass and as well as mixing of neutrinos.

One can look at some of the limiting cases of Eq. 2.6 involving the oscillation length L_{21} and understand its importance:

1. If $x << L_{21}$, then there is no oscillation.

2. If x is an integer multiple of $L_{21}, P_{\nu_e\nu_\mu} = 0$ i.e. $P_{\nu_e\nu_e} = 1$

3. If $x \neq$ integer multiple of L_{21} then oscillation takes place.

4. If $x >> L_{21}$ then the transition probability oscillates very fast, resulting in the averaged probability at the detector, $< P_{\nu_e\nu_\mu} > \; = \frac{1}{2}\sin^2 2\theta$.

2.1.2 Three flavor Vacuum Oscillations

In this subsection we will discuss very briefly about vacuum oscillation among three generation. For the simple case with CP conservation one can derive the probability that a $\nu_{l'}$ will be found in ν_l beam at a distance x, i.e.

$$\begin{aligned} P_{\nu_l \nu_{l'}}(x) = & \quad \sum_{\alpha=\beta} u_{l\alpha}^2 u_{l'\alpha}^2 + 2\sum_{\alpha>\beta} u_{l\alpha} u_{l'\alpha} u_{l\beta} u_{l'\beta} \cos\left(\frac{\Delta^2_{\alpha\beta} x}{2E}\right), \\ = & \quad (\sum_{\alpha} u_{l\alpha} u_{l'\alpha})^2 - 4\sum_{\alpha>\beta} u_{l\alpha} u_{l'\alpha} u_{l\beta} u_{l'\beta} \sin^2\left(\frac{\Delta^2_{\alpha\beta} x}{4E}\right). \end{aligned} \tag{2.7}$$

If one assumes that

$$\frac{\Delta^2_{21}}{2E} x \ll 1 \qquad [i.e.\ m_1 \sim m_2] \ \ and \ \ \Delta^2_{32} \cong \Delta^2_{31}.$$

$$P_{\nu_l \nu_{l'}}(x) = \delta_{ll'} - 4 u_{l3} u_{l'3} (\delta_{ll'} - u_{l3} u_{l'3}) \sin^2\left(\frac{\Delta^2_{32} x}{4E}\right). \tag{2.8}$$

Now consider the mixing matrix for 3 generation with CP violation

$$U = \begin{pmatrix} c_{12}\, c_{13} & -s_{12}\, c_{13} & s_{13}\, e^{-i\delta} \\ s_{12}\, c_{23} + c_{12}\, s_{23}\, s_{13}\, e^{i\delta} & c_{12}\, c_{23} - s_{12}\, s_{23}\, s_{13}\, e^{i\delta} & -s_{23}\, c_{13} \\ s_{12}\, s_{23} - c_{12}\, c_{23}\, s_{13}\, e^{i\delta} & c_{12}\, s_{23} + s_{12}\, c_{23}\, s_{13}\, e^{i\delta} & c_{23}\, c_{13} \end{pmatrix}. \tag{2.9}$$

Here $c_{ij} = \cos\theta_{ij}$ and $s_{ij} = \sin\theta_{ij}$ and δ is the CP phase. If one ignores CP violation i.e, CP phase $\delta = 0$ or π, the survival probability of ν_e is

$$P_{\nu_e \nu_e}(x) = 1 - \sin^2 2\theta_{13} \sin^2\left(\frac{\Delta^2_{32} x}{4E}\right). \tag{2.10}$$

This coincides with the survival probability in the 2 flavor case if we assume the mass squared differences to be such that $\Delta^2_{31} \cong \Delta^2_{32}$ and mixing angle is θ_{13}.

Consider another limiting case:

$$\frac{\Delta^2_{31}}{2E} x \ \cong \ \frac{\Delta^2_{32}}{2E} x \ \gg \ 1.$$

In this case the oscillations due to Δ^2_{31} and Δ^2_{32} are very fast and will lead to an averaged effect. Then the survival probability becomes

$$P_{\nu_l \nu_{l'}}(x) = \delta_{ll'} - 2 u_{l3} u_{l'3} \left(\delta_{ll'} - u_{l3} u_{l'3}\right) - 4 u_{l1} u_{l'1} u_{l2} u_{l'2} \sin^2\left(\frac{\Delta^2_{21} x}{4E}\right). \tag{2.11}$$

From here the survival probability for ν_e is :

$$P_{\nu_e \nu_e}(x) = \cos^4\theta_{13} \left[1 - \sin^2 2\theta_{12} \sin^2\left(\frac{\Delta^2_{21} x}{4E}\right)\right] + \sin^4\theta_{13}. \tag{2.12}$$

Oscillation parameter	Best fit $\pm 1\sigma$
Δm^2_{21}	$7.65^{+0.23}_{-0.20}$
$\mid \Delta m^2_{31} \mid$	$2.40^{+0.11}_{-0.12}$
$sin^2\theta_{12}$	$0.304^{+0.022}_{-0.016}$
$sin^2\theta_{23}$	$0.500^{+0.07}_{-0.06}$
$sin^2\theta_{13}$	$0.010^{+0.016}_{-0.011}$

Table 2.1: Present best-fit values of the three-flavor neutrino oscillation parameters with 1σ errors. These best fit values are obtained from global analysis with solar, atmospheric, reactor (KamLAND and CHOOZ) and accelerator (K2K and MINOS) experiments [2]. The mass squared differences Δm^2_{21} and $\mid \Delta m^2_{31} \mid$ are given in units of $10^{-5}eV^2$ and $10^{-3}eV^2$ respectively.

Again assuming small θ_{13} will lead to the same results as in two flavor case i.e

$$P_{\nu_e\nu_e}(x) \;\rightarrow\; 1 - \sin^2\theta_{12}\sin^2\left(\frac{\Delta^2_{21}x}{4E}\right). \tag{2.13}$$

To summarize we have five neutrino oscillation parameters in 3 flavor analysis without CP violation: They are the two mass squared differences and three mixing angles. Out of them only four are more or less well determined. The atmospheric $(\Delta^2_{31}, \theta_{23})$ and solar $(\Delta^2_{21}, \theta_{12})$ neutrino parameters are known from the oscillation experiments, while θ_{13} and the sign of Δ^2_{31} remain unknown. The present best fit limits on the parameters are given in the Table 2.1. For the 13-mixing angle, at this moment we have upper bounds coming from null results of the short-baseline CHOOZ reactor experiment with some effects also from solar and KamLAND data. Finally if one considers CP violation in the analysis then no limit at all has been yet obtained for the CP violating phase in neutrino oscillation experiments.

Though from solar experiments we know that the solar mass squared difference ($\Delta^2_{21} = \Delta^2_{sol}$), is positive, while the sign ofΔ^2_{31} or Δ^2_{atm}, is yet unknown. This sign determines what is called the neutrino mass hierarchy, Δ^2_{31} = $|\Delta^2_{31}|$ corresponds to normal hierarchy, and Δ^2_{31} = -$|\Delta^2_{31}|$ to inverted hierarchy.

2.2 Neutrino Oscillations in Matter

Oscillation of neutrinos in matter is significantly different from the vacuum oscillation. Most importantly matter effects on neutrino oscillations can give rise to the resonance enhancement of the oscillation probability - the Mikheyev-Smirnov-Wolfenstein(MSW) effect [3]. The neutrino conversion probability in vacuum can go upto a maximum of $sin^2 2\theta$, and for small mixing angles it is always small. Matter can enhance neutrino mixing and the probability can even reach close to 1 even when mixing angle is very small.

Neutrino Oscillations in supernova and solar environment are strongly affected by matter. Neutrinos can get absorbed and scattered through matter constituents and hence their momentum and energy can get changed. But the probabilities of these processes are typically very small as they are proportional to the square of the Fermi constant G_F. Neutrinos can also experience elastic forward scattering i.e their momentum remains same. This process is coherent and creates mean potential (V) for neutrinos and this potential (V) is proportional to the number densities of the scatterers. The potentials are in 1st order of G_F so they are also quiet small, but if we compare them with characteristic neutrino kinetic energy differences $\Delta^2_{\alpha\beta}/2E$ they are comparable or even larger than $\Delta^2_{\alpha\beta}/2E$ and can affect neutrino oscillation.

2.2.1 Evolution of neutrino states in matter

All three flavors ν_e, ν_μ, ν_τ of neutrinos can interact with electrons, protons and neutrons of matter through Neutral Current (NC) mediated by Z^0 boson whereas ν_e can have Charge Current (CC) interactions with the e^- of the medium and this CC is mediated by $W^\pm$ exchange.

Consider the CC interaction. At low energy the effective Hamiltonian is

$$\begin{aligned} H_{CC} &= \frac{G_F}{\sqrt{2}}[\bar{e}\gamma_\mu(1-\gamma_5)\nu_e][\bar{\nu_e}\gamma^\mu(1-\gamma_5)e], \\ &= \frac{G_F}{\sqrt{2}}[\bar{e}\gamma_\mu(1-\gamma_5)e][\bar{\nu_e}\gamma^\mu(1-\gamma_5)\nu_e] \quad \text{[By Fierz Transformation]}. \end{aligned} \tag{2.14}$$

To obtain the matter induced potential of ν_e, we fix the variables associated with ν_e and integrate over the variables that corresponds to electrons. Therefore,

$$H_{eff}(\nu_e) = \langle H_{cc}\rangle_{electron} = \bar{\nu_e} V_e \nu_e.$$

Moreover

$$\langle \bar{e}\gamma_0 e\rangle = \langle e^+ e\rangle = N_e, \quad \langle \bar{e}\gamma e\rangle = \langle V_e\rangle,$$
$$\langle \bar{e}\gamma_0\gamma_5 e\rangle = \left\langle \frac{\bar{\sigma}_e \cdot \bar{p}_e}{E_e} \right\rangle, \quad \langle \bar{e}\gamma\gamma_5 e\rangle = \langle \sigma_e\rangle,$$

where, N_e is the electron number density. For an unpolarized medium of zero total momentum only the 1st term of the above expectations survive. Thus we obtain,

$$(V_e)_{CC} = V_{CC} = \sqrt{2} G_F N_e.$$

Similarly the NC contribution, V_{NC} to the matter induced neutrino potentials,can also be found . As NC interactions are flavor independent it has same contribution for all three flavors.

For an electrically neutral medium the number densities of protons and electrons are same, hence the corresponding contribution to V_{NC} cancels. The contribution due to the NC scattering of neutrinos gives $(V_a)_{NC} = -G_F N_n/\sqrt{2}$ where, N_n is the neutron number density.

Together we get,

$$V_e = \sqrt{2} G_F \left(N_e - \frac{N_n}{2}\right), \quad V_\mu = V_\tau = \sqrt{2} G_F \left(-\frac{N_n}{2}\right).$$

In case of antineutrinos, $V_a \to -V_a$

For evolution of a system of oscillating neutrinos in matter we have to go back to the flavor basis as the effective potential of neutrinos are diagonal in this basis.

Let us consider the two flavor case with ν_e and ν_μ,

$$|\nu_l\rangle = u_{l\alpha}|\nu_\alpha\rangle \quad [l = e, \mu] \qquad U = \begin{pmatrix} \cos\theta & \sin\theta \\ -\sin\theta & \cos\theta \end{pmatrix}.$$

In absence of matter the evolution equation in mass basis is

$$i\frac{d}{dt}|\nu_\alpha\rangle = H|\nu_\alpha\rangle \quad [\alpha = 1, 2]. \tag{2.15}$$

$$\text{H is diagonal in this basis} \quad H = \begin{pmatrix} E_1 & 0 \\ 0 & E_2 \end{pmatrix}. \tag{2.16}$$

For flavor basis the evolution equation is,

$$i\frac{d}{dt}|\nu_l(t)\rangle = \tilde{H}|\nu_l(t)\rangle. \tag{2.17}$$

Expanding the flavor eigenstates in terms of mass eigenstates,

$$i\frac{d}{dt}|\nu_l(t)\rangle = i\frac{d}{dt}[u_{l\alpha}|\nu_\alpha\rangle] = iu_{l\alpha}\frac{d}{dt}|\nu_\alpha\rangle = u_{l\alpha}H|\nu_\alpha\rangle = u_{l\alpha}Hu^\dagger_{l\alpha}|\nu_l(t)\rangle, \tag{2.18}$$

$$i\frac{d}{dt}|\nu_l(t)\rangle = uHu^\dagger|\nu_l(t)\rangle.$$

Comparing them,

$$\tilde{H} = uHu^\dagger.$$

For relativistic neutrinos

$$E_\alpha \simeq p + \frac{m_\alpha^2}{2E}.$$

Therefore,

$$H = \begin{pmatrix} p & 0 \\ 0 & p \end{pmatrix} + \begin{pmatrix} \frac{m_1^2}{2E} & 0 \\ 0 & \frac{m_2^2}{2E} \end{pmatrix}.$$

Thus the evolution equation is

$$i\frac{d}{dt}\begin{pmatrix} |\nu_e(t)\rangle \\ |\nu_\mu(t)\rangle \end{pmatrix} = \begin{pmatrix} \left(p + \frac{m_1^2+m_2^2}{2E}\right) - \frac{\Delta_{21}^2}{4E}\cos 2\theta & \frac{\Delta_{21}^2}{4E}\sin 2\theta \\ \frac{\Delta_{21}^2}{4E}\sin 2\theta & \left(p + \frac{m_1^2+m_2^2}{2E}\right) + \frac{\Delta_{21}^2}{4E}\cos 2\theta \end{pmatrix} \begin{pmatrix} |\nu_e(t)\rangle \\ |\nu_\mu(t)\rangle \end{pmatrix}.$$

Since the terms within the first brackets in the diagonal elements modify the common phase only and since neutrino oscillations depend on the phase differences, this term have no effect on the evolution.

Therefore, the evolution equation in vacuum in the flavor basis is

$$i\frac{d}{dt}\begin{pmatrix} |\nu_e\rangle \\ |\nu_\mu\rangle \end{pmatrix} = \begin{pmatrix} -\frac{\Delta_{21}^2}{4E}\cos 2\theta & \frac{\Delta_{21}^2}{4E}\sin 2\theta \\ \frac{\Delta_{21}^2}{4E}\sin 2\theta & \frac{\Delta_{21}^2}{4E}\cos 2\theta \end{pmatrix}\begin{pmatrix} |\nu_e\rangle \\ |\nu_\mu\rangle \end{pmatrix}.$$

For matter induced ν evolution equation as there are free electrons in the matter (and no free muons) one has to add V_e to the first diagonal element of the effective Hamiltonian $\tilde{H}$ in the above equation.

$$i\frac{d}{dt}\begin{pmatrix} |\nu_e\rangle \\ |\nu_\mu\rangle \end{pmatrix} = \begin{pmatrix} -\frac{\Delta_{21}^2}{4E}\cos 2\theta + \sqrt{2}G_F N_e & \frac{\Delta_{21}^2}{4E}\sin 2\theta \\ \frac{\Delta_{21}^2}{4E}\sin 2\theta & \frac{\Delta_{21}^2}{4E}\cos 2\theta) \end{pmatrix}\begin{pmatrix} |\nu_e\rangle \\ |\nu_\mu\rangle \end{pmatrix}.$$

The evolution equation depends on N_e, which can depend on co-ordinate and time. We will consider two cases one with N_e a constant and another one with N_e varying with distance.

Constant Density Case

Here we take N_e to be constant. Diagonalization of the effective Hamiltonian gives the following eigenstates in the matter.

$$\nu_A = \nu_e \cos\phi + \nu_\mu \sin\phi,$$

$$\nu_B = -\nu_e \sin\phi + \nu_\mu \cos\phi,$$

where, the mixing angle ϕ is given by

$$\tan 2\phi = \frac{2\tilde{H}_{12}}{\tilde{H}_{22} - \tilde{H}_{11}} = \frac{(\Delta_{21}^2/2E)\sin 2\theta}{(\Delta_{21}^2/2E)\cos 2\theta - \sqrt{2}G_F N_e}. \tag{2.19}$$

This ϕ is different than vacuum mixing angle θ and ν_A and ν_B do not coincide with mass eigenstates ν_1 and ν_2.

The difference of the ν energy eigenvalues in matter is

$$E_A - E_B = \sqrt{\left(\frac{\Delta_{21}^2}{2E}\cos 2\theta - \sqrt{2}G_F N_e\right)^2 + \left(\frac{\Delta_{21}^2}{2E}\right)^2 \sin^2 2\theta}. \tag{2.20}$$

Therefore, the conversion probability

$$P_{\nu_e\nu_\mu}(x) = \sin^2 2\phi \sin^2\left(\pi\frac{x}{L_{mat}}\right), \tag{2.21}$$

where,

$$L_{mat} = \frac{2\pi}{E_A - E_B} = \frac{2\pi}{\sqrt{\left(\frac{\Delta^2_{21}}{2E}\cos 2\theta - \sqrt{2}G_F N_e\right)^2 + \left(\frac{\Delta^2_{21}}{2E}\right)^2 \sin^2 2\theta}}. \tag{2.22}$$

At limit $N_e \sim 0$, we can recover vacuum oscillation probability as then $\phi \sim \theta$ and $L_{mat} \sim L_{osc}$. From the formula of the mixing angle one can obtain

$$\sin^2 2\phi = \frac{\frac{\Delta^2_{21}}{2E}\sin^2 2\theta}{(E_A - E_B)^2}. \tag{2.23}$$

Thus it has a typical resonance form, with the maximum value $\sin^2 2\phi = 1$ obtained for

$$N_e = \frac{\frac{\Delta^2_{21}}{2E}\cos 2\theta}{2\sqrt{2}G_F E}. \tag{2.24}$$

This is called MSW Resonance condition and at this MSW condition mixing in matter is maximal $\phi = 45^0$ independent of the vacuum mixing angle θ. Thus even for very small θ (vacuum mixing angle) one can get resonance enhancement of ν-oscillation.

Again the resonance needs,

$$\Delta^2_{21}\cos 2\theta > 0,$$

i.e., $(m_2^2 - m_1^2)(\cos^2\theta - \sin^2\theta) > 0$.

Therefore MSW resonance of ν-oscillation requires

1. If $m_2 > m_1$ one needs $\cos^2\theta > \sin^2\theta$.

2. If $m_2 < m_1$ then $\cos^2\theta < \sin^2\theta$.

If one chooses the convention $\cos 2\theta > 0$, then $\Delta^2_{21} > 0$. Then for anti neutrinos one has $\Delta^2_{21} < 0$. Thus for a given sign of Δ^2_{21} one can not have both ν and $\bar{\nu}$ matter induced resonances.

Varying Density

Often in realistic situations a beam of non monochromatic neutrinos propagates in a medium with varying density profile. Then for a mass squared difference in the right order of magnitude, a significant portion of neutrino energy finds a matter density for which resonance is possible. If the neutrino beam is monochromatic, even then resonance can happen. Thus the MSW resonance condition does not involve any fine tuning. Consider two possible scenarios of varying density: The Adiabatic and the non-adiabatic.

The Adiabatic Case

For oscillation in a matter of an arbitrary non-uniform density. the evolution equation does not allow an analytic solution and has to be solved numerically. However, there is an important particular case which can give an approximate analytic solution. This is the case of slowly (adiabatically) varying matter density.

Consider ν_e born in matter densities far above MSW resonance, and assume matter density is decreasing monotonically. For the mixing angle given by Eq. 2.19 we have

$$\tan 2\phi = \frac{(\Delta_{21}^2/2E)\sin 2\theta}{(\Delta_{21}^2/2E)\cos 2\theta - \sqrt{2}G_F N_e},$$

Thus from this equation it follows that

1. Initial mixing angle (ϕ_i) in matter at neutrino production point $\phi_i \sim 90^0$ i.e., mixing is strongly suppressed by matter.

2. As ν's go towards smaller densities mixing increases and becomes maximal at resonance point (R), thus mixing at resonance $(\phi_R) = 45^0$.

3. At smaller densities the final mixing angle (ϕ_f) again decreases i.e.$\phi_f = \theta$ (vacuum mixing angle) when $N_e << N_{e(MSW)}$.

From

$$\begin{pmatrix} \nu_A \\ \nu_B \end{pmatrix} = \begin{pmatrix} \cos\phi & \sin\phi \\ -\sin\phi & \cos\phi \end{pmatrix} \begin{pmatrix} \nu_e \\ \nu_\mu \end{pmatrix},$$

one can say, at production point ($\phi \sim 90^0$) ν_e almost coincides with ν_B. If the matter density changes slowly enough (adiabatically) along the neutrino path, the neutrino system has enough time to adjust itself to the changing external conditions. In this case the transitions between ν_A and ν_B is completely suppressed, whereas the flavor composition of this matter eigenstates changes as neutrino propagates in matter because the mixing angle ϕ that determines this composition is a function of the matter density.

At the final point of neutrino evolution $\phi \simeq \theta$ then the matter eigenstates ν_B at this point has the component of originally produced ν_e with the weight $\sin^2\theta$ and the component of ν_μ with the weight $\cos^2\theta$, i.e., the transition probability is

$$P(\nu_e \to \nu_\mu) = \cos^2\theta,$$

i.e., in case of small vacuum mixing angle, one can have almost complete adiabatic conversion of ν_e to ν_μ.

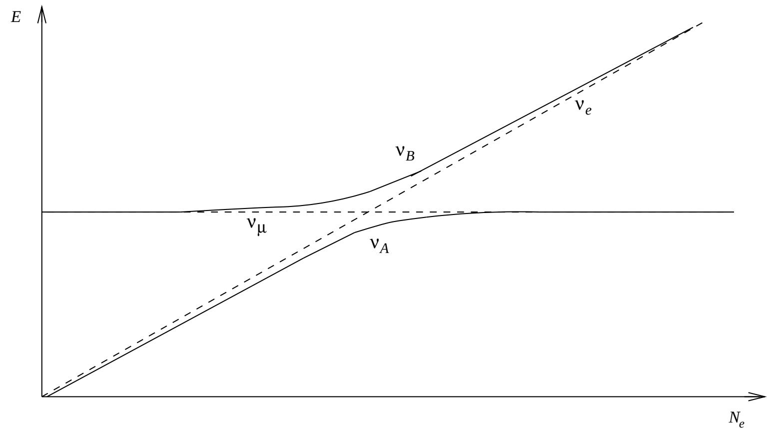

Figure 2.1: Neutrino energy levels in matter vs electron number density N_e. Dashed line – in the absence of mixing, solid line – with mixing.

Figure. 2.1 illustrates the energy levels of ν_A and ν_B along with those in the absence of mixing (i.e., ν_e and ν_μ) as the function of electron number density.

In case of absence of mixing the energy levels cross at MSW resonance point however with nonvanishing mixing the levels repel each other and the avoided level crossing results. For small transition probability between the two matter eigenstates, neutrinos which are produced as ν_e at high densities and also propagating towards smaller densities follow the upper (ν_B) branch and end up on the level that corresponds to ν_μ at small electron densities N_e.

In a more quantitative description of ν conversion, consider the effective Hamiltonian (i.e.,the non-diagonal part of $\tilde{H}$) at some instant t. Consider an unitary transformation to diagonalize this $\bar{H}(t)$ i.e.,

$$\begin{pmatrix} \nu_e \\ \nu_\mu \end{pmatrix} = \bar{U}(t) \begin{pmatrix} \nu_A(t) \\ \nu_B(t) \end{pmatrix}$$

and

$$\bar{U}^\dagger(t)\bar{H}\bar{U}(t) = \bar{H}_d(t) = \mathrm{diag}(E_A(t), E_B(t)),$$

where, $E_A(t)$ and $E_B(t)$ are instantaneous e-values of $\bar{H}(t)$ and $\bar{U}(t)$ are described as

$$\bar{U}(t) = \begin{pmatrix} \cos\phi & \sin\phi \\ -\sin\phi & \cos\phi \end{pmatrix},$$

where, $\phi = \phi(t)$ as $N_e = N_e(t)$. The evolution equation in the basis of the instantaneous eigenstates is

$$\begin{aligned} i\frac{d}{dt}\begin{pmatrix} |\nu_A\rangle \\ |\nu_B\rangle \end{pmatrix} &= i\frac{d}{dt}\left[\bar{u}^+(t)\begin{pmatrix} |\nu_e(t)\rangle \\ |\nu_\mu(t)\rangle \end{pmatrix}\right] \\ &= \begin{pmatrix} E_A(t) & -i\dot{\phi} \\ i\dot{\phi} & E_B(t) \end{pmatrix}\begin{pmatrix} |\nu_A\rangle \\ |\nu_B\rangle \end{pmatrix}. \end{aligned} \tag{2.25}$$

In this basis the effective Hamiltonian is not diagonal since the mixing angle ϕ is not constant, i.e. the matter e-state basis changes with time. For small off-diagonal terms, i.e., $|\dot{\phi}| << |E_A - E_B|$, the transitions between the instantaneous eigenstates ν_A and ν_B are suppressed. This is described as adiabatic approximation. The condition of adiabatic approximation is written as

$$\gamma^{-1} = \frac{2|\dot{\phi}|}{|E_A - E_B|} = \frac{\sin 2\theta_0 \Delta_{21}^2 |\dot{V}_{CC}|}{|E_A - E_B|^3 2E} << 1, \tag{2.26}$$

where $E_A - E_B$ and V_{CC} are given before. This parameter γ is called the adiabaticity parameter. In the adiabatic limit, the effective Hamiltonian is diagonal and then the time evolution of the matter eigenstates simply receive phase factors. Suppose ν_e was born at time $t = t_i$ with $\phi_i = \phi_(t_i)$,

$$\nu(t_i) = \nu_e = \cos\phi_i \nu_A + \sin\phi_i \nu_B.$$

Then in the adiabatic approximation at time t_f we have

$$\nu(t_f) = \cos\phi_i e^{-i\int_{t_i}^{t_f} E_A(t')dt'}\nu_A + \sin\phi_i e^{-i\int_{t_i}^{t_f} E_B(t')dt'}\nu_B.$$

At $t = t_f$, $\phi(t_f) = \phi_f$ is different form ϕ_i.

$$P(\nu_e \to \nu_\mu) = \frac{1}{2} - \frac{1}{2}\cos\phi_i \cos\phi_f - \frac{1}{2}\sin 2\phi_i \sin 2\phi_f \cos\beta,$$

where

$$\beta = \int_{t_i}^{t_f} (E_A - E_B)dt'.$$

The 2nd term in the above equation is a smooth function of t_f, whereas the 3rd term oscillates with time. If N_e at ν_e production point is very large compare to the MSW resonance matter density, then $\sin 2\phi_i \simeq 0$ and the 3rd term ~ 0. The non oscillatory neutrino conversion takes place with the probability $P(\nu_e \to \nu_\mu) = \cos^2 \phi_f$. Usually the final point has low density then $\phi_f = \theta$ i.e. we get back $P(\nu_e \to \nu_\mu) = \cos^2 \theta$,i.e. high oscillation in even low θ.

The Non-Adiabatic case

For the non-adiabatic situation the adiabatic condition is not satisfied ($|\phi| \not< |E_A - E_B|$) and γ is of the order of one. This breakdown is very much important at the position of resonance. Basically the off-diagonal terms in the effective Hamiltonian in Eq. 2.25 becomes comparable to the diagonal terms and give rise to a finite probability of transition from one mass eigenstates to other. This transition probability is called the level crossing or jump probability and defined as

$$P_J = | < \nu_B(x_+)|\nu_A(x_-) > |^2, \tag{2.27}$$

here $x_\pm$ refer to the points on either side of the resonance. P_J is found by solving the Eq.2.25 for the given matter density profile. For a linearly varying density, P_J is given by the Landau-Zener formula [4, 5]

$$P_J = exp(-\frac{\pi}{2}\gamma). \tag{2.28}$$

Thus the electron neutrino survival probability in a scenerio of breakdown of adiabaticity is given by

$$P_{\nu_e\nu_e} = \frac{1}{2} + (\frac{1}{2} - P_J)\ cos2\phi_f\ cos2\phi_i. \tag{2.29}$$

2.3 Discussion

In this chapter, we studied the general structure of neutrino oscillation. We showed how in vacuum neutrinos can oscillate among different flavors and give signature of their mass. We then discussed the neutrino interaction with matter and the change in the evolution equation of the neutrinos. This in turn led to the MSW resonance. Importance of both the costant density and varying density cases in this context has been discussed. These variation of matter densities can be very important in stellar environment. In particular in the scenario of supernovae where the matter density changes over a huge length this effects have to be considered.

BIBLIOGRAPHY

[1] B Pontecorvo, *Sov. Phys. JETP* **6**, 429 (1958).

[2] T. Schwetz, M. Tortola and J. W. F. Valle, *New J. Phys.* **10**, 113011 (2008).

[3] L. Wolfenstein,*Phys. Rev.* **D17**, 2369 (1978); S.P. Mikheyev and A.Yu. Smirnov, *Sov. J. Nucl. Phys.* **42(6)**, 913 (1985); *Nuovo Cimento* **9c**, 17 (1986).

[4] L. Landau, Phys. Z. Sowjetunion 2 (1932) 46; C .Zener, Proc. R. Soc. London, Ser. A 137 (1932) 696.

[5] T. K. Kuo and J. Pantaleone, Phys. Rev. D 39 (1989) 1930

CHAPTER 3

Core Collapse Supernova and Neutrinos

The death of a large massive star is a sudden and violent event. Peaceful evolution of the star for millions of year through various stages of development comes to an end when the star runs out of nuclear fuel and collapses under its own weight in the fraction of a second. The most interesting and important events occur in time scales of tens of milliseconds. That is followed by an outgoing shock wave causing the explosion, called supernova. This death of the massive star leaves the remnant as a neutron star or a black hole.

The explosion comes at the end of a sequence of fusion reactions which cover the life history of a star. These fusion reactions synthesize elements with atomic number upto 56. In fact even heavier elements in nature are thought to be created in the outer mantle of the exploding star.

3.1 Supernova Classification and Core Collapse Supernovae

Supernovae are broadly classified into two groups depending on their spectral nature. If the emitted radiation does not show hydrogen lines in their spectra then they are called type I otherwise it is a type II SN. On the other hand SN can also be classified according to the explosion mechanism : thermonuclear and core collapse explosions.

1. **Thermonuclear Explosion:**

   These kind of SNe also fall in one of the subgroup of type I/SNIa. They show similarity in luminosity and spectral evolutions and considered to be homogeneous events. In fact this is the reason why these SNIa explosions are used as standard candles in determining cosmological distances. The main feature of the SNIa are their spectra; other than the absence of hydrogen lines one can also find silicon lines in such events. They are usually formed by old stars in a binary system where one of the stars is a white dwarf accreting matter from the other one. This accretion gives rise to increase in mass and temperature for the central region of the star, eventually resulting in a thermonuclear explosion. Usually such explosions do not have any compact remnant and the progenitor is destroyed in the debris.

2. **Core Collapse Supernovae (CCSNe):** Core collapse events can be both type I and type II, with or without hydrogen line. Theses explosions are mainly observed in massive ($M \geq 8M_{\odot}$) stars. Their evolution is much faster than the SNIa and also less luminous. The main feature of these evemts are formation of an iron core at the center at the end of several stages of nuclear burning.

   The main difference in different core collapse SN comes from the spectrum of emitted radiation:

   (a) **SNIb and SNIc:** SNIb and SNIc similar to the SNIa, are characterized by the absence of hydrogen line. However unlike SNIa they also show absence of silicon lines. The explosion mechanisam of these events are similar in nature but the main difference between SNIa and SNIb is the following : SNIb are characterized by the presence of helium lines, whereas SNIc spectra do not show any helium line .

   (b) **Type II SN:** These are core collapse events but they have hydrogen in the spectrum. There are many subclasses of the type II depending on the luminosity curves and spectra. Whereas SNIb and SNIc lose the outer hydrogen/helium layers during their evolution, type II SNe retain all the layers resulting in different observed spectra.

Total energy released in core collapse events is a few times 10^{53} erg, out of which only about 1% is carried as kinetic energy of the expelled material. The energy in the electromagnetic radiation is approximately 0.01% of the total energy. However neutrinos emitted during the core collapse events carry the rest of the energy.

Therefore neutrinos play a very crucial role in the core collapse SN explosions and detection of SN neutrinos from such events would be really important.

However for thermonuclear explosions (SNIa) the total energy emitted by neutrinos is only about 1%. Thus compare to the CCSNe, the importance of neutrinos in such events is much less. In this thesis we study the oscillation of SN neutrinos; and we shall focus only on core collapse events as they are the main source of SN neutrinos. Henceforth by SN we will mean only core collapse events (CCSNe). In the next section we discuss how neutrinos are produced and emitted during a stellar core collapse and explosion.

3.2 Neutrino Production in Core Collapse Supernova

Neutrinos from CCSNe have some unique features, they carry information from deep inside the core of the SN and while coming out interact with the outside mantle as well. These SN neutrinos not only cary information about the SN but also can throw light on the neutrino properties. Now let us discuss the different stages of core collapse SN and the production of neutrinos [1, 2].

3.2.1 Stellar evolution and core collapse

A star during its evolution is kept in equilibrium by two opposite forces. One is a gravitational force trying to collapse the star and the other is the thermal pressure expanding it. The star goes through a series of nuclear burning reactions as described below.

In the beginning the hydrogen in the star gets transformed into helium through nuclear fusion reactions and this process is exothermic, i.e. the excess mass gets converted to energy. The gravitational attraction which tries to collapse the star is counteracted by the radiation pressure coming from fusion reactions. This hydrogen burning continues till the hydrogen in the core is used up. This is followed by contraction of the core which heats up the core and its surrounding layers. When the core becomes hot enough the next stages of fusion reactions are sequentially ignited, i.e., He burning to C, C to Ne, O and finally Si. Silicon burning lead to nuclei centered around the nucleus ${}^{56}_{26}Fe$ which has maximum binding energy per nucleon and no further fusion take place. Actually radially the star's burning is like an onion shell i.e. having shells of Si, S, O, C, He with increasing radius and finally hydrogen in the outermost envelope.

This onion shell like structure holds for larger stars while a star of size of the sun stops at the He burning stage whereas even smaller ones often stop with the hydrogen fusion. Only the massive stars ($> 8M_\odot$) continue upto Si burning. If the stellar core mass is more than the limiting Chandrasekhar mass (M_{Ch}) [1], then the electron degeneracy pressure cannot compensate the gravitational pressure and the star collapses after reaching iron type nuclei at the center. The collapse is initiated by the photodisintegration reactions and by loss of neutrinos produced in electron capture both of which reduce the pressure support.

With the collapse the core density increases with time. When it reaches the value of 10^{11} gm/cm^3, the matter becomes opaque to the neutrinos. At such high densities even the weakly interacting neutrinos get scattered many times. Eventually these neutrinos escape but the process has timescale longer than the collapse timescale. This effective trapping of neutrinos means that no energy can get out of the core.

For a simple model one can define a neutrinosphere with radius (R_ν) and neutrinos escape freely from the surface of the neutrinoshere. More precisely the neutrinosphere is defined as having a surface where the optical depth of neutrinos is unity. But since neutrinos in general do not emerge radially, optical depth for neutrinos are considered to be 2/3 instead of 1.

This neutrino trapping is important for the remaining evolution of the star. After the trapping most of the neutrinos generated through electron capture remain in the star and hence the lepton number per baryon (Y_l) at this stage does not change.

Now in the inner part of the core the collapse is homogeneous with the speed of infall being proportional to the distance from the center of the star. Thus the inner core collapses subsonically and at some radius the velocity becomes supersonic and the point at which the speed is equal to sound speed is called the sonic point. Thus the inner core decouples from the outer core and collapses homologously as a unit. This homologous core collapse continues until the density becomes around of 8×10^{14}gm cm^{-3}, which is

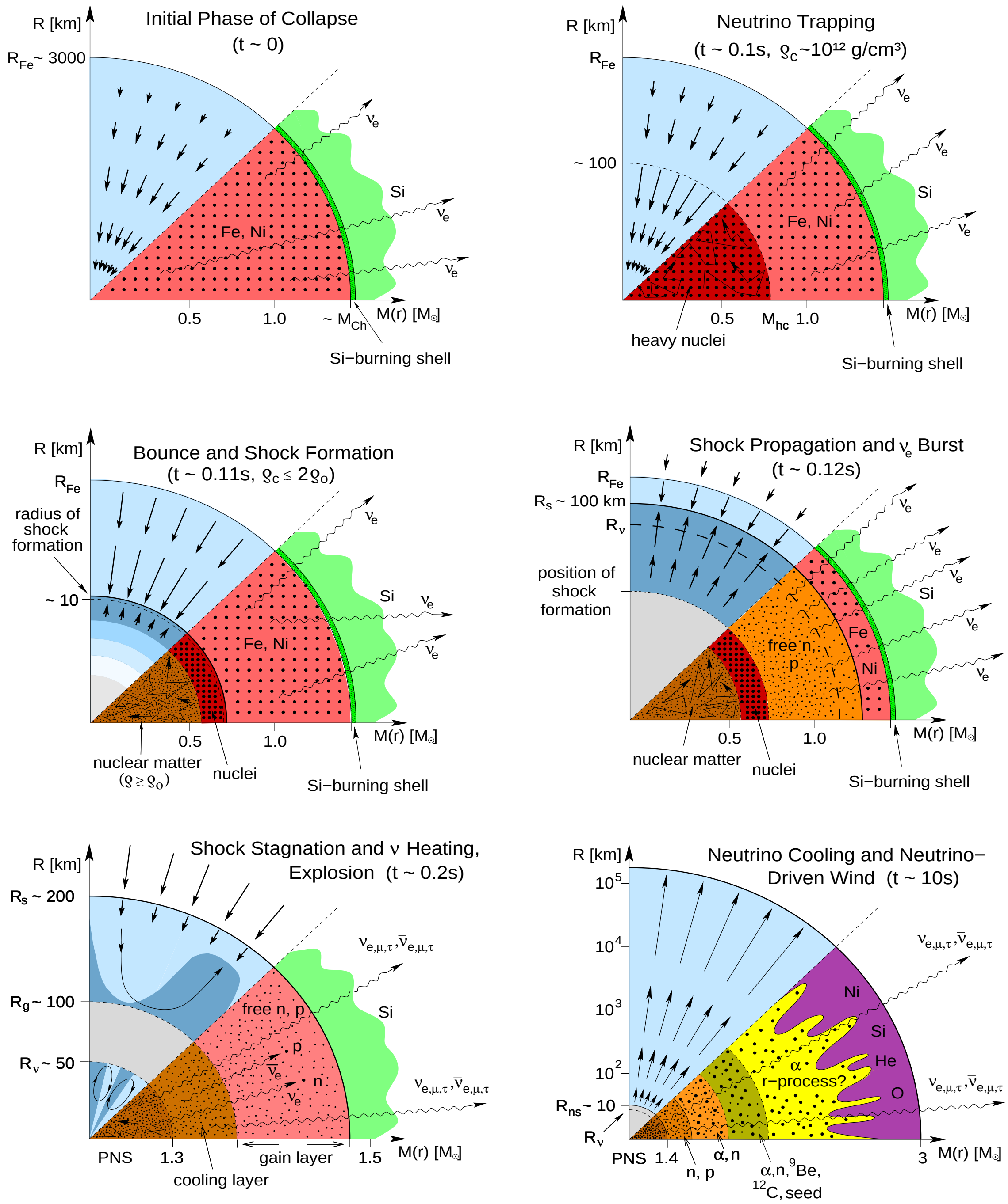

Figure 3.1: Schematic representation of the different stages of SN evolution. The panels show stages from the beginning of the supernova explosion upto the neutrino-driven wind during the neutrino-cooling phase. The upper half of the panels display the dynamical conditions, where the arrows represent the velocity vectors. The lower half of each panel indicates the nuclear composition with the nuclear and weak processes. The X-axis denotes mass in units of solar mass ($M_{\odot}$). M_{Ch} and M_{hc} mean the Chandrasekhar mass and the mass of the subsonically collapsing, homologous inner core respectively. The vertical axis indicates corresponding radii, with R_{Fe}, R_s, R_g, R_{ns} and R_{ν} being the iron core radius, shock radius, gain radius, neutron star radius, and neutrinosphere, respectively. The PNS has maximum densities (ρ) above the saturation density of nuclear matter (ρ_0). This figure has been taken from Janka et al. [3].

roughly 3 times the nuclear density. The collapse is halted around this density as the packed nuclei in the inner core feel the short distance repulsive part of the nuclear force. Consequently the inner core stiffens leading to a rebounding of the inner core, sending a radially propagating sound wave outwards through the infalling matter. This wave does not get to go very far as the supersonically infalling material from the outer core acts against it. Thus the infalling materials has to accumulate at the sonic point, giving rise to a discontinuity of density, pressure, and velocity. This is known as shock wave. This shock wave acquires more energy with time and starts traveling outward in the iron core.

3.2.2 Neutrino cooling

1. **Neutronization burst**

   The shock wave propagating outward on its way dissociates nuclei into free nucleons. The protons coming out due to this dissociation are perfect candidates for electron capture. The cross section of electron capture on free protons is much larger than that of on nuclei, hence one can expect creation of a huge number of electron neutrinos in the part of the star affected by the shock .

   $$e^- + p \to n + \nu_e$$

   $$e^- + (N, Z) \to \nu_e + (N + 1, Z - 1)$$

   These neutrinos normally are trapped within the neutrinosphere like the initial neutronization neutrinos due to the large density of the medium. However now some of the neutrinos can freely escape as the shock wave dissociates the iron nuclei of the neutrinosphere relieving some pressure. This sudden neutrino emission is known as the neutronization burst and leads to a shortlived rise in the luminosity. It is also known as the prompt neutrino burst as the time scale or duration of this peak is only about 10 ms. The shock wave gets stalled in the iron core within a few hundred km from the center of as both this dissociation of iron nuclei and neutrino emission takes out energy from the shock. The revival of this shock is a much discussed problem of stellar collapse.

2. **Thermal neutrinos**

   At the center of the expanding shock lies a proto-neutron star (PNS). At the end of the SN explosion the PNS forms a neutron star or a black hole. The PNS has a "colder" part below the shock starting radius whereas above this radius the shock affected region is more hot and less dense compared to the inner part. The electrons in the hot mantle of PNS are nondegenerate and relativistic thermal positrons can also be created. The presence of positrons are really important as it can give rise to neutrinos through the interactions

   $$e^{+} + n \longrightarrow \bar{\nu}_e + p$$

   and

   $$e^{+} + e \longrightarrow \bar{\nu}_x + \nu_x$$

   reactions. Note that contrary to the neutronization burst thermal neutrinos and antineutrinos can be produced in all three flavors denoted by 'x'. Emission of these thermal neutrinos eventually cool the mantle. Meanwhile the external core accretes mass over the PNS. The thermal neutrinos carry away the thermal energy transformed from the gravitational energy released in this process. This stage is longer compare to the neutronization burst phase and lasts between 10 ms and 1 s. Thus the accretion and neutronization/deleptonization give rise to cooling of the outer regions. After the accretion phase when the explosion starts the neutrino luminosity falls exponentially. This fall is a basic characteristic of neutron star formation and its cooling.

3.2.3 Supernova explosion

The final picture of the shock wave propagation and the late stages of SN explosions are not completely clear. By and large numerical simulations put forward two possible cases.

1. As the shock propagates outwards through inner core it will disintegrate the iron nuclei. As already discussed this is a costly process in terms of energy. If the iron core

is not too massive the shock can emerge at the outer region without too much loss of energy. When the shock energy is deposited in the outer material, an explosion can occur, throwing away the mantle. This process is called a prompt hydrodynamic explosion and for it to take place at all one needs a number of conditions in its favor, like a small and cold star and a soft equation of state. However simulations do not generally confirm this scenario.

2. On the contrary for a fairly massive iron core, the shock loses a fair amount of energy and the propagation stalls. Now to explain the SN explosions of such massive stars one need other ingredients. The need comes from the fact that SN are real events happening around the universe so somehow in nature the shock must have been revitalized.

   The possible solutions to the problem proposed and analyzed in literature are quite interesting. In the neutrino reheating mechanism [4] electron neutrinos and antineutrinos coming out the PNS reactivate the stalled shock. A small fraction of neutrino energy is deposited in the matter behind the shock as the neutrinos and antineutrinos are absorbed by protons and neutrons deposit their energy there.This additional energy heats up the matter to continue the shock forward, leads to an explosion. One also talks about the magneto-rotational or magneto-hydrodynamic (MHD) mechanics [5, 6]

   Another idea is the acoustic mechanism [7, 8], which mainly relies on the acoustic power from the core of the PNS. The energy produced in the core motions is transported by sound waves to the stalled shock, eventually giving rise to the explosions.

   All these scenarios still have different problems like the neutrino reheating does not generate enough energy of explosion, the acoustic mechanism is not well confirmed by different simulations. More realistic two or three dimensional calculations are needed for this last phase of explosion.

BIBLIOGRAPHY

[1] H.A. Bethe, *Rev. Mod. Phys.* **62**, 801 (1990).

[2] H.A. Bethe and G. Brown, *Sc. American* May (1984).

[3] H. T. Janka, K. Langanke, A. Marek, G. Martinez-Pinedo and B. Mueller, Phys. Rept. **442**, 38 (2007) [arXiv:astro-ph/0612072].

[4] H.A. Bethe and J.R. Wilson, *Astrophys. J* 295 (1985) 14

[5] K. Kotake, K. Sato, H. Sawai and S. Yamada, *Astrophys. J* 608 (2004) 391.

[6] T. Takiwaki, K. Kotake, S. Nagataki and K. Sato, *Astrophys. J* 616 (2004) 1086

[7] A. Burrows, E. Livne, L. Dessart, C. Ott and J. Murphy, *Astrophys. J.* 640 (2006) 878.

[8] A. Burrows, E. Livne, L. Dessart, C. D. Ott and J. Murphy, *Astrophys. J.* 655 (2007) 416.

CHAPTER 4

Collective Neutrino Oscillation in Supernova

The neutrinos from a core-collapse supernova can play an important role in probing both neutrino properties as well as throwing in light on the supernova mechanism [1, 2]. The neutrino evolution in SN is divided in two regions: inside the core below neutrino sphere and above neutrinosphere through the envelope. The neutrino oscillations of our interest happen outside the neutrino sphere so our focus will be only on neutrino evolution above the neutrinosphere and will consider the surface of the neutrinosphere as the source emitting the neutrinos.

These Neutrinos emitted during the explosion of core-collapse supernovae (SN) pass through very large density variation of matter and can undergo MSW resonant flavor conversion [3]. The MSW oscillation of SN neutrinos can give useful information on neutrino mass hierarchy and the third leptonic mixing angle θ_{13}. This idea of neutrino interaction with matter and its impact by giving rise to MSW effect is well understood. However the effect on neutrino evolution due to neutrino-neutrino interactions needs more clarifications. In fact the common assumption used in literatures before a few years was that neutrino-neutrino interactions are too feeble to cause any flavor conversion.

These interactions had been studied in previous literature [4, 5, 6], it has only very recently been appreciated that they induce sizable flavor conversion in supernovae [7, 8, 9, 10, 11]. Motivated by this interesting result, the effects of these neutrino-neutrino interactions have been explored in the context of supernovae, in a series of papers [12, 13, 14, 15, 16, 17, 18, 19, 20, 21, 22, 23, 24, 25, 26, 27, 28, 29, 30, 31, 32, 33, 34, 35, 36, 37, 38, 39].

The basic idea is that close to the neutrinosphere, due to the large neutrino density, neutrinos form a background to themselves. This neutrino-neutrino interaction effect is nonlinear and can give rise to flavor transition of neutrinos and antineutrinos. The interesting aspect of these conversions is that the neutrinos and antineutrinos of different energies undergo conversions together, and are almost in-phase. Therefore these conversions are referred to as being "collective". In other words the neutrino-neutrino interactions lead to coherent oscillations of neutrinos of different energies with some average frequency, giving rise to synchronized oscillations. However, there is no effective flavor conversion due to these synchronized oscillations as the effective mixing angle is highly suppressed due to the large MSW potential in the region close to the neutrinosphere. With the neutrino density decreasing outward, bipolar oscillations begin to take place beyond a distance of 50-100 km from the center. These oscillations can lead to complete or partial swapping (spectral split) of the $\bar{\nu}_e$ (ν_e) and $\bar{\nu}_x$ (ν_x) spectra depending on their initial luminosities and average energies. Finally, after a few hundred kilometers, the neutrino-neutrino interactions become negligible and it is the MSW transitions which dominate.

In this chapter we will address the question of collective effects in SN neutrino transformations in a two flavor scenario. We will show how different choice of initial relative luminosity neutrino and antineutrinos can give rise to different flux. In the beginning let us first discuss the main characteristics of this collective conversion caused by the dense neutrino background.

4.1 Neutrino-neutrino interaction and Supernova

Here the three flavor $(\nu_e, \nu_\mu, \nu_\tau)$ neutrino system behaves like an effective two flavor (ν_e, ν_x) scenerio under the collective evolution, where ν_x can be ν_μ or ν_τ or a linear combination of ν_μ and ν_τ [24, 31]. The flavor evolution for this system is driven by the effective mass squared difference Δm^2_{atm} and the mixing angle θ_{13}. This two flavor scenerio which has been extensively studied [11, 16, 17, 20] shows that for inverted hierarchy (IH, $\Delta m^2 < 0$), above a critical energy (split energy E_c), the spectrum in both the electron neutrino (ν_e) and antineutrino ($\bar{\nu}_e$) sectors end up with a complete exchange or swap with ν_x and $\bar{\nu}_x$ respectively, this is referred as "spectral swap". However the studies in [32, 33, 34] analyzed the role of equipartition in energy and variation of luminosity and showed the interesting possibility of multiple splits in the supernova neutrino spectrum for IH. Single spectral split for Normal Hierarchy (NH, $\Delta m^2 > 0$) was also reported for certain values of luminosities.

4.1.1 Evolution equations of SN neutrinos

We assume an ensemble of relativistic neutrinos and antineutrinos coming in 2 flavors (ν_e, ν_x) depicting the exact situation of dense neutrino gas close to the SN core. The ensemble is best described by a set of dimensionless density matrices ρ_p and $\bar{\rho}_p$, one for each momentum mode. The diagonal entries of the density matrices are the usual occupation numbers whereas the off-diagonal terms encode phase information. The evolution of such a system is driven by Liouville equations.

Thus the equations of motion (EOMs) are

$$\partial_t \rho_p = -i[H_p, \rho_p] \quad , \quad \partial_t \bar{\rho}_p = -i[\bar{H}_p, \bar{\rho}_p]. \tag{4.1}$$

Here the neutrino Hamiltonian (H_p) has contributions from the usual vacuum Hamiltonian (H_{vacuum}), the matter interaction or MSW Hamiltonian (H_{MSW}) and also from the new neutrino-neutrino interaction potential termed as $H_{\nu\nu}$.

$$H_p = H_{vacuum} + H_{MSW} + H_{\nu\nu}. \tag{4.2}$$

The antineutrino Hamiltonian ($\bar{H}_p$) has exactly the same form as (4.2) with the only change that the vacuum (H_{vacuum}) term picks a negative sign .

Under our analysis of two flavor system the different contributions of neutrino Hamiltonian are given by,

$$H_{vacuum} = \frac{\triangle m^2}{4E} \begin{pmatrix} -cos2\theta & sin2\theta \\ sin2\theta & cos2\theta \end{pmatrix} , \qquad H_{MSW} = \begin{pmatrix} \sqrt{2}G_F N_e & 0 \\ 0 & 0 \end{pmatrix} , \tag{4.3}$$

where

$$\triangle m^2 = m_2^2 - m_1^2 \ ; \ \ \theta = Mixing \ \ Angle \ \ and \ \ N_e = Electron \ \ Number \ \ Density. \tag{4.4}$$

For the term $H_{\nu\nu}$, considering the contribution from $\nu - \nu$ forward scattering to the leading order of G_F give [5]

$$H_{\nu\nu} = \sqrt{2}G_F \int d^3q(1 - cos\theta_{pq})(n\rho_q - \bar{n}\bar{\rho}_q). \tag{4.5}$$

The factor $(1 - cos\theta_{pq})$ arises from the V - A nature of the weak interaction. Thus neutrinos moving in different directions will experience a different refractive effect caused by the other neutrinos. On the other hand, the effect is also energy dependent, and SN neutrinos are emitted with a range of energy hence this dependence is an important point to understand.

Thus due to this angular factor, neutrinos from the SN core traveling along different trajectories encounter different neutrino-neutrino interaction potential. These 'multi angle' effects may give rise to kinematical decoherence [13] which in turn can wash out the collective features described above. But for spherically symmetric cases "single angle" [11] approximation i,e neutrino-neutrino interactions averaged along a single trajectory seems to be a fine approximation as the 'multi angle' decoherence in this case is rather weak against the collective features [14].

Then under the "single angle" approximation the $H_{\nu\nu}$ term becomes

$$H_{\nu\nu} = \sqrt{2}G_F D(r) \int dq\ q^2(n\rho_q - \bar{n}\bar{\rho}_q). \tag{4.6}$$

D(r) is called the geometrical factor and depends on the particular launching angle. The geometrical factor D(r) for a launching angle of zero degree is given by

$$D(r) = \frac{1}{2}\left(1 - \sqrt{1 - \left(\frac{R_\nu}{r}\right)^2}\right)^2. \tag{4.7}$$

In Eq. 4.6 the n and $\bar{n}$ denote the total effective neutrino and antineutrino number per unit volume per unit energy. They are discussed in detail in the later part of this chapter. The term R_ν denotes the neutrinosphere radius.

In this two-flavor system, the density matrices can be reduced to polarization vectors by using the Pauli matrices and the unit matrix. Therefore the EOMs can be expressed in terms of the polarization vectors using:

$$M = \frac{1}{2}(1 + \mathbf{m}.\bar{\sigma}). \tag{4.8}$$

Where M is any 2×2 Hermetian Matrix, σ's are Pauli spin Matrices and $\mathbf{m}$ (m_x, m_y, m_z) is called the Bloch Vector.

Define Bloch vectors corresponding to ρ , $\bar{\rho}$, H_{vacuum} , H_{MSW}, $H_{\nu\nu}$ as $\mathbf{P}$, $\mathbf{P}^{'}$, $\mathbf{B}$, $\mathbf{L}$, $\mathbf{D}$ respectively.

Thus the evolution equations in the two-family Bloch vector notation for the polarization vectors of the neutrino ($\mathbf{P}$) and antineutrino ($\mathbf{P}^{'}$) sector are,

$$\dot{\mathbf{P}} = \mathbf{P} \times (\omega \mathbf{B} - \lambda \hat{\mathbf{z}} - \mu \mathbf{D}) \ , \tag{4.9}$$

$$\dot{\mathbf{P}}^{'} = \mathbf{P}^{'} \times (-\omega \mathbf{B} - \lambda \hat{\mathbf{z}} - \mu \mathbf{D}) \ , \tag{4.10}$$

where the terms involving ω, λ and μ are the ones having the vacuum, matter and neutrino-neutrino interaction effects and the frequencies are represented by

$$\mathbf{B} = (-\sin 2\theta, 0, \cos 2\theta)^T \quad , \quad \omega = \frac{\Delta m^2}{2E} \ , \tag{4.11}$$

$$\hat{\mathbf{z}} = (0,0,1)^T \quad , \quad \lambda = \sqrt{2} G_F N_e \ , \tag{4.12}$$

$$\mathbf{D} = \frac{1}{(N_{\nu_e} + N_{\nu_x} + N_{\bar{\nu}_e} + N_{\bar{\nu}_x})} \int dE (n\mathbf{P} - \bar{n}\mathbf{P}^{'}) \quad , \quad \mu = \sqrt{2} G_F (N_{\nu_e} + N_{\nu_x} + N_{\bar{\nu}_e} + N_{\bar{\nu}_x}) \ , \tag{4.13}$$

respectively.

$\mathbf{D}$ can be defined in terms of the global polarization vectors $\mathbf{J}$ and $\bar{\mathbf{J}}$ i,e $\mathbf{D} = \mathbf{J} - \bar{\mathbf{J}}$. Where

$$\mathbf{J} = \tfrac{1}{(N_{\nu_e} + N_{\nu_x} + N_{\bar{\nu}_e} + N_{\bar{\nu}_x})} \int dE \ n\mathbf{P} \quad , \quad \bar{\mathbf{J}} = \tfrac{1}{(N_{\nu_e} + N_{\nu_x} + N_{\bar{\nu}_e} + N_{\bar{\nu}_x})} \int dE \ \bar{n}\mathbf{P}^{'}.$$

As usual, θ and Δm^2 are the mixing angle and mass squared difference respectively. In what follows θ_{eff} is taken as 10^{-5} and $|\Delta m^2| = |\Delta m^2_{31}| = |m_3^2 - m_1^2|$ $=3 \times 10^{-3}$ eV^2. N_α's represent the total effective number density of the αth species.

$$N_\alpha = \int dE \ n_\alpha \ , \tag{4.14}$$

where,

$$n = n_{\nu_e} + n_{\nu_x} \quad , \quad \bar{n} = n_{\bar{\nu}_e} + n_{\bar{\nu}_x} \ , \tag{4.15}$$

n_α's are the effective number density per unit energy for the α'th species of neutrino and can be expressed as [11]

$$n_\alpha(r,E) = \frac{D(r)}{2\pi R_\alpha^2}\frac{L_\alpha}{\langle E_\alpha\rangle}\Psi_\alpha(E)\ , \tag{4.16}$$

where L_α and $\langle E_\alpha\rangle$ are the luminosity and average energy for the αth (anti)neutrino species, R_α is the neutrinosphere radius. The initial flux of the αth species at the neutrinosphere is given by $\frac{L_\alpha}{\langle E_\alpha\rangle}$ whereas the initial energy distribution is represented by $\Psi_\alpha(E)$. $D(r)$ is allready defined earlier.

The matter effect is removed from the evolution equations as the equations are considered in a frame rotating with angular velocity -$\lambda\mathbf{z}$ [10]. [1] In such a frame all the physical observable remain the same. Thus the evolution equations are

$$\dot{\mathbf{P}} = \mathbf{P}\times(\omega\mathbf{B}-\mu\mathbf{D})\ , \tag{4.17}$$

$$\dot{\mathbf{P}}' = \mathbf{P}'\times(-\omega\mathbf{B}-\mu\mathbf{D})\ . \tag{4.18}$$

These are nonlinear coupled equations (due to the 2nd term containing $\mathbf{D}$) and have to be solved numerically. It is evident from the evolution Eqs. 4.9 and 4.10 that there are two relevant frequencies, the usual vacuum frequency (ω) and the neutrino-neutrino interaction strength parameter (μ). For our chosen Δm^2 the vacuum frequency is

$$\omega = \frac{\Delta m^2}{2E} = \frac{30}{(4E/MeV)}\ \ km^{-1}\ . \tag{4.19}$$

The usual SN neutrino energy considered is in the range of 0 to 50 MeV, as the SN neutrino flux beyond 50 MeV is very small. Hence we use neutrino energy upto 50 MeV for our calculation.

The other frequency (μ) representing neutrino-neutrino interaction is nontrivial, and is given by

$$\mu = \sqrt{2}G_F(N_{\nu_e}+N_{\nu_x}+N_{\bar\nu_e}+N_{\bar\nu_x})\ . \tag{4.20}$$

[1]Note that though the matter potential is mostly rotated away, it may affect the evolution by delaying the collective effect [12] or by some early decoherence [27] or even modifying very low energy (order of 0.1 MeV) split features [20, 21, 2].These early effects have very little impact on the over all split patterns at the end of the collective region (400 Km) and the low energy split features below 1 MeV are negligible compared to the total spectra. Moreover the matter potential can be accounted for by choosing a matter suppressed hence small effective mixing angle, as we have chosen a $\theta_{eff} = 10^{-5}$ [14]. So in the subsequent discussions we neglect the above mentioned roles of the matter term and work with a very small θ_{eff} to compensate the matter term. We have explicitly checked that the inclusion of the matter term does not change our results.

The Eqs. 4.13 to 4.16 imply that contribution of the α-th species to μ is dependent on radial distance (r), neutrinosphere radius (R_α), initial flux ($\frac{L_\alpha}{\langle E_\alpha \rangle}$) and initial energy distribution ($\Psi_\alpha(E)$).

In our analysis, neutrinosphere radius is taken as 10 km whereas other inputs like initial flux and energy distribution depend on the choice of initial neutrino spectrum model. We analyze the evolution for several neutrino spectrum model.

4.1.2 Models of initial neutrino spectrum

In a core-collapse SN, the gravitational binding energy (about a few times 10^{53} erg) is converted to neutrinos and antineutrinos with energies of the order of 10 MeV and gets emitted in the subsequent $\sim$ 10 sec. Initially a neutronization burst comes out consisting of pure ν_es but with only a very small fraction of the total energy and after that the thermal neutrinos and antineutrinos of all three flavors are emitted. For the thermal neutrinos the initial energy distribution is expected to be Fermi-Dirac (FD), but the results of several simulations [40, 41, 42] found that the distribution must be close to pinched thermal spectra [42] i.e. with a deficit on the high energy side compared to FD. Fermi-Dirac(FD) distribution in energy implies

$$\Psi_\alpha^{FD}(E) \propto \frac{\beta_\alpha \ (\beta_\alpha E)^2}{e^{\beta_\alpha E} + 1} \ , \tag{4.21}$$

and for a choice of average energies of different flavors

$$\langle E_{\nu_e} \rangle = 10 \text{ MeV}, \quad \langle E_{\bar{\nu}_e} \rangle = 15 \text{ MeV}, \quad \langle E_{\nu_x} \rangle = \langle E_{\bar{\nu}_x} \rangle = 24 \text{ MeV}, \tag{4.22}$$

the inverse temperature parameters are [20]

$$\beta_{\nu_e} = 0.315 \text{ MeV}^{-1}, \quad \beta_{\bar{\nu}_e} = 0.210 \text{ MeV}^{-1}, \quad \beta_{\nu_x} = \beta_{\bar{\nu}_x} = 0.131\text{MeV}^{-1}. \tag{4.23}$$

Whereas the pinched spectra for different simulations are parameterized as [42]

$$\Psi_\alpha(E) = \frac{(1+\zeta_\alpha)^{1+\zeta_\alpha}}{\Gamma(1+\zeta_\alpha)} \left(\frac{E_\alpha}{\langle E_\alpha \rangle}\right)^{\zeta_\alpha} \frac{\exp\left(-(1+\zeta_\alpha)\frac{E_\alpha}{\langle E_\alpha \rangle}\right)}{\langle E_\alpha \rangle} \ , \tag{4.24}$$

$\langle E_\alpha \rangle$ is the average energy of ν_α, and ζ_α is the pinching parameter.

The effective number density for the αth species per unit energy is given by

$$n_\alpha(r,E) = \frac{D(r)}{2\pi R_\alpha^2}\frac{L_\alpha}{\langle E_\alpha\rangle}\Psi_\alpha(E) \ . \tag{4.25}$$

For a specific choice of $\Psi_\alpha(E)$ the initial flux ($\phi_\alpha = \frac{L_\alpha}{\langle E_\alpha\rangle}$) for the αth flavor need to be specified and are very crucial input parameters in our study. Supernova models tell us that almost all the gravitational energy released in core collapse supernovae comes out as $\nu\bar{\nu}$s of all flavors. Only one or two percent of it goes into the explosion and the electromagnetic radiation emitted in all wavelengths. The total luminosity scales as $L(t) = L_0(e^{-t/\tau}/\tau)$ but for a first study we take a time-averaged value for it as done in [20] and [33]. One can of course look at the problem for specific instants of time by changing the total luminosity, early times having larger values.

The total SN binding energy released ($E_B = 3\times 10^{53}$ erg) is related to the individual flavor luminosities by

$$L_{\nu_e} + L_{\bar{\nu}_e} + 4L_{\nu_x} = \frac{E_B}{\tau} \ , \tag{4.26}$$

assuming no distinction between ν_x and $\bar{\nu}_x$. We also assume a time-independent constant luminosity over the time τ. We take $\tau = 10$ seconds. Thus the initial fluxes of different flavors get constrained by

$$\phi^0_{\nu_e}\langle E_{\nu_e}\rangle + \phi^0_{\bar{\nu}_e}\langle E_{\bar{\nu}_e}\rangle + 4\phi^0_{\nu_x}\langle E_{\nu_x}\rangle = 3\times 10^{52} \ . \tag{4.27}$$

If we denote the ratio between the initial fluxes of different flavors by

$$\phi^0_{\nu_e} : \phi^0_{\bar{\nu}_e} : \phi^0_{\nu_x} = \phi^r_{\nu_e} : \phi^r_{\bar{\nu}_e} : 1 \ , \tag{4.28}$$

where $\phi^r_{\nu_e}$, $\phi^r_{\bar{\nu}_e}$ are positive numbers, then Eq.4.27 can be written as

$$\phi^0_{\nu_x}(\phi^r_{\nu_e}\langle E_{\nu_e}\rangle + \phi^r_{\bar{\nu}_e}\langle E_{\bar{\nu}_e}\rangle + 4\langle E_{\nu_x}\rangle) = 3\times 10^{52} \ . \tag{4.29}$$

Note that $\phi^r_{\nu_e} = \frac{\phi^0_{\nu_e}}{\phi^0_{\nu_x}}$, $\phi^r_{\bar{\nu}_e} = \frac{\phi^0_{\bar{\nu}_e}}{\phi^0_{\nu_x}}$ are basically initial relative fluxes. Thus different choices of $\phi^r_{\nu_e}$ and $\phi^r_{\bar{\nu}_e}$ imply different relative luminosities or relative fluxes.

Four representative sets for the energy spectra (in terms of $\langle E_\alpha\rangle$ and the pinching factor ζ_ν) and flux ratios usually discussed in literature, are given in Table 4.1. One simulation by the Lawrence Livermore group (LL) [40] and two different simulations by the Garching group (G1, G2) [42] are presented. Recently [32] used another set of "plausible" flux parameters giving rise to multiple splits in the neutrino spectra is also given. We call this 'G3'. For the LL spectra we use the FD distribution for Ψ given in Eq. 4.21. The β_α for LL are given in Eq. 4.23. For G1, G2 and G3 spectra we use the pinched spectrum defined in Eq. 4.24. We assume ζ_{ν_x}=$\zeta_{\bar{\nu}_x} = 4$ and ζ_{ν_e}=$\zeta_{\bar{\nu}_e} = 3$ for G1 and G2. For G3 all $\zeta_\alpha = 3$.

Model	$\langle E_{\nu_e}\rangle$	$\langle E_{\bar{\nu}_e}\rangle$	$\langle E_{\nu_x,\bar{\nu}_x}\rangle$	$\phi^r_{\nu_e}$=$\frac{\phi^0_{\nu_e}}{\phi^0_{\nu_x}}$	$\phi^r_{\bar{\nu}_e}$=$\frac{\phi^0_{\bar{\nu}_e}}{\phi^0_{\nu_x}}$
LL	12	15	24	2.00	1.60
G1	12	15	18	0.80	0.80
G2	12	15	15	0.50	0.50
G3	12	15	18	0.85	0.75

Table 4.1: The parameters of the used primary neutrino spectra models motivated from SN simulations of the Garching (G1, G2) and the Lawrence Livermore (LL) group. We assume ζ_{ν_x}=$\zeta_{\bar{\nu}_x} = 4$ and ζ_{ν_e}=$\zeta_{\bar{\nu}_e} = 3$ for G1 and G2. For G3 all $\zeta_\alpha = 3$. For LL we use a pure FD spectrum.

Note that the LL simulation obtained a large hierarchy $\langle E_{\nu_e}\rangle < \langle E_{\bar{\nu}_e}\rangle < \langle E_{\nu_x}\rangle \approx \langle E_{\bar{\nu}_x}\rangle$, and an almost complete equipartition of energy among the flavors. The Garching simulations predict a smaller hierarchy between the average energies, incomplete equipartition, and increased spectral pinching. The differences in the values of these parameters arise from the different physics inputs.

The equipartition of energy implies

$$L_{\nu_e} = L_{\bar{\nu}_e} = L_{\nu_x} \ . \tag{4.30}$$

In terms of our notation it means

$$\phi^r_{\nu_e} = \frac{\langle E_{\nu_x}\rangle}{\langle E_{\nu_e}\rangle}; \quad \phi^r_{\bar{\nu}_e} = \frac{\langle E_{\nu_x}\rangle}{\langle E_{\bar{\nu}_e}\rangle} \ . \tag{4.31}$$

So complete equipartition for the Garching simulations would imply flux ratios (Table 4.2) different from the values in Table 4.1. Recent analyses [33] have shown that the multiple split cases have origin in the departure from energy equipartition.

Actually there is no reason that equipartition should be strictly followed for the energy

Model	$\phi^r_{\nu_e}=\frac{\phi^0_{\nu_e}}{\phi^0_{\nu_x}}$	$\phi^r_{\bar{\nu}_e}=\frac{\phi^0_{\bar{\nu}_e}}{\phi^0_{\nu_x}}$
G1	1.50	1.20
G2	1.25	1.00
G3	1.50	1.20

Table 4.2: The flux ratios for the Garching models with equipartition of energy

released from a real supernova. In the next subsection we make extensive analysis of this multiple split phenomena with varying initial fluxes, which is equivalent to varying $\phi^r_{\nu_e}$ and $\phi^r_{\bar{\nu}_e}$.

4.1.3 Survival probability and flux

As stated above in this subsection we discuss the impact due to the variation of initial relative fluxes ($\phi^r_{\nu_e}$ and $\phi^r_{\bar{\nu}_e}$) on the final spectrum. The final spectrum is calculated at 400 km as collective effect is expected to vanish at around 400 km. We also analyze this effect for different models of initial neutrino spectrum spectrum LL, G1 and G3.

In principle the values of $\phi^r_{\nu_e}$ and $\phi^r_{\bar{\nu}_e}$ can lie in a large range. Thus analysing this variation would require study in a wide range of the $\phi^r_{\nu_e}$-$\phi^r_{\bar{\nu}_e}$ parameter space. Instead we consider the suggestion [43] that the uncertainty in the relative luminosities of different flavors must be in the range

$$\frac{1}{2} \leq \frac{L_{\nu_e}}{L_{\nu_x}} \leq 2 \quad ; \quad \frac{1}{2} \leq \frac{L_{\bar{\nu}_e}}{L_{\nu_x}} \leq 2 \, . \tag{4.32}$$

These limits in turn will put a constraint on the parameters $\phi^r_{\nu_e}$ and $\phi^r_{\bar{\nu}_e}$

$$\frac{1}{2}\frac{\langle E_{\nu_x}\rangle}{\langle E_{\nu_e}\rangle} \leq \phi^r_{\nu_e} \leq 2\frac{\langle E_{\nu_x}\rangle}{\langle E_{\nu_e}\rangle} \quad ; \quad \frac{1}{2}\frac{\langle E_{\nu_x}\rangle}{\langle E_{\bar{\nu}_e}\rangle} \leq \phi^r_{\bar{\nu}_e} \leq 2\frac{\langle E_{\nu_x}\rangle}{\langle E_{\bar{\nu}_e}\rangle} \, . \tag{4.33}$$

In Table 4.3 we present the lower limits (ll) and upper limits (ul) of the initial relative fluxes for different spectrum models LL, G1 and G3.

Model	$\langle E_{\nu_e} \rangle$	$\langle E_{\bar{\nu}_e} \rangle$	$\langle E_{\nu_x,\bar{\nu}_x} \rangle$	$\phi^r_{\nu_{e;ll}}$	$\phi^r_{\nu_{e;ul}}$	$\phi^r_{\bar{\nu}_{e;ll}}$	$\phi^r_{\bar{\nu}_{e;ul}}$
LL	10	15	24	1.20	4.80	0.80	3.2
G1	12	15	18	0.75	3.00	0.60	2.4
G3	12	15	18	0.75	3.00	0.60	2.4

Table 4.3: The average energies, upper limits (ul) and lower limits (ll) of the initial relative flux for the models used.

To compare different flux models and study more of the parameter space we vary $\phi^r_{\nu_e}$ and $\phi^r_{\bar{\nu}_e}$ in the range [0.5,5.0] and [0.5,3.5] respectively, for all the models. We find that varying $\phi^r_{\nu_e}$ and $\phi^r_{\bar{\nu}_e}$ give rise to different possibilities of final spectra as discussed in [33]. In addition to that we check it for different initial spectrum models. Here it is notable that usually the initial spectrum models come with a fixed value of $\phi^r_{\nu_e}$ and $\phi^r_{\bar{\nu}_e}$ (see Table 4.1) but the main idea in this analysis is about varying $\phi^r_{\nu_e}$ and $\phi^r_{\bar{\nu}_e}$. So here by initial spectrum models (like LL, G1, G3) we mean the energy dependence (ζ_{ν_α}) and neutrino average energies ($\langle E_{\nu_\alpha} \rangle$) of the models. In what follows, we will see that for the Inverted Hierarchy (IH) the final spectrum is very sensitive to the values of $\phi^r_{\nu_e}$, $\phi^r_{\bar{\nu}_e}$ and the model of initial spectrum. Whereas for Normal Hierarchy (NH), the results are less dependent on these quantities. We will discuss the reasons for this behavior.

Probability and Flux: NH

As already discussed in [32, 33], large flux (luminosity) of ν_x can induce simultaneous swap in both neutrino and antineutrino sector for NH. In these cases initially the system is in an unstable equilibrium. As it evolves, it partially swaps the flavor in both neutrino as well as antineutrinos, to end up in a stable state. We further study this over different spectrum models and initial relative fluxes. For each of the different models we vary $\phi^r_{\nu_e}$ and $\phi^r_{\bar{\nu}_e}$ in the range [0.5,5.0] and [0.5,3.5] respectively. We find that for several choices of ($\phi^r_{\nu_e}$,$\phi^r_{\bar{\nu}_e}$) there is simultaneous swap in both neutrino and antineutrino spectrum and this swap may generate prominent split in the final spectrum. For a specific model these split energies (E_c) may vary from low to high energies, depending on the value of ($\phi^r_{\nu_e}$,$\phi^r_{\bar{\nu}_e}$).

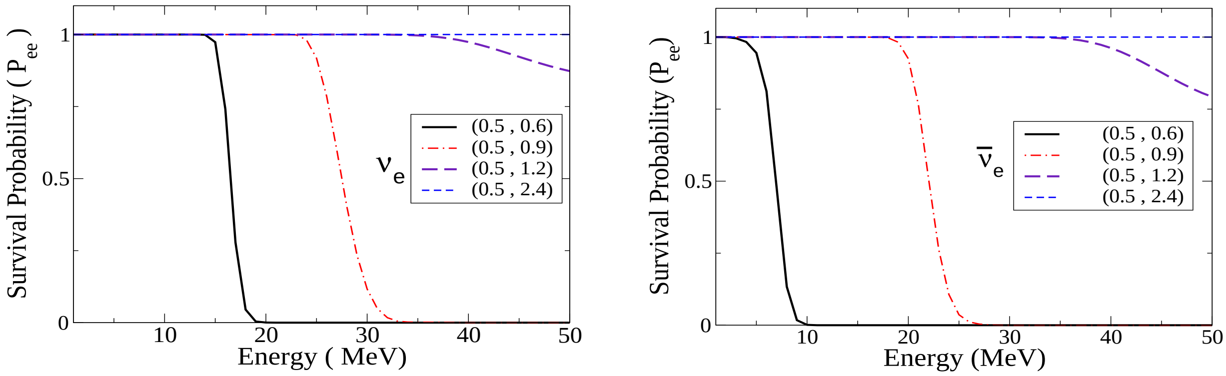

Figure 4.1: Survival probability for G3 spectrum in NH with different ($\phi^r_{\nu_e}$,$\phi^r_{\bar{\nu}_e}$).

Independent of the choice of spectrum models, these split features are seen for low values of ($\phi^r_{\nu_e}$,$\phi^r_{\bar{\nu}_e}$), which implies large flux of ν_x compared to other flavors [33]. As the values of ($\phi^r_{\nu_e}$,$\phi^r_{\bar{\nu}_e}$) increase, the split energy (E_c) also increases, and close to the equipartition point the split energy tends to infinity.

As an example see fig. 4.1 where survival probabilities are plotted for the spectrum G3. The left panel is for neutrino and right one for antineutrino. For a low value of $\phi^r_{\nu_e}$ (0.5), $\phi^r_{\bar{\nu}_e}$ is increased from 0.6 to 2.4 for both neutrino and antineutrino. From the figures it is evident that with this increment, split energies (E_c) also increase. For the same combination of $\phi^r_{\nu_e}$ and $\phi^r_{\bar{\nu}_e}$ the split energy is higher for neutrinos than for antineutrinos. We find these features are same for other spectrum models too.

In fig. 4.2 we have shown the above mentioned features for LL and G3. The left panels are for LL and the right ones are for G3. The red straight lines are for neutrino and the blue dashed lines are for antineutrino. In the top panels the initial relative spectrum ($\phi^r_{\nu_e}$,$\phi^r_{\bar{\nu}_e}$) are chosen to be close to the equipartition point for both the models and for these values there is no split whereas for the lower panels ($\phi^r_{\nu_e}$,$\phi^r_{\bar{\nu}_e}$) are smaller and these panels show split for both neutrino and antineutrino sectors.

The flux corresponding to G3 and (0.5,0.6) are plotted in fig. 4.3. Left and right panels in this figure are respectively for neutrinos and antineutrinos. The upper panels are without collective effects (initial flux) and the lower ones are with collective effect (flux beyond collective region). The black lines in the panels are for electron type whereas the

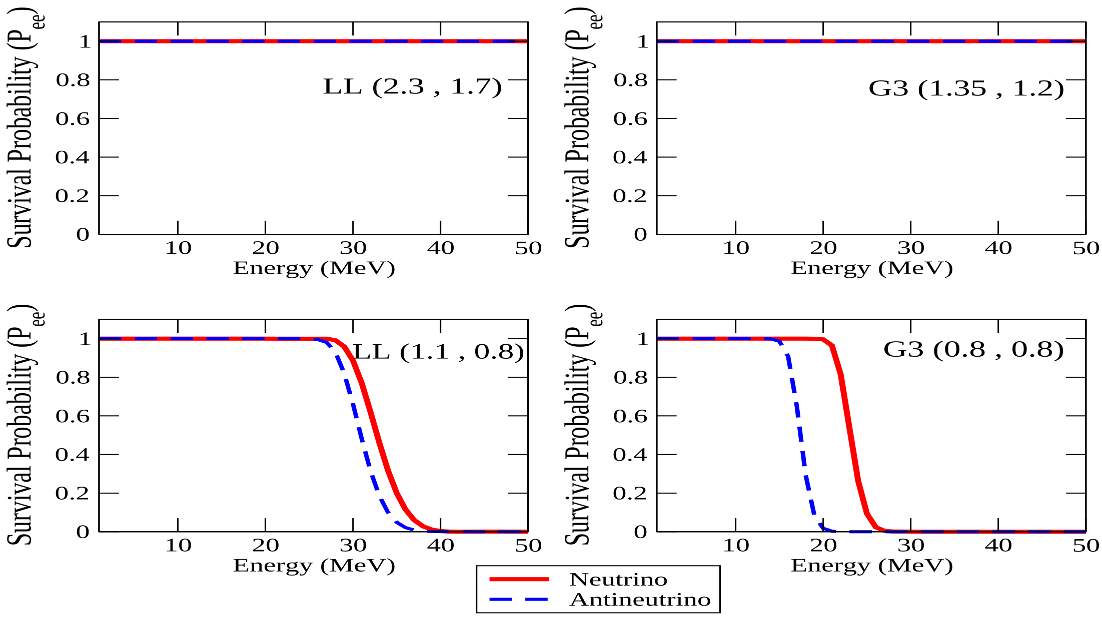

Figure 4.2: Survival probability for LL and G3 spectrum in NH with different ($\phi^r_{\nu_e}$,$\phi^r_{\bar{\nu}_e}$).

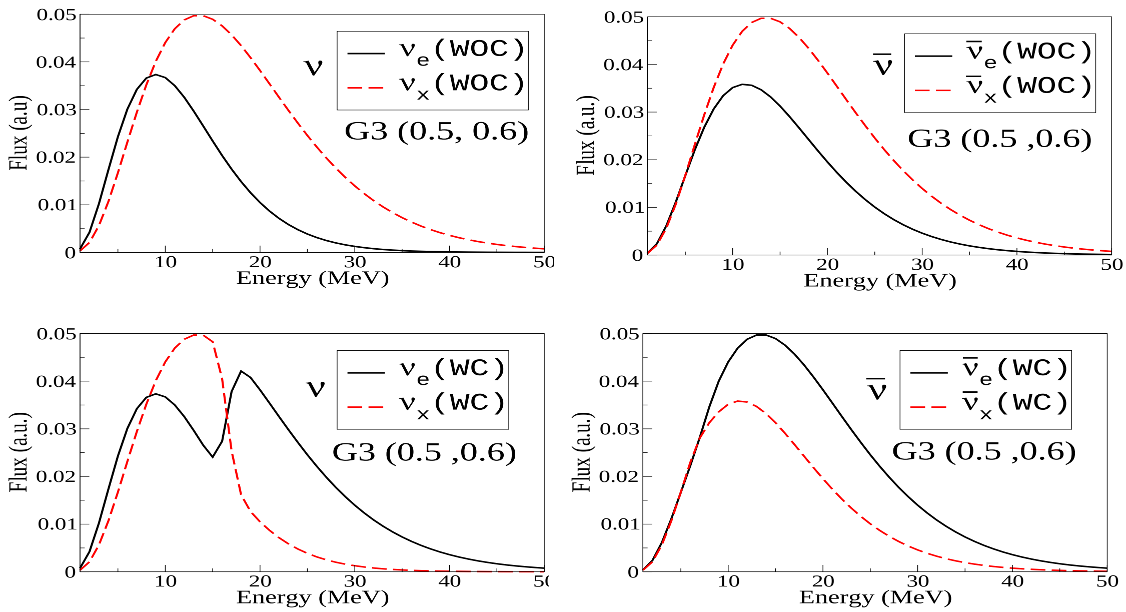

Figure 4.3: Flux for the different neutrino species for G3 with NH in arbitrary units (a.u.); WOC stands for "Without Collective" effects and WC for "With Collective" effects.

red dashed lines are for x-type. Clearly the lower panels show swap in both neutrino and antineutrino sector. The swap in both sectors are partial, that is, a part of the spectra below the "split energy" remains same. The antineutrino split feature is not clearly visible since E_c for them is low and the $\bar{\nu}_e$ and $\bar{\nu}_x$ fluxes are very close to each other at these energies. The probability plots for (0.5,0.6) in fig. 4.1 also show the low split energy for antineutrino. Note that the swap for neutrino spectra happens at a higher energy compared to the antineutrino spectra, this feature is also consistent with the probability plots in fig. 4.1.

Probability and Flux: IH

Probability and flux in the IH is much more complex and interesting than NH. Here also we vary the initial relative flux for different spectrum models and find wide variation of the final spectrum depending on the choice of ($\phi^r_{\nu_e}$,$\phi^r_{\bar{\nu}_e}$). These variations in spectrum with initial relative flux ($\phi^r_{\nu_e}$,$\phi^r_{\bar{\nu}_e}$) have been attributed to meeting the instability condition of the initial system and adiabaticity violation [32] as well as to change of global initial condition with luminosity variation and minimization of potential energy [33]. We find that these changes in final spectrum are similar for different choices of spectrum models.

As discussed in [33], the different spectral features arise from the initial conditions, which may or may not lead the system to swap to minimize "potential energy". We also find that in some cases the multiple swaps actually do take place but the swaps are so close that they can not be resolved numerically [32] and thus appear as if the swap or split features are absent. We find five spectral split patterns as mentioned in [33]. These five patterns are found for all three models of initial energy spectra LL, G1, G3. These are displayed (for LL and G3) in successive panels from top to bottom in fig. 4.4.

1. Dual split in both neutrino and antineutrino flux (II,II).

2. Dual split in neutrino but no split in antineutrino flux (II,0).

3. One split in both neutrino and antineutrino flux with the split energy of the neutrino higher (H) than that of antineutrino (L) split energy (I,I)(H,L).

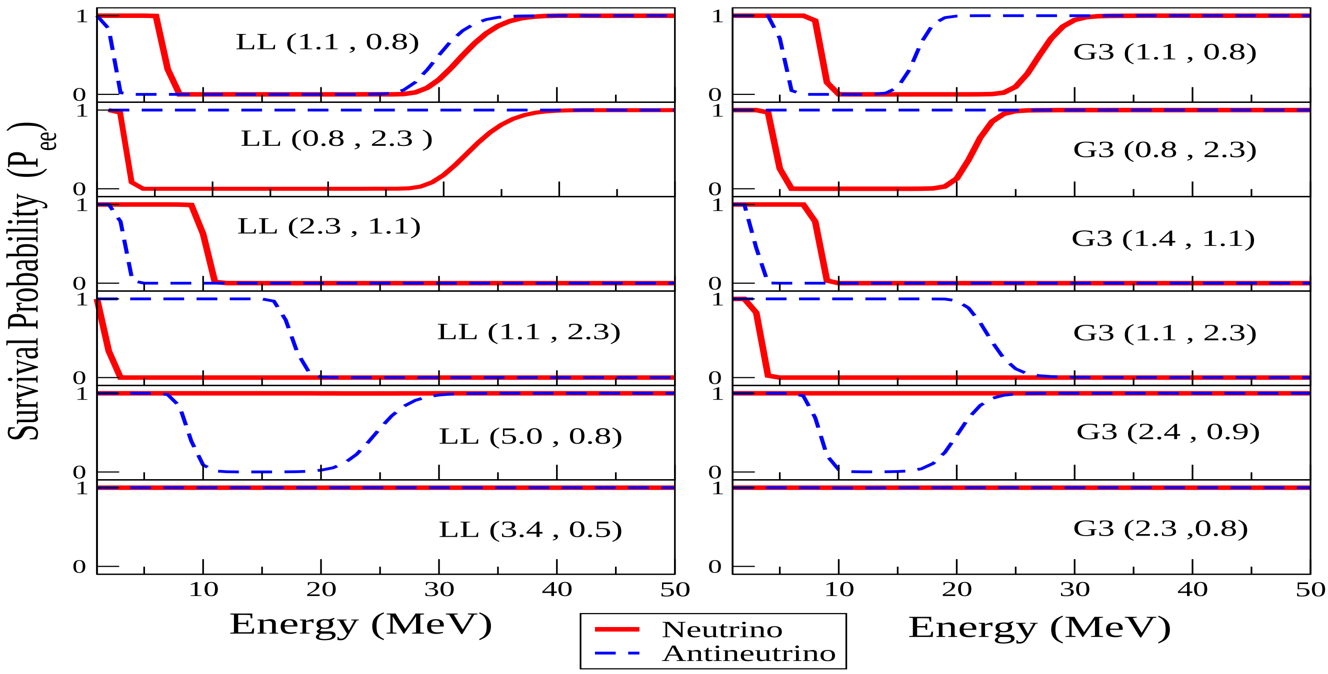

Figure 4.4: Survival Probability for LL and G3 spectrum in IH with different ($\phi^r_{\nu_e}$, $\phi^r_{\bar{\nu}_e}$).

4. One split in both neutrino and antineutrino flux with the split energy of the neutrino lower (L) than that of antineutrino (H) split energy (I,I)(L,H).

5. No split in neutrino but dual split in antineutrino flux (0,II).

Apart from these five patterns we find a sixth possible pattern in which neither neutrino nor antineutrino show any swap in the spectrum. We call this (0,0). For this pattern (0,0) the effect of neutrino-neutrino interaction on both neutrino and anti neutrino flux is undetectable.

The physical reasoning behind the patterns in the top five panels are well explained [33] from the idea of potential energy minimization. Our analysis shows that in some sense all the different spectrum models are in the same footing as all of them give rise to similar split patterns with the change of initial relative flux or relative luminosity. As explained in [32] the basic feature is that there are multiple swaps or splits in both the neutrino and antineutrino sector but the swaps may disappear depending on the adiabaticity violation

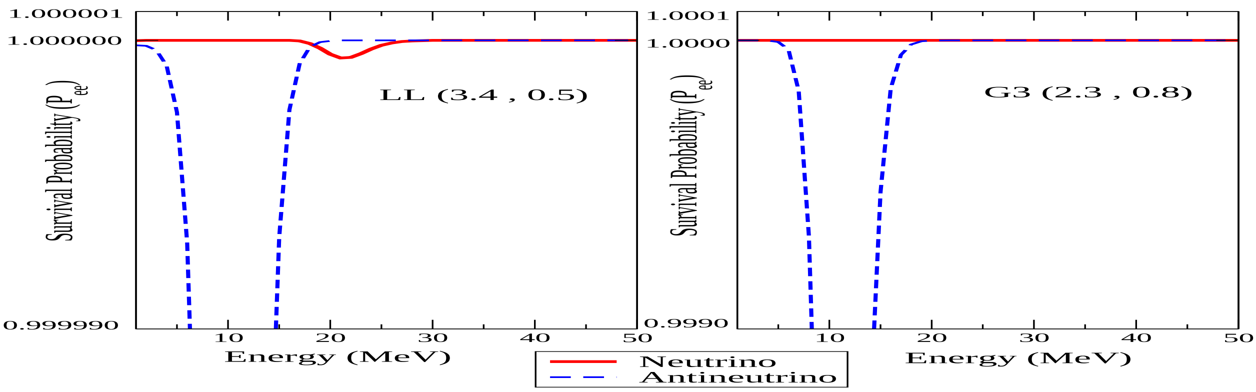

Figure 4.5: Survival Probability for LL (3.4, 0.5) and G3 (2.3, 0.8) spectrum in IH .

or it may be numerically unresolvable. Consider the new pattern, described in the lowest panel of fig. 4.4, where it seems that there is no swap in both neutrino and antineutrino sectors. When we study these cases carefully (fig. 4.5, left panel LL (3.4,0.5) and right panel G3 (2.3,0.8)) we find that they also show changes in survival probability similar to the other patterns. But the swaps here are incomplete and numerically undetectable. While in fig. 4.4 the change in probability for this case is visually unresolvable for all practical purposes, in fig. 4.5 it is visible, as we have increased the resolution.

For the fluxes we just give one example of the case (II,II) in fig. 4.6. Here we plotted the G3 neutrino spectrum in the left panel and the G3 antineutrino spectrum in right one. In both panels, the solid sky blue lines are for electron type without collective effect (WOC) and the solid red lines are for ν_x without collective effect (WOC). For the spectrum with collective effects (WC) dashed black lines are for electron type whereas dot-dashed blue lines are for ν_x. Here the spectrum model used is G3 and the initial relative fluxes are (1.1,0.8). We can see prominent dual split pattern in this flux figure as expected from the upper right panel of fig. 4.4.

Thus, depending upon the choice of initial relative fluxes $(\phi^r_{\nu_e},\phi^r_{\bar{\nu}_e})$ the spectra can have different patterns, especially for IH. The possible values of $(\phi^r_{\nu_e},\phi^r_{\bar{\nu}_e})$ can be in a wide

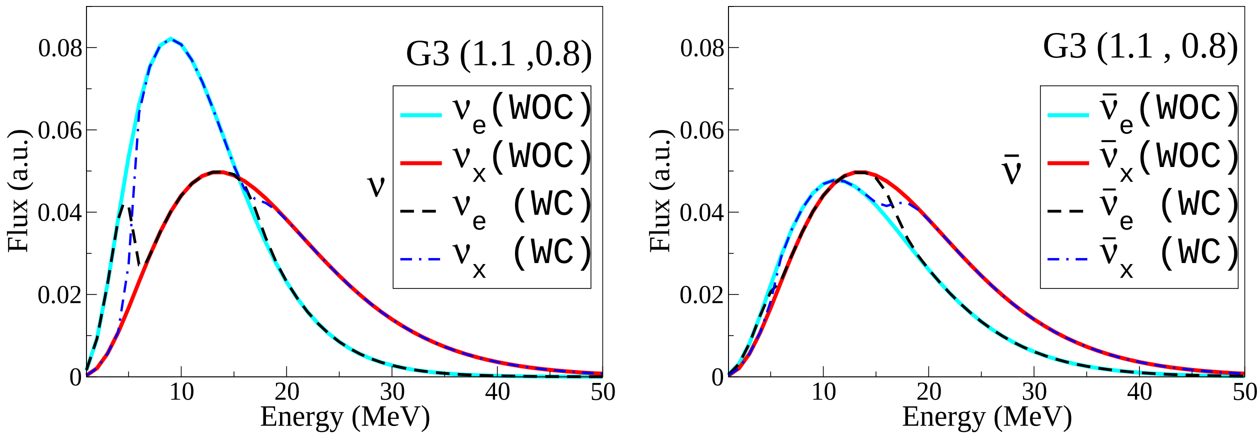

Figure 4.6: The neutrino and antineutrino fluxes in arbitrary units (a.u.) for the model G3 with the relative luminosities (1.1,0.8), with and without collective effect for IH.

range. Even if one assumes a factor-of-two-uncertainty in the relative luminosity [43], there can be considerable variations in the final flux characteristics.

We study the variation in spectral split features over the $\phi^r_{\nu_e}$-$\phi^r_{\bar{\nu}_e}$ plane for LL, G1, G3 and found a pattern showing different kind of spectral splits at different $\phi^r_{\nu_e}$-$\phi^r_{\bar{\nu}_e}$ region. In fig. 4.7 we show this in the $\phi^r_{\nu_e}$-$\phi^r_{\bar{\nu}_e}$ plane. The plane is divided into zones by the values of the global polarization vectors J_z, $\bar{J}_z$ and D_z. The black dashed line divides the plane into zones with $D_z > 0$ and $D_z < 0$. The purple long dashed corresponds to $\bar{J}_z = 0$ and demarcates the area which has $\bar{J}_z$ positive and negative. The blue thick dashed is for $J_z = 0$. These lines therefore divide the $\phi^r_{\nu_e}$-$\phi^r_{\bar{\nu}_e}$ plane into 6 zones. The split patterns observed in the different zones are shown on the plane. The global polarization vectors J_z, $\bar{J}_z$ and D_z, define the "phase transitions" across different split patterns. It should be noted that the global polarization vectors were initially in the z direction hence the sign changes of their z components mark the stability of the system and spectral splits [33]. fig. 4.7 shows that

1. (I,I)(H,L) patterns are for $J_z > 0, \bar{J}_z > 0$ and $D_z > 0$,

2. (I,I)(L,H) for $J_z > 0, \bar{J}_z > 0$ and $D_z < 0$,

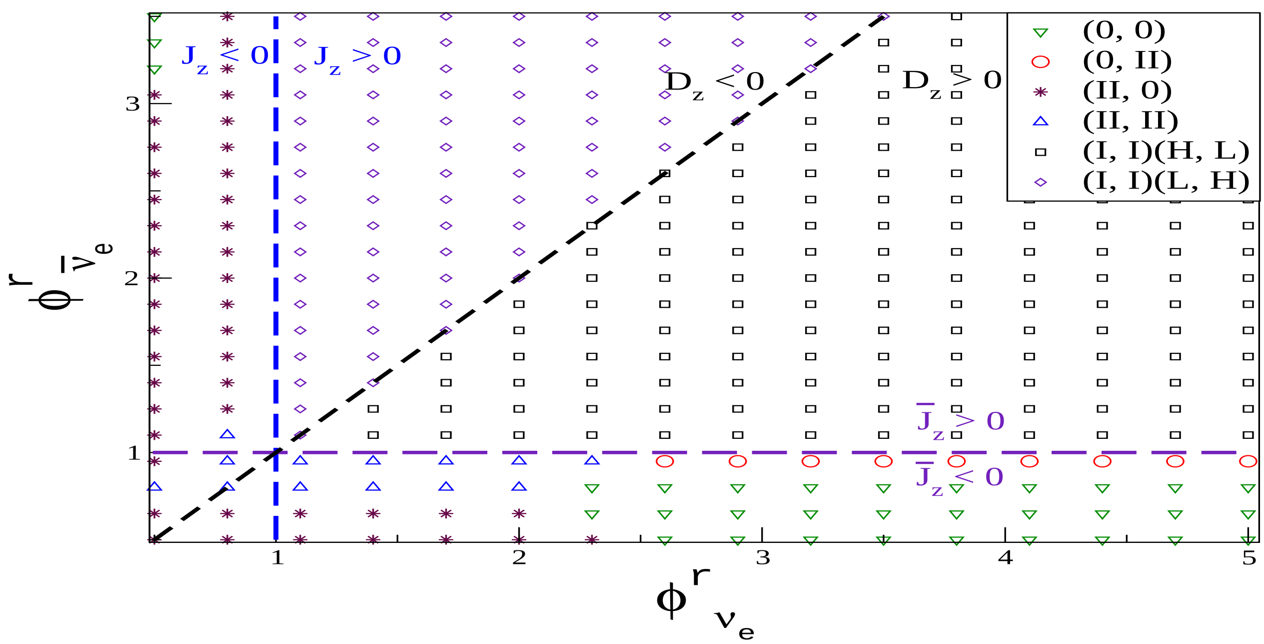

Figure 4.7: The different split pattern regions in the $\phi^r_{\nu_e}$-$\phi^r_{\bar{\nu}_e}$ plane for IH and G3. The black dashed, purple long dashed, blue thick dashed denotes $D_z = 0$, $\bar{J}_z = 0$ and $J_z = 0$ lines respectively. The six zones in $\phi^r_{\nu_e}$-$\phi^r_{\bar{\nu}_e}$ plane have different split patterns.

3. (a) (II,II) patterns are seen in the $J_z < 0, \bar{J}_z < 0$ region, and also in the $J_z > 0, \bar{J}_z < 0$ region,

   (b) (0,0) appear mostly in $\bar{J}_z < 0$ with a very few occurrence in $J_z < 0$,

   (c) (II,0) is the most dominant pattern in the $J_z < 0$ region, although it can appear in the $J_z > 0$, $\bar{J}_z < 0$ region,

   (d) (0,II) pattern occurs only in $\bar{J}_z < 0$.

Thus for the double split patterns described in point 3 above, the so called "phase transition" lines seem inconclusive. [33] established that the $J_z < 0$ or $\bar{J}_z < 0$ region (i.e, the rectangle covering the zone with $J_z < 0$ alongwith the rectangle covering the zone with $\bar{J}_z < 0$) lead to (II,II) pattern when the adiabaticity is increased artificially. Hence due to the incomplete adiabaticity in the actual case some of the (II,II) patterns appear as (II,0), (0,II), (0,0) pattern. So with complete adiabaticity one will not see any of the (II,0), (0,II), (0,0) patterns in fig. 4.7. For example see the discussion regarding the (0,0) pattern in context of fig. 4.4.

With so many possible patterns it will be really difficult to predict the initial relative neutrino fluxes, the energy distribution model and the extent of collective neutrino effect, even for a future galactic supernova event.

4.2 Discussion

Collective flavor oscillations driven by neutrino-neutrino interaction at the very high density region of core collapse supernovae control the emitted flux of neutrinos of different flavors. In the process one or more swaps of flavors for both neutrinos and antineutrinos take place depending on the initial neutrino flux and distributions. We study the phenomena of spectral splits and consequent flavor swaps for different models of neutrino spectrum, varying the relative luminosities of neutrinos and antineutrinos for both normal and inverted mass hierarchy. The effect of spectral splits is found to be more pronounced for inverted hierarchy and depending on the initial luminosities one can get single or dual splits in neutrinos and/or antineutrinos. For a specific choice of relative luminosity we also find a case for inverted hierarchy where the splits are not resolvable numerically and is akin to no spectral splits for all practical purposes. Single split patterns are also obtained for normal hierarchy for some choices of the luminosities.

To summarize this chapter showed how the variation of relative luminosity can give rise to different possible split pattern in both hierarchies. This different possibilities in a way increase the uncertainty in SN neutrino flux and decrease the predictivity. Hence we would need other information to have a hold on this flux uncertainty. For example in the next chapter we discuss to what extent one can constrain the luminosities by demanding a neutron rich condition at the end of the collective region, required for successful r-process.

Here we would like to mention the fact that recent studies [35, 38] show that the atmospheric mass squared driven effective two flavor collective evolution of the actual three flavor system may not be adequate. The total 3 flavor analysis together with solar mass squared difference may give rise to another swap in the inverted hierarchy

(IH). However for a little lower (reduced by a factor of 10) neutrino-neutrino interaction potential (μ) this three flavor effect disappear [38]. Also this swap starts a little late than the atmospheric mass squared difference driven one. Though not in the scope of this thesis, in future it would be interesting to see how the above analysis of different split patterns changes under this three flavor analysis.

BIBLIOGRAPHY

[1] G. Raffelt, *Stars as Laboratories for Fundamental Physics* (U. of Chicago Press, Chicago, 1996), 664 pp.

[2] A. Dighe, J. Phys. Conf. Ser. **136**, 022041 (2008).

[3] L. Wolfenstein,*Phys. Rev.* **D17**, 2369 (1978); S.P. Mikheyev and A.Yu. Smirnov, *Sov. J. Nucl. Phys.* **42(6)**, 913 (1985); *Nuovo Cimento* **9c**, 17 (1986).

[4] J. T. Pantaleone, Phys. Lett. B **287**, 128 (1992).

[5] G. Sigl and G. Raffelt, Nucl. Phys. B **406**, 423 (1993).

[6] V. A. Kostelecky and S. Samuel, Phys. Rev. D **52**, 621 (1995).

[7] S. Pastor, G. G. Raffelt and D. V. Semikoz, Phys. Rev. D **65**, 053011 (2002).

[8] S. Pastor and G. Raffelt, Phys. Rev. Lett. **89**, 191101 (2002).

[9] R. F. Sawyer, Phys. Rev. D **72**, 045003 (2005).

[10] H. Duan, G. M. Fuller and Y. Z. Qian, Phys. Rev. D **74**, 123004 (2006).

[11] H. Duan, G. M. Fuller, J. Carlson and Y. Z. Qian, Phys. Rev. D **74**, 105014 (2006).

[12] S. Hannestad, G. G. Raffelt, G. Sigl and Y. Y. Y. Wong, Phys. Rev. D **74**, 105010 (2006); Erratum ibid. **76**, 029901 (2007).

[13] G. G. Raffelt and G. Sigl, Phys. Rev. D **75**, 083002 (2007).

[14] A. Esteban-Pretel *et al.*, Phys. Rev. D **76**, 125018 (2007).

[15] H. Duan, G. M. Fuller, J. Carlson and Y. Z. Qian, Phys. Rev. D **75**, 125005 (2007).

[16] G. G. Raffelt and A. Yu. Smirnov, Phys. Rev. D **76**, 081301 (2007); Erratum ibid. **77**, 029903 (2008).

[17] G. G. Raffelt and A. Yu. Smirnov, Phys. Rev. D **76**, 125008 (2007).

[18] H. Duan, G. M. Fuller and Y. Z. Qian, Phys. Rev. D **76**, 085013 (2007).

[19] H. Duan, G. M. Fuller, J. Carlson and Y. Z. Qian, Phys. Rev. Lett. **99**, 241802 (2007).

[20] G. L. Fogli, E. Lisi, A. Marrone and A. Mirizzi, JCAP **0712**, 010 (2007).

[21] G. L. Fogli *et al.*, Phys. Rev. D **78**, 097301 (2008).

[22] H. Duan, G. M. Fuller, J. Carlson and Y. Z. Qian, Phys. Rev. Lett. **100**, 021101 (2008).

[23] B. Dasgupta, A. Dighe, A. Mirizzi and G. G. Raffelt, Phys. Rev. D **77**, 113007 (2008).

[24] B. Dasgupta and A. Dighe, Phys. Rev. D **77**, 113002 (2008).

[25] H. Duan, G. M. Fuller and Y. Z. Qian, Phys. Rev. D **77**, 085016 (2008).

[26] B. Dasgupta, A. Dighe and A. Mirizzi, Phys. Rev. Lett. **101**, 171801 (2008).

[27] A. Esteban-Pretel *et al.*, Phys. Rev. D **78**, 085012 (2008).

[28] B. Dasgupta, A. Dighe, A. Mirizzi and G. G. Raffelt, Phys. Rev. D **78**, 033014 (2008) [arXiv:0805.3300].

[29] J. Gava and C. Volpe, Phys. Rev. D **78**, 083007 (2008).

[30] G. G. Raffelt, Phys. Rev. D **78**, 125015 (2008).

[31] G. Fogli, E. Lisi, A. Marrone and I. Tamborra, JCAP **0904**, 030 (2009) [arXiv:0812.3031 [hep-ph]].

[32] B. Dasgupta, A. Dighe, G. G. Raffelt and A. Y. Smirnov, Phys. Rev. Lett. **103**, 051105 (2009) [arXiv:0904.3542 [hep-ph]].

[33] G. Fogli, E. Lisi, A. Marrone and I. Tamborra, arXiv:0907.5115 [hep-ph].

[34] S. Chakraborty, S. Choubey, S. Goswami and K. Kar, JCAP **1006**, 007 (2010) [arXiv:0911.1218 [hep-ph]].

[35] A. Friedland, Phys. Rev. Lett. **104**, 191102 (2010) [arXiv:1001.0996 [hep-ph]].

[36] H. Duan, G. M. Fuller and Y. Z. Qian, arXiv:1001.2799 [hep-ph].

[37] B. Dasgupta, G. G. Raffelt and I. Tamborra, Phys. Rev. D **81**, 073004 (2010) [arXiv:1001.5396 [hep-ph]].

[38] B. Dasgupta *et al.* [arXiv:1002.2943 [hep-ph]]

[39] G. G. Raffelt and I. Tamborra, arXiv:1006.0002 [hep-ph].

[40] T. Totani, K. Sato, H. E. Dalhed, J. R. Wilson, Astrophys. J. 496,216 (1998) [astro-ph/9710203],

[41] T. A. Thompson, A. Burrows, P. Pinto, Astrophys. J. 592,434 (2003). [astro-ph/0211194]

[42] M. T. Keil, G. G. Raffelt and H. T. Janka, Astrophys. J. **590**, 971 (2003) [arXiv:astro-ph/0208035].

[43] C. Lunardini and A. Yu. Smirnov, JCAP **0306**, 009 (2003) [hep-ph/0302033].

CHAPTER 5

Collective Conversion and r-Process Nucleosynthesis

In this chapter we discuss the effect of the flux of neutrinos radiated out in core collapse supernovae on the electron fraction and discuss the possibility of getting allowed regions for r-process nucleosynthesis and the resulting constraints on relative luminosities. As most simulations of core-collapse supernovae do not lead to explosions, there are uncertainties in the understanding of the late stage of the SN shock propagation. But the generally accepted scenario supported by simulations is that for core collapse supernovae starting with iron cores the shock wave gets initially stalled due to loss of energy through nuclear dissociation and then over timescale of a second, gets revived by the energy deposited by neutrinos radiating out, the so-called late-time neutrino heating mechanism leading to the delayed core collapse supernova. This results in the development of a low density "hot bubble" region just behind the SN shock. Normally the hot bubble regions are taken between the infalling neutron star radius and the forward shock, that is, up to 30-40 km initially. The huge flux of neutrinos emitted from the proto-neutron star leads to the "neutrino-driven wind" which remains active for about 10 seconds after the core bounce. This creates neutron-rich regions of high entropy which are conducive to the development of the r-process. Different delayed core-collapse SN calculations give rise to different values for the entropy per baryon leading to conflicting conclusions about the r-process. However the ν-driven wind is still considered to be one of the most probable sites for the r-process [1]. The ν-driven wind models consider the r-process site to be at a few hundred kilometers (within 1000 km) [1]. Since, as discussed before, this is also the region where collective oscillations are active, it is expected that r-process will get affected. In what follows, we study this effect in the ν-driven wind region and numerically check if criteria of successful r-process can be used to constrain initial neutrino flux parameters.

5.1 Minimal Condition for r-Process

The criteria for r-process on which we focus here is the the electron fraction Y_e, *i.e.*, the number of electrons (equal to the number of protons, due to charge neutrality) per baryon. The Y_e will depend on the relative strengths of the two reactions – neutrino capture on neutrons and antineutrino capture on protons. Therefore, Y_e can be expressed as [2]

$$Y_e = 1/(1 + \lambda_{\bar{\nu}_e p}/\lambda_{\nu_e n}) \ , \tag{5.1}$$

where $\lambda_{\nu_e n}$ and $\lambda_{\bar{\nu}_e p}$ are the reaction rates for $\nu_e + n \rightarrow e^- + p$ and $\bar{\nu}_e + p \rightarrow e^+ + n$ respectively. Note that these reactions can in principle occur on both free and bound nucleons. However for the purpose of this work, we will not consider the reactions on heavy nuclei[2]. Note also that in principle, the inverse reactions also happen inside the supernova and should be considered. However, we neglect the inverse reactions here since the matter temperature of the region is small compared to the neutrino temperature as one goes away from the neutrinosphere and has very small effect at radius of 30 km and beyond [2, 4]. The reaction rates $\lambda_{\nu N}$ (where $N = n$ or p) are given as

$$\lambda_{\nu N} \approx \frac{L_\nu}{4\pi r^2} \frac{\int_0^\infty \sigma_{\nu N}(E) f_\nu(E) dE}{\int_0^\infty E f_\nu(E) dE} \ , \tag{5.2}$$

where $L_\nu = \phi^0_\nu \langle E_\nu \rangle$, and f_ν denotes the neutrino flux. The cross section used are

$$\sigma_{\nu_e n}(E_{\nu_e}) \approx 9.6 \times 10^{-44} \left(\frac{E_{\nu_e} + \triangle_{np}}{MeV} \right)^2 \text{cm}^2 \ , \tag{5.3}$$

$$\sigma_{\bar{\nu}_e p}(E_{\bar{\nu}_e}) \approx 9.6 \times 10^{-44} \left(\frac{E_{\bar{\nu}_e} - \triangle_{np}}{MeV} \right)^2 \text{cm}^2 \ , \tag{5.4}$$

where $\triangle_{np} = 1.293$ MeV is the mass difference between neutron and proton.

Note that the neutrino flux denoted as f_ν in Eq. (5.2) is the flux including collective flavor oscillations. The swap between the active neutrinos due to collective effect can change f_ν and hence Y_e. To illustrate this better we show the ratio of the reaction rates

[2]For a detailed study of the effect of nuclear compositions on Y_e we refer to [3]. Our main conclusions come from impact of collective oscillations on r-process nucleosynthesis and are not expected to drastically change as a result of reactions on bound nucleons.

for $\bar{\nu}_e$ and ν_e explicitly in terms of the collective oscillation probabilities

$$\frac{\lambda_{\bar{\nu}_e p}}{\lambda_{\nu_e n}}(r) = \frac{\int_0^\infty \sigma_{\bar{\nu}_e p}(E) P^c_{\bar{\nu}_e}(r,E)\phi^r_{\bar{\nu}_e}\Psi_{\bar{\nu}_e}(E)dE + \int_0^\infty \sigma_{\bar{\nu}_e p}(E)(1-P^c_{\bar{\nu}_e}(r,E))\Psi_{\nu_x}(E)dE}{\int_0^\infty \sigma_{\nu_e n}(E) P^c_{\nu_e}(r,E)\phi^r_{\nu_e}\Psi_{\nu_e}(E)dE + \int_0^\infty \sigma_{\nu_e n}(E)(1-P^c_{\nu_e}(r,E))\Psi_{\nu_x}(E)dE} , \tag{5.5}$$

where $P^c_{\bar{\nu}_e}(r,E)$ and $P^c_{\nu_e}(r,E)$ are the anti-neutrino and neutrino survival probabilities with collective oscillations and are calculated numerically as functions of radius and energy. The minimal condition for the SN environment to become neutron reach is $Y_e < 0.5$ which translate as the condition $\lambda_{\bar{\nu}_e p}/\lambda_{\nu_e n} > 1$.

Let us begin by understanding the impact of collective flavor oscillations on r-process

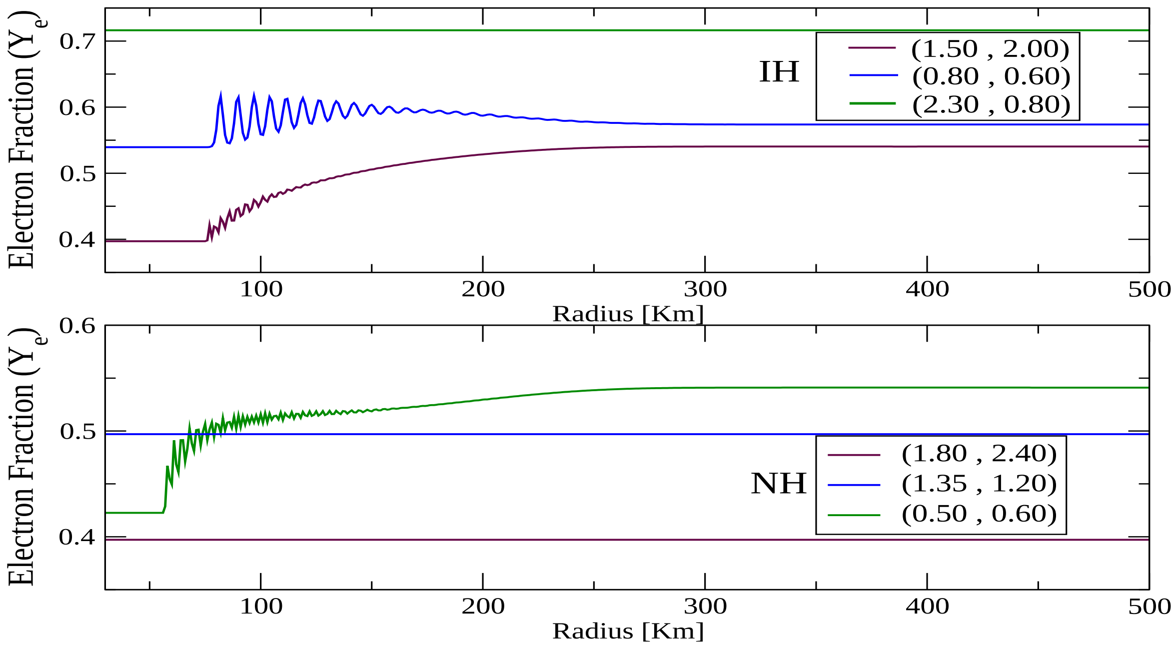

Figure 5.1: The electron fraction Y_e for both hierarchies as a function of ‘r’, the distance of the region from the center of the core.The spectrum model used is G3.

by discussing some limiting cases. In the no flavor oscillation limit, i.e. $P^c_{\bar{\nu}_e} = P^c_{\nu_e} = 1.0$

for all energies, Eq. (5.5) reduces to

$$\left(\frac{\lambda_{\bar{\nu}_e p}}{\lambda_{\nu_e n}}\right)_{\text{no osc}} \simeq \frac{\phi^r_{\bar{\nu}_e}}{\phi^r_{\nu_e}} \frac{\int_0^\infty (E-\Delta_{np})^2 \Psi_{\bar{\nu}_e}(E) dE}{\int_0^\infty (E+\Delta_{np})^2 \Psi_{\nu_e}(E) dE} \simeq \frac{\phi^r_{\bar{\nu}_e}}{\phi^r_{\nu_e}} \frac{\langle (E-\Delta_{np})^2 \rangle_{\bar{\nu}_e}}{\langle (E+\Delta_{np})^2 \rangle_{\nu_e}} \tag{5.6}$$

Since the average energy of $\bar{\nu}_e$ is greater than that of ν_e for all the three SN models that we have considered, it is expected that $\langle (E-\Delta_{np})^2\rangle_{\bar{\nu}_e} > \langle (E+\Delta_{np})^2\rangle_{\nu_e}$. Therefore under this approximation, for $\phi^r_{\bar{\nu}_e}/\phi^r_{\nu_e} \geq 1$, $Y_e < 0.5$ always and r-process can proceed. The condition $Y_e \leq 0.5$ in fact gives $\phi^r_{\bar{\nu}_e}/\phi^r_{\nu_e} \geq 0.62$ for LL and ≥ 0.88 for G1/G3 . For all values of $\phi^r_{\bar{\nu}_e}/\phi^r_{\nu_e}$ greater than this value, r-process can happen while for all values of $\phi^r_{\bar{\nu}_e}/\phi^r_{\nu_e}$ below this, r-process is forbidden.

Likewise one could consider the case where we have complete conversion of both neutrinos and antineutrinos where $P^c_{\bar{\nu}_e} = P^c_{\nu_e} = 0$ for all energies. One can easily show that for this case $\lambda_{\bar{\nu}_e p}/\lambda_{\nu_e n} = \langle (E - \triangle_{np})^2\rangle_{\nu_x}/\langle (E + \triangle_{np})^2\rangle_{\nu_x}$. As a result here one always gets $Y_e > 0.5$ as $\triangle_{np}$ is positive. Note however that this case never happens in collective oscillations and is therefore not realistic.

5.2 r-Process and Initial Relative Flux

We consider effect of collective effects on r-process for the realistic case, where the flavor conversions are calculated numerically, as outlined in the previous section. In fig. 5.1 we show the electron fraction Y_e as a function of the radius (r), for different combinations of $\phi^r_{\nu_e}$ and $\phi^r_{\bar{\nu}_e}$. We have taken the G3 model for the ν_e and $\bar{\nu}_e$ spectra. The upper panel is for IH while the lower one is for NH. In the upper panel, the green line is for ($\phi^r_{\nu_e}$, $\phi^r_{\bar{\nu}_e}$) of (1.5, 2.0), the blue line for (0.8, 0.6), while the maroon line is for (2.3, 0.8). We can note from the figure that for IH and (2.3, 0.8) case, there is no flavor conversion due to oscillations for the inverted hierarchy. The probability $P^c_{\bar{\nu}_e}$ and $P^c_{\nu_e}$ for this case was shown in the lowest right-hand panel of fig. 4.4, where we can see that $P^c_{\bar{\nu}_e} = P^c_{\nu_e} = 1$. Therefore as discussed above, the $\lambda_{\bar{\nu}_e p}/\lambda_{\nu_e n} = (0.8/2.3) * \langle (E-\triangle_{np})^2\rangle_{\bar{\nu}_e}/\langle (E+\triangle_{np})^2\rangle_{\nu_e} = 0.396$, giving $Y_e \sim 0.72$. For the two other cases considered with IH we have oscillations due to single and multiple splits. A scan of fig. 4.7 reveals that we have double splits in both neutrino and antineutrino channels for the blue line with (0.80, 0.60) whereas for the maroon lines of (1.50, 2.00) we have single splits in both neutrino and antineutrino channels with the split energy of neutrino lower than that of antineutrino. For both these cases we can see very fast oscillations in Y_e within the first 200 km, which can be attributed to the bipolar collective oscillations. Beyond 300 km the value of Y_e approaches a fixed value as the neutrino density decreases very fast and the collective effects end. The reason that one gets higher values of Y_e for both of them after the completion of collective effects compared to their values at 30 km can become clear from Eq. (5.5). For double splits for fixed value of $\phi^r_{\bar{\nu}_e}/\phi^r_{\nu_e}$ the contribution from the integrals in denominator in between the split energies is more than the corresponding contribution in the numerator making the ratio lower, resulting in higher Y_e. On the other hand for the single split case of (1.50, 2.00) the low split energies in the denominator for neutrinos make the ratio of Eq. (5.5) lower.

In the lower panels we assume NH and show Y_e for (0.5, 0.6) by the green line, for (1.35, 1.2) by the blue line, and (1.8, 2.4) by the maroon line. For the (1.35, 1.2) case, we had noted before in fig. 4.2, that $P^c_{\bar{\nu}_e} = P^c_{\nu_e} = 1$ over the entire energy range. For the case (1.8, 2.4) there is no conversion as well. Hence for these case there is no flavor conversion and Y_e stays constant for all r, given solely in terms of the $\phi^r_{\bar{\nu}_e}/\phi^r_{\nu_e}$ and $\langle(E - \triangle_{np})^2\rangle_{\bar{\nu}_e}/\langle(E + \triangle_{np})^2\rangle_{\nu_e}$ ratios. For the case (0.5, 0.6) (cf. fig. 4.1) we have single split in both the neutrino and antineutrino channels. For this case therefore we see a variation in Y_e as a function of the radius. Since we have noted that for cases of ($\phi^r_{\nu_e}$, $\phi^r_{\bar{\nu}_e}$) for which there is flavor conversion due to collective effects, Y_e fluctuates non-trivially with the radius for $r \lesssim 400$ km, therefore in what follows, we will show all results for $r \gtrsim 400$ km. That implies that we consider only the neutrino-driven wind region henceforth.

Figure. 5.1 also shows the most significant aspect of flavor conversion due to collective effects. At $r = 30$ km, one is in the synchronization phase and the collective bipolar oscillations are yet to set in. This is the limiting case of no conversion already discussed, while by $r = 400$ km, they are complete. The maroon line (1.5, 2.0) for IH and green line (0.5, 0.6) for NH show that collective effects can change the value of the electron fraction from $Y_e < 0.5$ (at $r = 30$ km) to $Y_e > 0.5$ (at $r = 400$ km). Hence, we can explicitly see that these combination of values of $\phi^r_{\nu_e}$ and $\phi^r_{\bar{\nu}_e}$ (for the respective hierarchies) will not allow r-process once collective effects are taken into account and hence will be ruled out

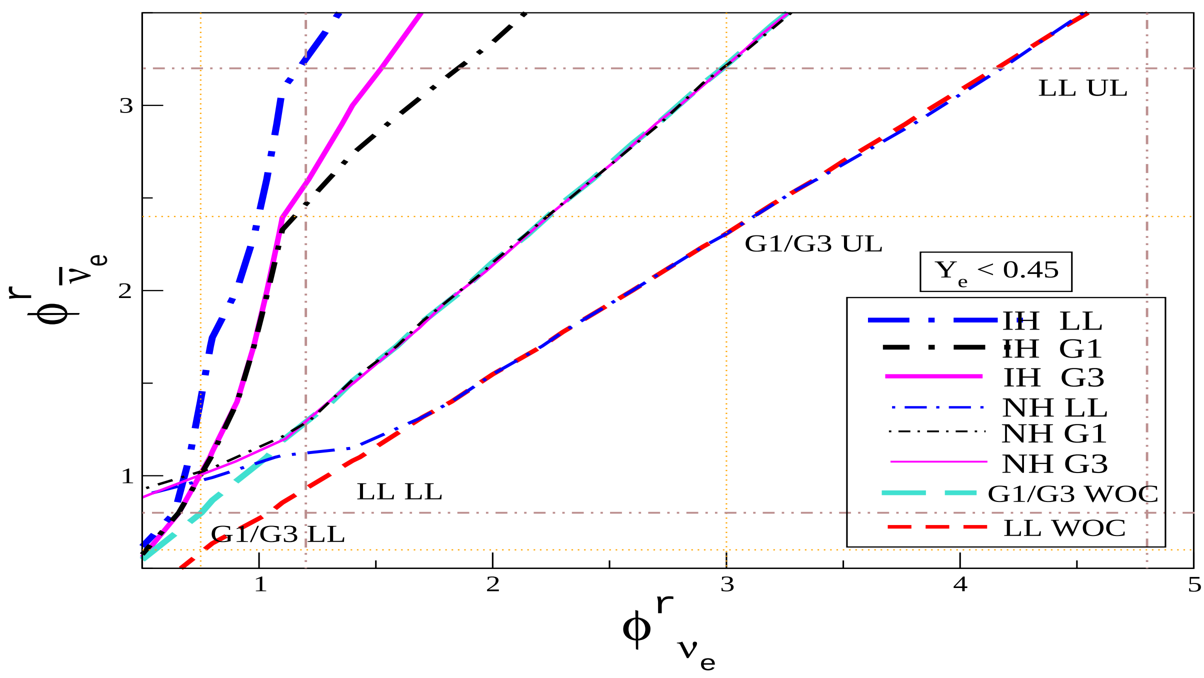

Figure 5.2: The exclusion plot consistent with $Y_e < 0.45$ for the spectrum G1, G3 and LL for both NH and IH. The allowed area is to the left of the curves. The dotted orange lines denote the Lower Limit (LL) and Upper Limit (UL) of $\phi^r_{\nu_e}$ and $\phi^r_{\bar{\nu}_e}$ for G1 and G3, arising from the two fold uncertainty defined in Eq. 4.32. Similarly double dotted dashed brown lines denote the Lower Limit (LL) and Upper Limit (UL) for the Lawrence Livermore spectrum model (LL).

if one imposes the criteria that Y_e must be less than 0.5. Therefore, it is expected that the exclusion plot for any specific limit on Y_e will change once collective effects are taken into account.

In fig. 5.2 we show the exclusion plot in the $\phi^r_{\nu_e}$-$\phi^r_{\bar{\nu}_e}$ plane for $Y_e < 0.45$. The lines themselves correspond to the case when $Y_e = 0.45$, while the allowed area (which gives $Y_e < 0.45$ or $\lambda_{\bar{\nu}_e p}/\lambda_{\nu_e n} > 1.22$) is to the left of the curves. We reiterate that the survival probabilities for these plots have been calculated at $r = 400$ km. We vary $\phi^r_{\nu_e}$ and $\phi^r_{\bar{\nu}_e}$ in the ranges (0.5,5.0) and (0.5,3.5) respectively. We plot exclusion curves for both IH and NH, and for all the three spectra models. We also plot the exclusion curves when collective oscillations are absent (WOC) for LL (thick red dashed) and G1/G3 (thick sky blue long dashed). These lines correspond to the no conversion case discussed earlier. We can see that they are almost straight lines in the $\phi^r_{\nu_e}$-$\phi^r_{\bar{\nu}_e}$, with $\phi^r_{\bar{\nu}_e}/\phi^r_{\nu_e} =$

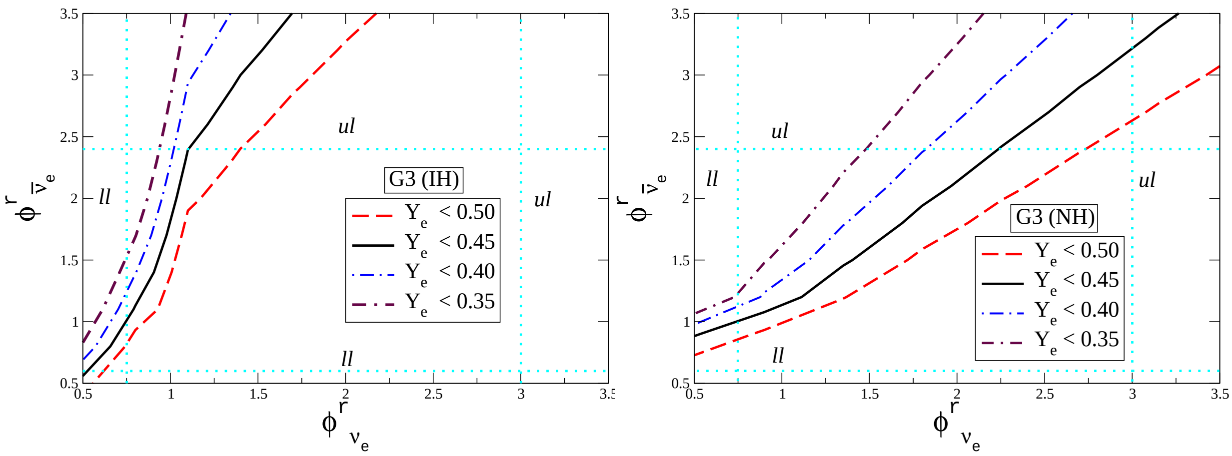

Figure 5.3: Exclusion plots for NH and IH for model G3. The exclusion condition is varied from $Y_e < 0.35$ to 0.5. The dotted sky blue lines denote the '*ll*' (Lower Limit) and '*ul*' (Upper Limit) from the assumed two fold uncertainty of $\phi^r_{\nu_e}$ and $\phi^r_{\bar{\nu}_e}$, for the spectrum model G3. The allowed region is on the left side of the exclusion curves.

$1.22 * \langle(E+\triangle_{np})^2\rangle_{\nu_e}/\langle(E-\triangle_{np})^2\rangle_{\bar{\nu}_e}$, for the respective spectral model. Since the average energy as well as the spectral shape (cf. Eq. (4.24)) for both G1 and G3 are the same, the exclusion lines for no oscillation case for them is identical. For LL, since the ratio of $\langle(E+\triangle_{np})^2\rangle_{\nu_e}/\langle(E-\triangle_{np})^2\rangle_{\bar{\nu}_e}$ is smaller (0.62) than for G1/G3 (0.88), the exclusion line for no oscillation case for LL corresponds to smaller $\phi^r_{\bar{\nu}_e}/\phi^r_{\nu_e}$. We see from the figure that for NH the effect of collective oscillations are mainly in the low $\phi^r_{\nu_e}$ and $\phi^r_{\bar{\nu}_e}$ region. This conforms to the observation of previous chapter, where we had shown that the split energy increased with increasing $\phi^r_{\nu_e}$ and/or $\phi^r_{\bar{\nu}_e}$. Since the flux begins to fall with increasing energy, the impact of collective oscillations fall for higher $\phi^r_{\nu_e}$ and $\phi^r_{\bar{\nu}_e}$. Hence for all the three models, the NH exclusion curves at higher relative luminosities agree with the WOC ones, as there is no observed collective effect there. Whereas at lower relative luminosities the curves deviate from the WOC ones due to the observed single splits, making the allowed region smaller. Again, as seen in fig. 5.1, the effect of collective oscillations is to increase Y_e for any given $\phi^r_{\bar{\nu}_e}/\phi^r_{\nu_e}$. Since Y_e decreases with $\phi^r_{\bar{\nu}_e}/\phi^r_{\nu_e}$, the exclusion plots shift to larger $\phi^r_{\bar{\nu}_e}/\phi^r_{\nu_e}$ values once collective oscillations are switched on. This results in the curves shifting to the left in the $\phi^r_{\bar{\nu}_e}$-$\phi^r_{\nu_e}$ plane.

Figure. 5.2 shows that for IH, the effect of collective oscillations can be very significant in constraining the relative luminosities. This can be understood from fig. 4.7 ,5.1 and Eq. 5.5. In fig. 5.1 we see that the effect of collective oscillation is to shift Y_e to a higher value. Eq. 5.5 shows that this can be balanced by increasing $\phi^r_{\bar{\nu}_e}$ compared to $\phi^r_{\nu_e}$. This results in shifting the contour plots to the left of the $\phi^r_{\bar{\nu}_e} - \phi^r_{\nu_e}$ plane in fig. 5.2. Since fig. 4.7 and 5.2 show the same $\phi^r_{\nu_e}$-$\phi^r_{\bar{\nu}_e}$ plane, we can see that for IH once collective oscillations are switched on, the only region in this plane which remains allowed is the one where we have double splits in the neutrino sector and no splits in the antineutrino sector. This is the (II, 0) zone where $J_z < 0$ and $D_z < 0$.

One understands that stronger constraint on Y_e reduces the allowed parameter space. Figure. 5.3 shows the exclusion plots for IH and NH for the model G3 for various constraints $Y_e < 0.35$, 0.40, 0.45, 0.50. The left panel is for IH and the right one for NH. Since higher values of $\phi^r_{\nu_e}$ gives higher Y_e, as one reduces the required value of Y_e, $\phi^r_{\bar{\nu}_e}$ gets more constrained. The constraint on $\phi^r_{\bar{\nu}_e}$ is relatively weak. But very low values of $\phi^r_{\bar{\nu}_e}$ are not allowed as we have seen that lower values of $\phi^r_{\bar{\nu}_e}$ increase the electron fraction.

Some final comments are in order. We would like to reiterate here that our analysis and the corresponding exclusion plots are meant as a proof of principle and merely indicate the ranges of the allowed fluxes for which one gets neutron-rich regions for r-process in the neutrino driven wind. They show that all r-process calculations should take collective effects into account and such detailed simulations can be used to extract more rigorous bounds on the initial fluxes.

Now we discuss the evolution as a function of time and its implication for our results. Early times have larger luminosities and may deviate more from energy equipartition. In realistic simulations in the cooling phase the luminosity for each species decreases with time as mentioned earlier but it may be reasonable to assume that the relative luminosities change very slowly with respect to time. With time the shock moves out, the neutrinospheres slowly fall in, the matter in the hot bubble and the wind driven region cools and the constituents change, first producing alpha-particles and then heavier nuclei. The alpha particles are strongly bound systems and their excitation by $\nu/\bar{\nu}$ can be neglected. The inclusion of α-particles in the matter was considered in [5] and the effect of the nuclear composition involving heavier nuclei on Y_e was looked at in [3]. A similar study including spectral splits in a self-consistent manner for the time-evolved system need to be undertaken separately in future.

One also realizes that there are many uncertainties that exist presently in the occurrence of the r-process in the supernovae. Firstly large entropy needed for the development of the r-process, as mentioned earlier, need to be observed consistently in all one dimensional simulations as well as in simulations going beyond one dimension. The hot bubble region does have the problem of having lower entropy [1]. This is compounded by the inability of simulations to give rise to outgoing shocks with the right explosion energy. Often the physics understanding comes from the use of 'semi-analytic models' [1] that critically depend on the three quantities Y_e, the entropy and the dynamic timescale.

5.3 Discussion

In this chapter we showed that the inclusion of collective effects can affect the value of Y_e for realistic values of mass and mixing parameters. The electron fraction (Y_e) as a function of the radius of the core is calculated and it shows an oscillatory behavior in the bipolar region due to collective effects, before saturating to a constant value which depends on the initial luminosities and the pattern of flavor swap. We analyze the dependence for different models of neutrino energy distributions. For each of the distributions initial fluxes of different flavors are varied and constraints on the initial neutrino fluxes consistent with successful r-process nucleosynthesis are shown in exclusion plots for these initial neutrino fluxes. While a detailed simulation of the r-process nucleosynthesis inside the supernova might bring some changes to the exclusion plots, this work illustrates the fact that such exclusion plots are possible to achieve.

The variation in the number of spectral splits with the variation in the luminosity gives rise to different possibilities of neutrino and antineutrino spectrum at the detector. The constraints on luminosities obtained by ensuring r-process nucleosynthesis can provide additional inputs in narrowing down the possible patterns.

BIBLIOGRAPHY

[1] M. Arnould, S. Goriely and K. Takahashi, Phys. Rep.**450** 97-213 (2007).

[2] Y. Z. Qian, G. M. Fuller, G. J. Mathews, R. Mayle, J. R. Wilson and S. E. Woosley, Phys. Rev. Lett. **71**, 1965 (1993).

[3] G. C. McLaughlin, G. M. Fuller and J. R. Wilson, Astrophys. J. **472**, 440 (1996) [arXiv:astro-ph/9701114].

[4] H.A.Bethe and J.R.Wilson, Astrophys. J. **295**, 14 (1985).

[5] A. B. Balantekin and H. Yuksel New J. Phys. **7**, 51 (2005). [astro-ph/0411159]

[6] James P. Kneller, Gail C. McLaughlin Phys. Rev. D **80**, 053002 (2009).

CHAPTER 6

Diffuse Supernova Neutrino Background (DSNB)

Future observation of neutrino signal from a core-collapse supernova (SN) is expected to contribute significantly towards determination of the neutrino mass hierarchy and the mixing angle θ_{13}. However, supernovae are relatively rare in our galaxy with an estimated rate of about $1-3$ per century [1], which prompts consideration of the alternative strategy to detect neutrinos from supernovae that are further away. Neutrinos accumulated in the universe from all the SN explosions in the past and present epoch form a cosmic background, known as the diffuse supernova neutrino background (DSNB) or supernova relic neutrinos [2, 3, 4].

6.1 Introduction

The expected flux of these DSNB neutrinos depends mainly on the SN rate and the flavor dependent flux of neutrinos from supernovae.

The SN rate can be either determined directly [5] or from the cosmic star formation rate, which is measured using a variety of ways like galaxy luminosity function of rest-frame ultraviolet radiation [6]–[14], far-infrared/sub-millimeter dust emission [15, 16] and near-infrared Hα fluorescent line emission [17]–[20] and radio emission [21]. Though these techniques suffer from various ambiguities and complications like dust extinction [22], careful studies have enabled a determination of the star formation rate [23].

The typical neutrino flux from a SN on the other hand is not experimentally available. The data from SN1987A do not allow a clean determination of the spectral parameters [24]. So one has to resort to using primary neutrino fluxes predicted using SN simulations. Fluxes predicted by different groups (and sometimes different simulations by the same group) are at considerable variance, because of their different physics input [25, 26].

Additionally, these primary fluxes are further mixed by flavor conversions as they stream through the SN, thus requiring knowledge of not only the typical primary spectra, but also the typical SN density profiles. The emitted neutrino fluxes are therefore ridden with uncertainties at present. However, they could be made precise with more sophisticated simulations or observation of a galactic SN.

Estimation of the DSNB flux has been performed earlier, with varying approaches and results [23], [27]–[40]. Most studies have focused on DSNB detection via $\bar{\nu}_e$ scattering off protons at water Čerenkov detectors [39] and large liquid scintillator detectors [33]. On the other hand, ν_e detection has been considered at a liquid argon detector [41] and at Sudbury Neutrino Observatory (SNO) [42, 43]. In [40], authors have performed a detailed comparative study of ν_e detection in different future large scale observatories – by interaction of ν_e on oxygen in water Čerenkov detectors, on carbon in liquid scintillator detectors and on argon in liquid argon detectors. Experimentally, the best upper limits at 90 % C.L. of 6.8×10^3 ν_e cm^{-2}s^{-1} (25 MeV< E_{ν_e} < 50 MeV) and 1.2 $\bar{\nu}_e$ cm^{-2}s^{-1} ($E_{\bar{\nu}_e} > 19.3$ MeV) come from the Liquid Scintillation Detector (LSD) [44] and the Super-Kamiokande (SK) detectors [45] respectively. However, stronger bounds can be placed on these fluxes, albeit using somewhat indirect arguments [43, 46]. Some of the theoretical estimates of the DSNB fluxes predict event-rates for $\bar{\nu}_e$ that are tantalizingly close to detection, *e.g.*, the observational upper limit set by the SK collaboration [45]. The prospects for discovery thus seem promising if a large water Čerenkov detector like SK is loaded with 0.02% $GdCl_3$ [47] or if one or more of the proposed next generation detectors become available.

The study presented in this chapter is very relevant as it focuses on the effect of neutrino oscillation on DSNB. While considering the oscillation we for the first time added effects of oscillations driven by neutrino-neutrino interaction in the DSNB fluxes. In this initial study we considered a simplistic view of collective oscillations. The split scenario assumed in this chapter is basically (I, I) (H,L) i.e, ν_e and ν_x spectra swap completely above a critical energy of 7 MeV, whereas the $\bar{\nu}_e$ and $\bar{\nu}_x$ spectra swap at a much lower critical energy around 1 MeV. As the fluxes below such low energies are negligible compare to the rest part of the spectrum it is equivalent to assume that the $\bar{\nu}_e$ and ν_x spectra are swapped completely. However for normal hierarchy (NH) we assume the fluxes are unaffected by the collective effect. Further out from the center of the star, the traditional picture of flavor evolution by Mikheyev-Smirnov-Wolfenstein (MSW) conversion is not changed, except that the primary fluxes emitted at the neutrinosphere undergo the above-mentioned "pre-processing" due to the collective effects. In this chapter, we take the SN rate deduced from the cosmic star formation rate calculated by Beacom *et al.* [23], and the standard Λ-CDM cosmological model [48] as inputs to calculate the DSNB flux. The expected DSNB flux in the case of IH turns out to be quite different from those contained in previous works that disregarded collective effects. Thus the prospects of DSNB detection at antineutrino and/or neutrino detectors are modified. We report the DSNB fluxes and their observability, with and without neutron tagging, at the present and proposed detectors.

6.2 DSNB in Terrestrial Detectors

SN explosions are fairly common events in the Universe. These explosions have injected a large number of neutrinos, with energies of tens of MeV, in the Universe. These neutrinos have created the diffuse SN neutrino background, as already mentioned. Evidently, the DSNB flux depends on the two ingredients:

- The rate of SN explosions $R_{SN}(z)$, as a function of cosmological redshift z.
- The differential flux of neutrinos $F_\nu(E_\nu)$, from a typical core-collapse event at redshift z.

The differential flux of neutrinos $F_\nu(E_\nu)$ depends on the primary neutrino fluxes $F^0_\nu(E_\nu)$, emitted from the neutrinosphere, which get modified due to

- Collective effects, i.e. neutrino-neutrino self interaction, close to the neutrinosphere.
- MSW effects, i.e matter driven neutrino oscillations in the SN mantle and envelope.

The total differential DSNB flux arriving at terrestrial detectors, expressed as the number of neutrinos of flavor ν (where $\nu = \nu_e, \nu_\mu, \nu_\tau$ and antineutrinos are denoted with a bar overhead) arriving per unit area per unit time per unit energy, due to all supernovae in the universe up to a maximum redshift z_{max}, is

$$F'_\nu(E_\nu) = \int_{z_{max}}^{0} (dz\,\frac{dt}{dz})\,(1+z)\,R_{SN}(z)\,F_\nu((1+z)E_\nu)\ . \tag{6.1}$$

Here E_ν is the neutrino energy at Earth and $R_{SN}(z)$ is the SN rate per comoving volume at redshift z. For our numerical calculations we have assumed $z_{max} = 7$. Note that the factor $(1+z)$ in the neutrino spectrum $F_\nu((1+z)E_\nu)$ incorporates the redshift of the energy spectrum.

From the Friedmann equation for a flat universe we have

$$\frac{dz}{dt} = -H_0(1+z)(\Omega_m(1+z)^3 + \Omega_\Lambda)^{1/2}\ . \tag{6.2}$$

Thus the differential number flux of DSNB is

$$F'_\nu(E_\nu) = \frac{c}{H_0}\int_0^{z_{max}} R_{SN}(z)\,F_\nu((1+z)E_\nu)\frac{dz}{\sqrt{(\Omega_m(1+z)^3 + \Omega_\Lambda)}}\ . \tag{6.3}$$

For the standard Λ-CDM cosmology, we have

$$\Omega_m = 0.3\ ;\ \Omega_\Lambda = 0.7 \text{ and } H_0 = 70\ h_{70}\ \text{km s}^{-1}\ \text{Mpc}^{-1}\ . \tag{6.4}$$

Therefore, we only need to know the SN rate $R_{SN}(z)$ and the differential flux of neutrinos $F_\nu(E_\nu)$, from a typical core-collapse event to calculate the DSNB flux at Earth.

6.2.1 The cosmic supernova rate

The SN rate $R_{SN}(z)$ is related to the cosmic star formation rate ($R_{SF}(z)$), through the initial mass function $\varphi(m)$, which describes the differential mass distribution of stars at formation [23, 34]. We assume that all stars that are more massive than $8M_\odot$ give rise to core-collapse events and die on a timescale much shorter than the Hubble time, and that the initial mass function $\varphi(m)$ is independent of redshift. This allows us to relate the star formation rate $R_{SF}(z)$ to the cosmic SN rate $R_{SN}(z)$ as

$$R_{SN}(z) = R_{SF}(z)\frac{\int_{8M_\odot}^{125M_\odot}\varphi(m)dm}{\int_{0.1M_\odot}^{125M_\odot}\varphi(m)mdm}\ . \tag{6.5}$$

For our estimates, we use the initial mass function from reference [49], i.e.

$$\varphi(m) \propto \begin{cases} m^{-1.50} & (0.1M_\odot < m < 0.5M_\odot) \\ m^{-2.15} & (m > 0.5M_\odot) \end{cases} . \tag{6.6}$$

Putting the above expression into Eq. (6.5) we find

$$R_{SN}(z) = 0.0132 \;\; R_{SF}(z) M_\odot^{-1} . \tag{6.7}$$

It should be noted that the factor connecting R_{SN} and R_{SF} is quite insensitive to the upper limit of the integrations in Eq. (6.5).

Recent careful studies on different indicators of the cosmic star formation rate have been used to calculate the R_{SF} and its normalization. We use the cosmic star formation rate per comoving volume, R_{SF}, from the concordance model advocated in [50, 51], which is given by

$$R_{SF}(z) \propto \begin{cases} (1+z)^{3.44} & z < 0.97 \\ (1+z)^{-0.26} & 0.97 < z < 4.48 \\ (1+z)^{-7.8} & 4.48 < z \end{cases} , \tag{6.8}$$

with the local star formation rate given by

$$R_{SF}(0) = 0.0197 \; M_\odot \mathrm{yr}^{-1} \mathrm{Mpc}^{-3} . \tag{6.9}$$

This model satisfies the experimental upper limit on DSNB set by SK [45], and hence is known as the concordance model [23, 52].

6.2.2 Neutrino fluxes from core-collapse supernovae

Primary Neutrino Fluxes

As already discussed in the previous chapter, after the neutronization burst, thermal neutrinos and antineutrinos of all three flavors are emitted with a pinched thermal spectrum, that is conveniently parameterized as [53]

$$F_\nu^0(E_\nu) = \frac{L_\nu^0}{\langle E_\nu \rangle^2} \frac{(1+\zeta_\nu)^{1+\zeta_\nu}}{\Gamma(1+\zeta_\nu)} \left(\frac{E_\nu}{\langle E_\nu \rangle} \right)^{\zeta_\nu} \exp\left(-(1+\zeta_\nu) \frac{E_\nu}{\langle E_\nu \rangle} \right) , \tag{6.10}$$

where L_ν^0 is the luminosity in the flavor ν, $\langle E_\nu \rangle$ is the average energy of ν, and ζ_ν is the pinching parameter at the neutrinosphere.

For our study, we take 3 sets of representative values of $\Phi_\nu^0 = L_\nu^0 / \langle E_\nu \rangle$, $\langle E_\nu \rangle$ and ζ_ν motivated by SN simulations. One simulation by the Lawrence Livermore group (LL),

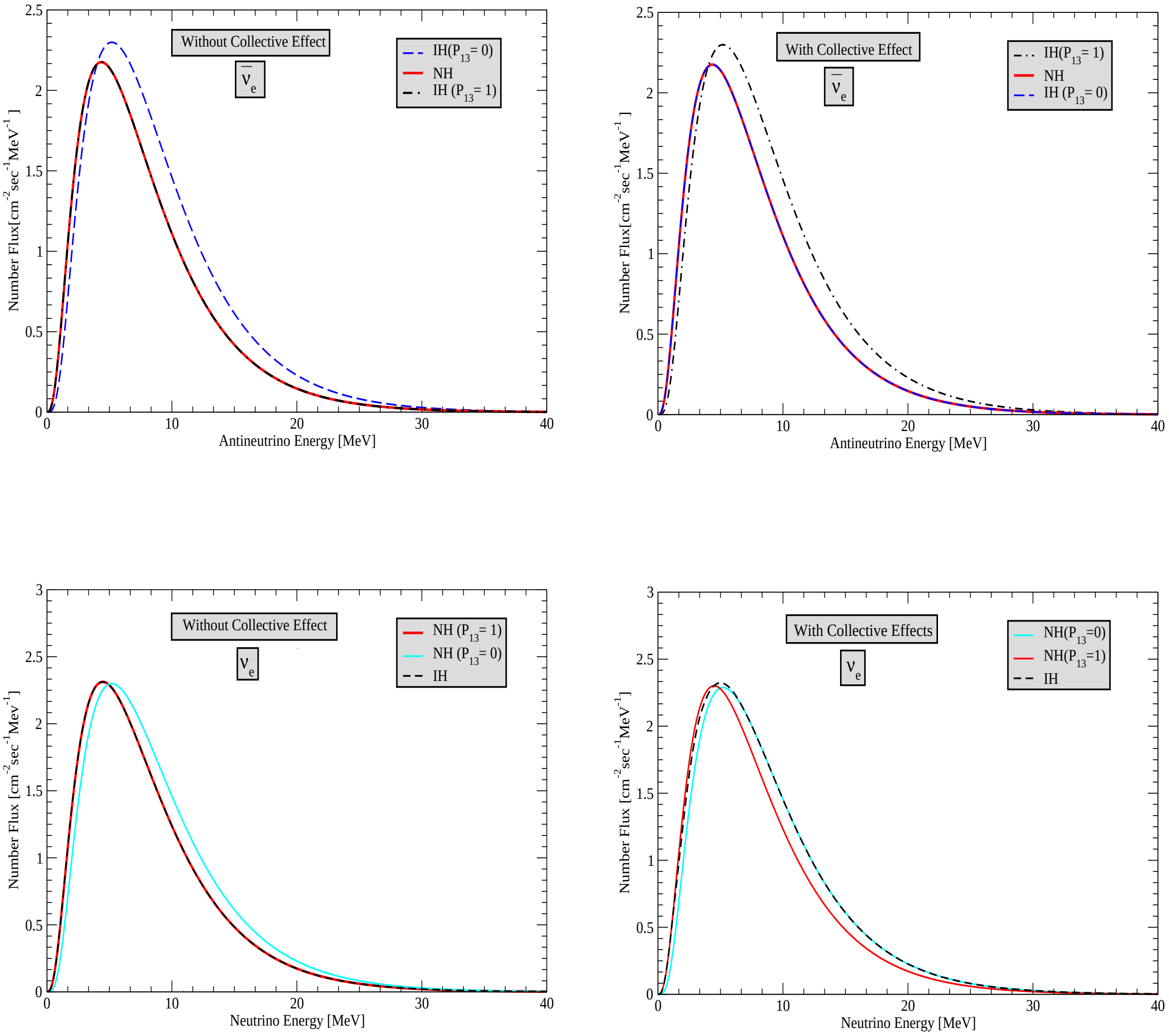

Figure 6.1: The DSNB flux spectrum arriving at Earth as a function of the (anti)neutrino energy at Earth. The upper panels show the $\bar{\nu}_e$ flux while the lower panels show the ν_e flux. The left panels correspond to the hypothetical case where we have only MSW matter effects in the SN while the right panels correspond to the case where we have both collective as well as MSW-driven flavor transitions. We have assumed that the initial neutrinos are given by the G1 model.

and two different simulations by the Garching group (G1, G2) have been chosen for our estimates, as shown in Table. 6.1.

Model	$\langle E_{\nu_e}\rangle$	$\langle E_{\bar{\nu}_e}\rangle$	$\langle E_{\nu_x,\bar{\nu}_x}\rangle$	$\Phi^r_{\nu_e} = \frac{\Phi^0_{\nu_e}}{\Phi^0_{\nu_x}}$	$\Phi^r_{\bar{\nu}_e} = \frac{\Phi^0_{\bar{\nu}_e}}{\Phi^0_{\bar{\nu}_x}}$
LL	12	15	24	2.0	1.6
G1	12	15	18	0.8	0.8
G2	12	15	15	0.5	0.5

Table 6.1: The parameters of the used primary neutrino spectra models motivated from SN simulations of the Garching (G1, G2) and the Lawrence Livermore (LL) group. We assume $\zeta_{\bar{\nu}_x} = 4$ and $\zeta_{\bar{\nu}_e} = 3$. The total luminosity is chosen to be 3×10^{53} erg.

Collective Effects and MSW Transitions

The primary fluxes (at the neutrinosphere) are further processed by collective effects and MSW conversions before they get emitted from the SN[3]. In the following paragraph the basic feature of collective conversion considered for this simplistic analysis is described.

Far from the neutrinosphere (at about a few hundred kilometers) as the neutrinos stream outward, the neutrino density becomes smaller, and bipolar oscillations begin to take place. In the case of IH, these oscillations have large amplitude even for a vanishingly small mixing angle. These oscillations thus can lead to a complete swapping of the $\bar{\nu}_e$ and $\bar{\nu}_x$ spectra. The ν_e and ν_x spectra cannot swap completely - the swap occurs only above a certain energy E_c, giving rise to a spectral split [54]. Eventually, beyond a few hundred kilometers, the neutrino-neutrino interaction becomes negligible, and collective effects cease to be important.

For normal hierarchy (NH), the collective effects do not affect the fluxes significantly and only MSW conversions are at work. In particular, the MSW resonances affect the ν_e flux, while the $\bar{\nu}_e$ flux remains almost unaffected. For IH, the collective effects swap the ν_e

[3]The detailed picture of collective effects presented herein is valid only for initial spectra that resemble the LL model. However we are interested in seeing the maximum effect that these new effects can cause, and for that purpose it suffices to ignore more complicated features in the spectrum [57, 58, 59] for G1 or G2 like models.

and ν_x above a certain energy E_c, determined by lepton number conservation [54, 55, 23]. On the other hand for antineutrinos, all $\bar{\nu}_e$ and $\bar{\nu}_x$ are swapped. This pre-processed flux now undergoes the traditional MSW conversions which now affect the $\bar{\nu}_e$ flux, and not the ν_e flux. The neutrinos then travel independently (while getting redshifted) as mass-eigenstates until they reach Earth, wherein they are detected as flavor eigenstates before or after having undergone regeneration inside the Earth. The fluxes of ν_e and $\bar{\nu}_e$ arriving at Earth are given in Table. 6.2. The quantities such as $F^0_{\nu_\alpha}$, are the initial SN neutrino fluxes while F_{ν_α} are the resultant fluxes emerging from the SN at redshift z. The quantities s^2_{12} and c^2_{12} stand for $\sin^2\theta_{12}$ (taken to be 0.3 for numerical studies) and

Normal hierarchy	Inverted hierarchy
$F_{\nu_e} = s^2_{12}\left(P_{13}F^0_{\nu_e} + (1-P_{13})F^0_{\nu_x}\right) + c^2_{12}F^0_{\nu_x}$	$F_{\nu_e} = \begin{cases} s^2_{12}F^0_{\nu_e} + c^2_{12}F^0_{\nu_x} & (E < E_c) \\ F^0_{\nu_x} & (E > E_c) \end{cases}$
$F_{\bar{\nu}_e} = c^2_{12}F^0_{\bar{\nu}_e} + s^2_{12}F^0_{\bar{\nu}_x}$	$F_{\bar{\nu}_e} = s^2_{12}F^0_{\bar{\nu}_x} + c^2_{12}\left((1-P_{13})F^0_{\bar{\nu}_e} + P_{13}F^0_{\bar{\nu}_x}\right)$

Table 6.2: Electron neutrino and antineutrino spectra emerging from a SN.

$\cos^2\theta_{12}$ respectively and P_{13} is the effective jump probability between the neutrino mass eigenstates due to the MSW resonance(s), and takes a value between 0 and 1. The value of P_{13} is approximately 0 if θ_{13} is large (i.e. $\theta_{13} \gtrsim 6$ degrees) and for smaller values of θ_{13} ($sin^2\theta_{13} \leq 10^{-6}$) P_{13} is one.

To calculate the DSNB flux at Earth $F'(E_\nu)$, we need to integrate the fluxes in Table. 6.2, correctly redshifted and weighted by the SN rate $R_{SN}(z)$, over redshift z. We show in fig. 6.1 the DSNB $\bar{\nu}_e$ (upper panels) and ν_e (lower panels) fluxes arriving on Earth as a function of their (anti)neutrino energy at Earth. We have assumed the G1 model for generating this figure. Note that the energy spectrum gets degraded to smaller energies due to redshift. The left panels show the predicted fluxes when one takes both collective as well as MSW transitions into account. To bring out the contrast with what the situation was earlier, we show in the right panels the predicted fluxes if one does not take collective effects. We can see that for NH the prediction have remained the same even after collective effects were taken, whereas for IH the fluxes are completely different.

6.2.3 Terrestrial detectors

An array of existing and planned detectors could catch the DSNB neutrinos. In what follows, we will consider in particular three types of detectors for observing DSNB $\bar{\nu}_e$:

- Water Čerenkov detectors
- Liquid scintillator detectors
- Gadolinium loaded water Čerenkov detectors

Detection of ν_e is more difficult. Both water and liquid scintillator detectors can in principle detect ν_e (as well muon and tau flavored neutrinos and antineutrinos). In water Čerenkov detectors this can be done through neutrino-electron scattering. On the other hand, in liquid scintillator in addition to the neutrino-electron scattering, one can detect ν_e through charged current interaction on ^{12}C, while the other species can be detected through the neutral current interaction on ^{12}C. However, the cross-section for these processes are rather low. Another detector technology that has been proposed for detecting ν_e is to use a high Z material, such as lead (and/or iron), interleaved with scintillators. Among such proposals are the OMNIS/ADONIS projects and the HALO experiment at SNOLAB [60]. Therefore the only chance for detecting the ν_e DSNB would be in a reasonably large

- Liquid argon detector

Water Čerenkov Detectors

An upper bound on the DSNB flux already exists from non-observation of these neutrinos at the SK experiment [45]. Using 1496 days of data with 22.5 kton of fiducial volume, the DSNB flux has been constrained to be less than 1.2 cm^{-2} s^{-1} for 19.3 MeV $< E_\nu <$ 30 MeV. SK is still running and could provide further constraint or evidence for DSNB fluxes in the future. Megaton water detectors with fiducial volume in the ballpark of 500 kton have been planned in Japan (Hyper-Kamiokande (HK)) [61], Europe (MEMPHYS) [62], and USA (UNO) [63]. These have been proposed to serve as the far detector for long baseline experiments with powerful accelerator beams. At the same time, they would be used to study neutrinos from natural sources, such as the Sun, atmosphere and nearby supernovae. In particular, they will be useful tools for the observation of DSNB fluxes. While in principle water detectors can detect neutrinos and antineutrinos of all flavors, the easiest to observe is $\bar{\nu}_e$, which is captured on protons via the inverse beta decay process

$$\bar{\nu}_e + p \rightarrow e^+ + n \ . \tag{6.11}$$

The emitted positron is observed through the Čerenkov cone produced by it. The "true" positron energy is approximately related to the neutrino energy by $E_\nu - 1.3$ MeV. The other types of neutrino species would scatter electrons and thereby could also be detected. However, the cross-section for neutrino-electron scattering is much lower compared to the reaction (6.11). Therefore, in this thesis we will consider the detection of only $\bar{\nu}_e$ in water Čerenkov detectors. The number of events per kton of detector mass is given as

$$N_e = n_T T \int_0^\infty dE_\nu \int_{E_e^{low}}^{E_e^{up}} dE_e \ F'_\nu(E_\nu)\sigma(E_\nu)R(E_\nu, E_e) \ , \tag{6.12}$$

where n_T is the number of protons in a kton of detector mass, T is the total exposure time, E_e the measured positron energy, E_e^{low} is the lower energy threshold, E_e^{up} is the upper energy threshold, $F'_\nu(E_\nu)$ is the DSNB flux at Earth, $\sigma(E_\nu)$ is the cross-section and $R(E_\nu - 1.3, E_e)$ is the energy resolution of the detector. For the energy resolution we assume a Gaussian form

$$R(E_\nu, E_e) = \frac{1}{\sqrt{2\pi}\sigma_E} \exp\left(\frac{-(E_\nu - 1.3 - E_e)^2}{2\sigma_E^2}\right) , \tag{6.13}$$

where all quantities are given in units of MeV and σ_E is the half width at half maximum (HWHM). For the water Čerenkov detector we use

$$\sigma_E = 0.47\sqrt{(E_\nu(\mathrm{MeV}) - 1.3)} \ . \tag{6.14}$$

From fig. 6.1 we can see that the DSNB fluxes being redshifted, arrive on Earth predominantly within the energy window $E_\nu = (0 - 35)$ MeV, above which the fluxes are negligible. In this energy range water Čerenkov detectors also register events coming from a myriad of other sources. The main sources of particles which would imitate the DSNB signal include reactor $\bar{\nu}_e$, atmospheric ν_e and $\bar{\nu}_e$, solar ν_e, spallation products induced by cosmic ray muons, and neutrinos from "invisible muons" produced by atmospheric ν_μ and $\bar{\nu}_\mu$. These form a background for the DSNB signal. Events due to reactor $\bar{\nu}_e$ appear roughly in the energy range $(1.8 - 8)$ MeV and these events can be estimated using the information from reactor power and their distances from the detector. In the case of SK for instance, it will be even easier to estimate them since KamLAND [64] directly observes these events. The events due to atmospheric ν_e and $\bar{\nu}_e$ are expected to be lower compared to those due to DSNB below $E \simeq 30$ MeV. Number of events expected from atmospheric ν_e and $\bar{\nu}_e$ can be anyway estimated using the predicted fluxes at these energies and can be included in the analysis of DSNB events. Therefore, these events do not pose a very serious threat to the DSNB analysis. Events due to neutrinos coming from the Sun fall in the energy range $E_\nu \lesssim 20$ MeV and can also be estimated fairly well using the fluxes from the standard solar model as well as from the direct observation of the ^{8}B fluxes at SNO [65]. These neutrinos can also be identified in the detector from their directionality. Indeed these are the solar neutrino events that SK observes. Therefore, these events do not pose a serious threat to DSNB observation either. The type of events which cause a serious concern are the ones produced from spallation. These events are typically important in the energy window relevant for solar neutrinos, *viz.* for $E \lesssim 20$ MeV. The SK collaboration in their paper [45] show that after suitable cuts there are almost no spallation events above $E_e > 18$ MeV. The lower threshold for the neutrino energy is hence restricted to $E_\nu \geq 19.3$ MeV. The upper limit is taken as 30 MeV.

Despite the different cuts and selection criteria there are two sources of neutrinos which still appear as backgrounds for the DSNB detection. The first has already been discussed above – the ν_e and $\bar{\nu}_e$ events from atmospheric neutrinos. These background events have to be estimated using the detector Monte Carlo. The second type of background comes from "invisible muons" produced by atmospheric ν_μ and $\bar{\nu}_\mu$. These are events where atmospheric ν_μ and/or $\bar{\nu}_\mu$ produce muons with kinetic energy less than 53 MeV, which is the threshold for emitting Čerenkov photons. These muons/antimuons therefore pass undetected and eventually decay into electrons/positrons which are observed by the detector. Estimates for the background due to both these sources have been made by the SK collaboration and can be found in [45].

Liquid Scintillator Detectors

Number of events expected in liquid scintillator are also given by Eq. (6.12). The predominant reaction is $\bar{\nu}_e$ capture of protons (cf. reaction (6.11)). The other detection reactions in liquid scintillators are charged and neutral current scattering off electrons, charged current capture of ν_e and $\bar{\nu}_e$ on ^{12}C, neutral current break-up of ^{12}C (see [66] for reactions of ^{12}C)[4] and neutral current scattering off protons [67]. However, the cross-section for these processes is small, especially at low energies [40, 68, 69], and we reiterate that due to redshift the DSNB fluxes are peaked at lower energies. Therefore, even for liquid scintillators the main detection weapon is the reaction (6.11). However, compared to the water detectors, liquid scintillators can use the reaction (6.11) more efficiently, whereby they tag the released neutron. While the positron is detected promptly, the neutron is captured by a proton in the detector, releasing a 2.2 MeV photon which is detected in delayed coincidence after 180 μs. This results in lesser problems with backgrounds, and liquid scintillator detectors can be used to observe the DSNB neutrino in the broader energy window of $E_\nu = (10 - 25)$ MeV [33].

The other major difference between the liquid scintillator detector and water Čerenkov detector is in the energy resolution, which is much better for the former. The HWHM for liquid scintillator detectors is expected to be better than

$$\sigma_E = 0.1\sqrt{E_\nu(\mathrm{MeV}) - 0.8}\ . \tag{6.15}$$

The KamLAND detector in Japan [64] and Borexino in Italy [70] are the currently running liquid scintillator detectors. While KamLAND has a total mass of 1 kton, Borexino is much smaller and comprises of about 300 ton of liquid scintillator. The detectors for the upcoming second generation reactor experiments designed to probe θ_{13} would be far too small to contribute to the study of DSNB neutrinos. However, one could look

[4] Liquid scintillator detectors can also detect the DSNB ν_e flux by their charged current interactions on ^{12}C [40].

forward to proposals such as LENA [33] which would be situated in the Pyhasalmi mine in Finland and is expected to have 50 kton of liquid scintillator. Such a big liquid scintillator detector could collect sizable number of DSNB events and prove to be a pivotal player in this game. Another large liquid scintillator detector proposal is the Hanohano project in Hawaii [71].

Gadolinium Loaded Water Čerenkov Detectors

The neutron released in the reaction (6.11) when captured on protons emits only a 2.2 MeV photon. This is below the detection threshold of water detectors and hence they cannot normally tag the released neutron by delayed coincidence, as liquid scintillators can. However, things could change dramatically if $GdCl_3$ is dissolved into the water. Gadolinium has a large cross-section for neutron capture and the capture of neutron on Gadolinium releases a 8 MeV gamma cascade. This being above the energy threshold, could be easy to observe in water detectors [47], transforming them into giant $\bar{\nu}_e$ detectors with statistics many times the statistics expected in scintillator detectors. This could give exceptional sensitivity to neutrino oscillation parameters using reactor antineutrinos [72]. This will help also in DSNB detection by lowering the lower energy threshold, and we should be able to use the same energy window as in liquid scintillators. Following [33], we present our results for the energy range $(10 - 30)$ MeV. The energy resolution of course continues to be given by Eq. (6.14).

Liquid Argon Detectors

Liquid argon TPCs are unique as they allow the detection of ν_e. The only other ν_e sensitive detector technology that we have so far seen built on a large scale was the heavy water detector at SNO. However, SNO is now dismantled. Significant amount of R&D on the other hand has gone into the liquid argon option. The ICARUS detector [73] in Italy already consists of a 600 ton module and has shown the feasibility of this detector technology. Since it is one of the few detector types which can be built on a large scale and allows for very fine granularity, good electron detection efficiency as well as detection of τ events, this is often considered as a far detector option for the Neutrino

Factory. Feasibility of probing galactic SN neutrinos was studied in [74, 75] and DSNB in [41, 40]. A future large liquid argon detector could have a mass of about 100 kton. Some of the currently pursued proposals include GLACIER [76], MODULAr [77] and FLARE [78]. Energy resolution in this detector is expected to be extremely good and at energies relevant for the neutrino factory it is believed to be in the ballpark of $\sigma_E \sim 0.03\sqrt{E\ (\text{GeV})}$ Therefore, at energies relevant for DSNB, one can assume that the energy reconstruction could be almost perfect. In what follows, we work under this assumption and give our results in terms of the neutrino energy. Since further R&D would be needed to determine the backgrounds in this detector, we will show results for an energy window of $(20 - 40)$ MeV.

6.3 Expected Events from DSNB

6.3.1 DSNB antineutrino events in water and scintillator detectors

We give in this subsection the number of DSNB $\bar{\nu}_e$ events expected in water and scintillator detectors. The total expected number of events are presented in Table. 6.3. The energy windows in which we have calculated the total number of events were discussed in the previous section and are shown in the parentheses in the first row of the table. The number of events per year have been calculated assuming a fiducial mass of 22.5 kton for SK and Gadolinium loaded SK (GDSK), 1 Mton for a future megaton detector (marked in the table symbolically as HK) and Gadolnium loaded megaton water detector (GDHK) and 50 kton for the scintillator detector (LENA). The results for NH remain the same for any value of θ_{13}. For IH the neutrino oscillation probability and hence the number of events depend on θ_{13}. We explicitly show results for two extreme values of θ_{13} – for small θ_{13} such that the jump probability $P_{13} = 1$ and for large θ_{13} such that the jump probability $P_{13} = 0$. For showcasing the impact of collective effects on the predictions for DSNB (anti)neutrino events, we also present in the Table. 6.3 expected number of events if collective effects were not taken into account. These are shown in parenthesis. When there are no collective effects, one has only standard MSW transitions in the SN and it is well known that in this case antineutrinos undergo maximal flavor transitions for IH when θ_{13} is large ($P_{13} = 0$), while for small values of θ_{13} or with NH (for any θ_{13})

Model	Hierarchy	SK (19.3 - 30.0) (MeV)	GDSK (10.0 - 30.0) (MeV)	HK (19.3 - 30.0) (MeV)	GDHK (10.0 - 30.0) (MeV)	LENA (10.0 - 25.0) (MeV)
G1	NH	1.7 (1.7)	4.9 (4.9)	67.8 (67.8)	196.0 (196.0)	6.4 (6.4)
	IH ($P_{13} = 0$)	1.7 (2.7)	4.9 (7.4)	67.8 (109.6)	196.0 (296.0)	6.4 (9.5)
	IH ($P_{13} = 1$)	2.7 (1.7)	7.4 (4.9)	109.6 (67.8)	296.0 (196.0)	9.5 (6.4)
G2	NH	1.1 (1.1)	3.5 (3.5)	42.6 (42.6)	139.5 (139.5)	4.6 (4.6)
	IH ($P_{13} = 0$)	1.1 (1.5)	3.5 (5.1)	42.6 (58.5)	139.5 (205.7)	4.6 (6.9)
	IH ($P_{13} = 1$)	1.5 (1.1)	5.1 (3.5)	58.5 (42.6)	205.7 (139.5)	6.9 (4.6)
LL	NH	2.5 (2.5)	6.2 (6.2)	98.2 (98.2)	246.0 (246.0)	7.7 (7.7)
	IH ($P_{13} = 0$)	2.5 (4.4)	6.2 (8.9)	98.2 (175.7)	246.0 (356.0)	7.7 (10.6)
	IH ($P_{13} = 1$)	4.4 (2.5)	8.9 (6.2)	175.7 (98.2)	356.0 (246.0)	10.6 (7.7)

Table 6.3: Number of expected events per year per 22.5 kton of SK and GDSK, 1000 kton of HK and GDHK, and 50 kton of LENA. The events without collective effects are shown in parenthesis for comparison.

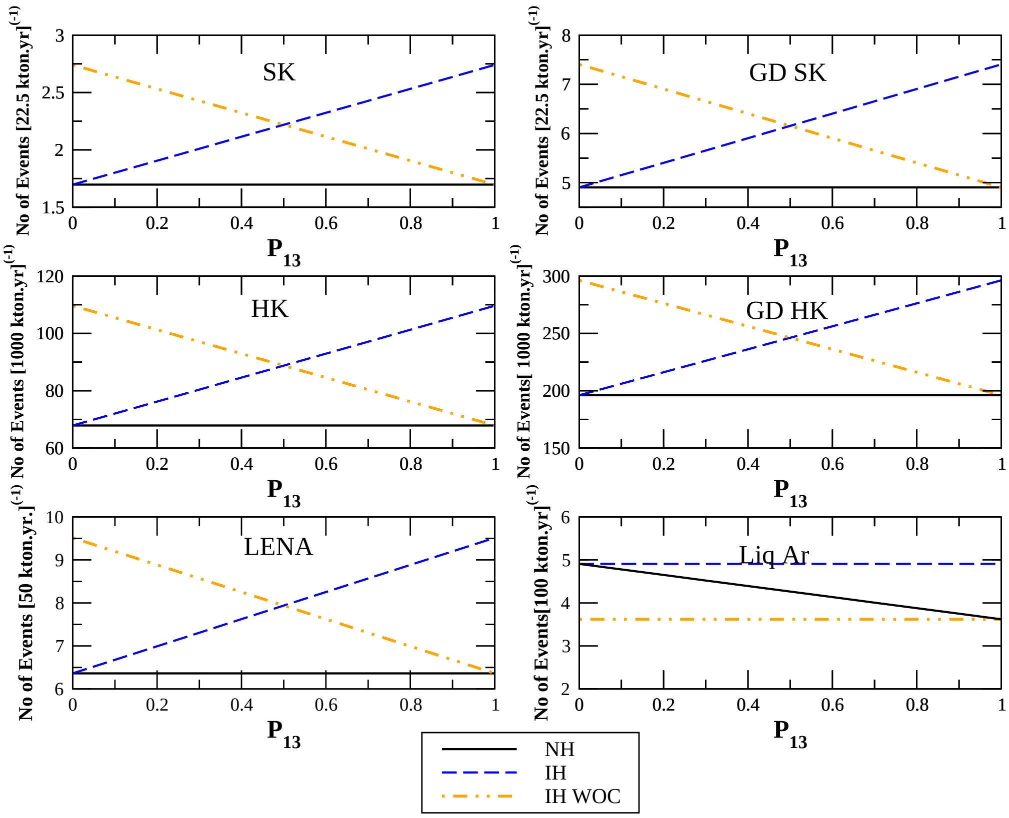

Figure 6.2: Number of expected events as a function of the jump probability P_{13} for the G1 model. Black lines are for NH and blue dashed lines for IH. The yellow dashed dotted lines show the case for IH without collective effects (WOC).

there is no matter enhanced resonant oscillations and these two scenarios give identical results. We therefore get larger number of events for IH and large θ_{13}. However, once the collective effects are switched on, the small and large θ_{13} cases of IH switch roles. Since there are now two stages of flavor conversions, first due to collective effects deep inside the SN and then due to MSW transitions, the final $\bar{\nu}_e$ fluxes are such that IH with large θ_{13} and NH give identical predictions, while IH with small θ_{13} predicts larger number of events (cf. upper right panel of fig. 6.1).

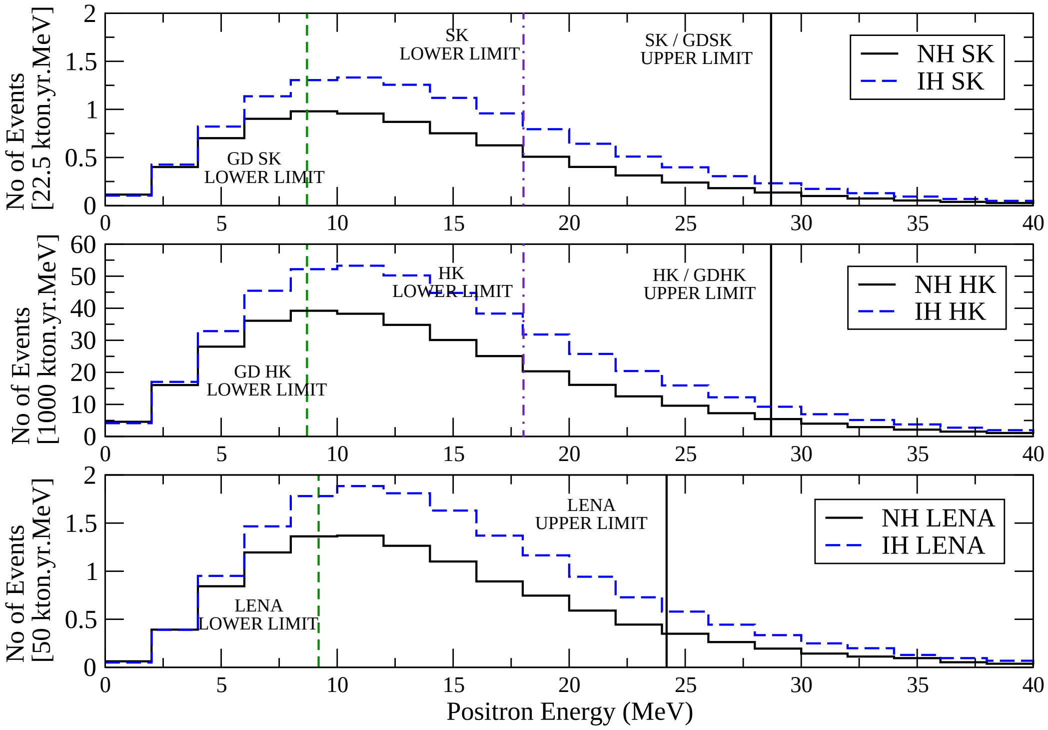

Figure 6.3: Number of expected events per year in 2 MeV positron energy bins in SK (upper panel) HK (middle panel) and LENA (lower panel). The solid black lines show the projected event spectrum for NH while the dashed blue lines are if IH was true with $P_{13} = 1$. The SN flux model corresponds to G1.

It can be seen, that we expect about a couple of events per year in SK [5]. This would go up by a factor of about $2-3$ if Gadolinium were to be added to the water. The corresponding number for a megaton of water would be scaled upwards by a factor of $1000/22.5$ and we expect about $40-176$ $(140-356)$ events per year in megaton water (Gadolinium loaded water) detectors depending on the choice of the neutrino mass hierarchy and θ_{13} and the SN model. After 10 years of running these numbers would be a factor of 10 higher,

[5]Note that there will also be a large number of background events in the detector and one has to find the signal by looking at excess of events above the fluctuations in the background. This makes DSNB detection more difficult.

and we could have a few thousand events in the Gadolinium loaded detector. It should therefore be straightforward for megaton water detectors, with or without Gadolinium, to be able to observe these DSNB fluxes. More importantly we note that for a given SN flux model, it should be easy for megaton water detectors to determine the hierarchy, if $\sin^2\theta_{13} \lesssim 10^{-5}$. For almost vanishing θ_{13}, we can see that for G1, NH predicts 1960 ± 44 (678 ± 26) events in 10 years of running of GDHK (HK) while IH predicts 2960 ± 54 (1096 ± 33). It would therefore be easy to distinguish one hierarchy from the other. Note that this is one of the very rare type of experiments which can give information about the neutrino mass hierarchy even if θ_{13} was below the reach of the most Neutrino Factory and Beta-beam experiments. A 50 kton liquid scintillator detector should be able to record $46 - 106$ events in 10 years of running.

We have shown in the table, number of events expected assuming either the G1, G2 or LL model for the initial SN neutrino fluxes. We find that the lowest number of events are predicted by the G2 model, while LL predicts the highest event rate. In fact, one can see that the event rate predicted by NH and G1 is close is that predicted by IH and G2. Likewise, the rate predicted by IH and G1 is close to the one predicted by NH and LL. We have discussed before the uncertainty associated with the SN models. Therefore, if the uncertainty in the model predictions for the initial fluxes remain at the current level, then it might be hard to distinguish the hierarchy from the DSNB itself, especially in the smaller detectors. However, for Gadolinium loaded megaton water detectors it might still be possible to say something about the hierarchy. Also, for G2 and NH (LL and IH) we have a prediction which is lower (higher) than any other case and therefore for these cases there is no confusion. For instance, if GDHK records less (greater) than 1500 (3000) events, we could say that the hierarchy is normal (inverted). Of course, we have nowhere taken into account the uncertainty in the star formation rate. That might bring additional complication, which we do not address in this thesis.

So far we have presented results only for two extreme cases of θ_{13}, very low corresponding to $P_{13} = 1$ and very high corresponding to $P_{13} = 0$. For intermediate values of the mixing angle the jump probability ranges between 0 and 1. We show in fig. 6.2 how the total event rate in the different detectors change as a function of P_{13}. The SN model assumed is G1. Solid black lines show the case for NH while the dashed blue lines show the case for IH, where we have included both collective as well as MSW transitions inside the SN. It is easy to see from the expressions given in Table. 6.2 that for IH, the event rate would rise almost linearly with P_{13}. If collective effects were not taken into account then the trend would have been the opposite, and we would see a decrease in the $\bar{\nu}_e$ event rate with P_{13}. These are shown for the different detectors by the yellow dot-dashed lines in the figure.

For sizable number of events, it might even be possible to do a spectral analysis of the DSNB events. We show in fig. 6.3 the event spectrum for 22.5 kton SK (upper panel), 1 Mton HK (middle) and 50 kton LENA (lower panel). The events per year are shown in 2 MeV energy bins. The solid black lines give the event spectrum for NH while the blue dashed lines are for IH with $P_{13} = 1$. We show results where both collective as well as MSW oscillations are taken into account. Upper and lower energy threshold for the different cases are indicated by vertical lines and we have assumed the G1 model for the initial fluxes.

6.3.2 DSNB neutrino events in liquid argon detectors

Liquid argon TPC could offer a unique laboratory to probe ν_e from a future galactic SN as well as from the DSNB around us. We show in Table. 6.4 the number of expected ν_e charged current events on ^{40}Ar. We show results for NH and large θ_{13} ($P_{13} = 0$), NH and small θ_{13} ($P_{13} = 1$), and IH for any value of θ_{13}. Expected number of events are shown for the three benchmark flux models. We see that the number of ν_e events expected in liquid argon detectors is extremely small. This is because the $\nu_e + ^{40}\text{Ar} \rightarrow e^- + ^{40}\text{K}^*$ cross-section (taken from [75]) is very small at low energies and rises very fast as the energy increases. The DSNB flux on the other hand gets redshifted to lower energies thereby reducing the number of events. In particular, the DSNB flux is peaked at around 5 MeV, with very few neutrinos in the energy window 20–40 MeV (cf. fig. 6.1). It might also be interesting to compare the number of expected ν_e events in a liquid argon detector, with the number of $\bar{\nu}_e$ events in a water detector, for same number of target nuclei/nucleons. It turns out that 100 kton of liquid argon has 1.5×10^{33} argon targets, while 22.5 kton water detector

	G1	G2	LL
NH ($P_{13} = 0$)	4.9 (4.9)	2.3 (2.3)	9.9 (9.9)
NH ($P_{13} = 1$)	3.6 (3.6)	1.7 (1.7)	7.3 (7.3)
IH	4.9 (3.6)	2.3 (1.7)	9.9 (7.3)

Table 6.4: Number of ν_e charged current events on ^{40}Ar per year per 100 kton of Liquid argon TPC in the energy window $E_\nu = (20 - 40)$ MeV. The events without collective effects are shown in parenthesis for comparison.

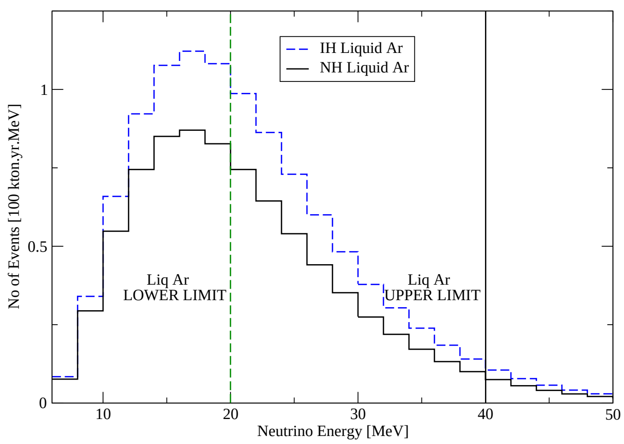

Figure 6.4: Number of expected events per year in 2 MeV neutrino energy bins in a 100 kton Liquid argon TPC. The solid black lines show the projected event spectrum for NH ($P_{13} = 1$) while the dashed blue lines are if IH was true. The SN flux model corresponds to G1.

(SK) also has 1.5×10^{33} proton targets. On the other hand, the cumulative cross-section in the energy window of 20–40 MeV for ν_e capture on ^{40}Ar is larger than the cross-section for $\bar{\nu}_e$ capture on protons by a factor of about 2. Signal in this energy window, for the LL SN model with complete flavor conversion[6], would be 9.9 and 5.8 events in 100 kton of liquid argon and 22.5 kton of water, respectively. This implies a ratio of about 1.7, which agrees with the rough estimate of the factor of 2 coming from the difference in the cross-sections. If we could lower the energy threshold in liquid argon to 5.5 MeV, we could expect about 8.1 events per year for NH with small θ_{13} and about 10.5 events per year for IH (and NH with large θ_{13}). In fig. 6.4 we show the event spectrum in bins of 2 MeV width. The black solid line shows the spectrum for NH with $P_{13} = 1$ while the blue dashed line is for IH.

6.4 Discussions

Neutrinos emitted by core-collapse supernovae over the entire history of the Universe, pervade us. This is the so-called diffuse supernova neutrino background. The DSNB fluxes are theoretically given by folding the neutrinos emitted from a typical SN with the rate of SN explosions as a function of the redshift, and integrating over all redshifts to take into account all possible SN explosions that might have happened in the Universe. Since the final fluxes emerging from the SN depend on neutrino flavor coversions inside the SN, the DSNB fluxes also depend very crucially on neutrino properties. Therefore, while a galactic SN event is eagerly awaited in order to shed light on SN theory on one hand and neutrino properties on the other, detecting the DSNB in currently running and future detectors could help us constrain SN dynamics, cosmic star formation rate as well as neutrino properties. However, the primary agenda is to successfully observe them in terrestrial detectors.

Being redshifted, the spectrum of DSNB fluxes is peaked at smaller energies, making their detection even more challenging. So far the running Super-Kamiokande detector

[6]For complete flavor conversion, the resultant flux at both liquid argon and water detector is ν_x, and is therefore the same. Of course in reality, complete flavor conversion can be possible only in one channel. The above example is just to illustrate the difference in the number of events for the two detector types being compared.

has managed to put an upper bound on the $\bar{\nu}_e$ DSNB flux. However, the situation might improve in the future with possibility of a signal in the upcoming large scale detectors which would be built to serve as the far detector for high performance neutrino beam experiments. Observing DSNB would be free for these detectors and the physics output from that would be immense. In this chapter we re-analyzed the potential of a selected class of future detectors to detect DSNB fluxes. Such an analysis has been warranted by the flurry of activity in the field of SN neutrino research, following the revival of interest in neutrino-neutrino self-interaction and it was necessary to revisit the issue of DSNB detection.

We considered water, Gadolinium loaded water and liquid scintillator detectors for $\bar{\nu}_e$ DSNB detection and liquid argon TPC for observing the ν_e DSNB flux. A major issue in this field is the model uncertainties in the SN neutrino fluxes themselves. We presented results for three SN neutrino flux models. We calculated the total number of events for both the hierarchies and for two extreme values of θ_{13} resulting in jump probability $P_{13} \to 0$ and 1. Number of events expected in future megaton water and 50 kton liquid scintillator detectors are large, with a few thousand events expected in Gadolinium loaded megaton water detectors running for 10 years. For true inverted hierarchy, it becomes possible to get very large flavor oscillations even if $\theta_{13} \to 0$. We showed that under fortunate circumstances, it might be possible to get information on the neutrino mass hierarchy by observing DSNB in megaton water detectors. Note that this is a very unique situation, since for $\theta_{13} \to 0$ it becomes almost impossible to determine the hierarchy using long baseline experiments. In this way, DSNB detection could be complementary to the long baseline program. We also showed how the total number of events change if θ_{13} increases from very small to very large values, decreasing P_{13} from 1 to 0. Finally, we showed the event spectrum by binning the prospective data in 2 MeV bins.

In conclusion, very large number of DSNB events are expected in the next generation detectors and therefore, it should be possible to observe DSNB $\bar{\nu}_e$ in the future. Collective effects inside SN significantly change the predicted number of DSNB events if the hierarchy is inverted. Under fortunate conditions it might be possible to determine the neutrino mass hierarchy using the DSNB signal and this could be done even if $\theta_{13} \to 0$, in which case long baseline experiments would not be able to tell the hierarchy at all. One might even feel optimistic about learning about neutrino oscillation parameters, cosmic star formation rate and maybe about SN physics, by observing these relic neutrinos in future detectors.

However it should always be kept in mind that the distinguishability of hierarchy is highly dependent on the initial flux models of the emitted neutrinos. Moreover different SNe may emit different fluxes. In that case the hierarchy sensitivity has to be averaged as DSNB is a collective background of all past SNe. In the next chapter we will show how the hierarchy distinguishability will get affected if all the SNe do not have identical neutrino flux.

BIBLIOGRAPHY

[1] R. Diehl *et al.*, Nature **439**, 45 (2006) arXiv:astro-ph/0601015.

[2] G. S. Bisnovatyi-Kogan and S. F. Seidov Annals N. Y. Acad. Sci. **422**, 319 (1984).

[3] L. M. Krauss, S. L. Glashow and D. N. Schramm, Nature **310**, 191 (1984).

[4] S. E. Woosley, J. R. Wilson and R. Mayle Astrophys. J. **302**, 19 (1986).

[5] F. Mannucci, D. Maoz, K. Sharon, M. T. Botticella, M. Della Valle, A. Gal-Yam and N. Panagia, arXiv:0710.1094 [astro-ph].

[6] Lilly S, Fèvre O L, Hammer F and Crampton D 1996 *Astrophys. J.* **460** L1

[7] Madau P, Ferguson H C, Dickinson M E, Giavalisco M, Steidel C C and Fruchter A 1996 *Mon. Not. R. Astron. Soc.* **283** 1388

[8] Cowie L, Songaila A, Hu E and Cohen J 1996 *Astron. J.* **112** 839

[9] Connolly A, Szalay A, Dickinson M, Rao M S and Brunner R 1997 *Astrophys. J.* **486** L11

[10] Sawicki M J, Lin H and Yee H K C 1997 *Astron. J.* **113** 1

[11] Treyer M, Ellis R, Milliard B, Donas J and Bridges T 1998 *Mon. Not. R. Astron. Soc.* **300** 303

[12] Madau P, Pozzetti L and Dickinson M 1998 *Astrophys. J.* **498** 106

[13] Pascarelle S M, Lanzetta K M and Fernandez-Soto A 1998 *Astrophys. J.* **508** L1

[14] Steidel C C, Adelberger K L, Giavalisco M, Dickinson M and Pettini M 1999 *Astrophys. J.* **519** 1

[15] Hughes D H *et al.* 1998 *Nature* **394** 241

[16] Flores H *et al.* 1999 *Astrophys. J.* **517** 148

[17] Gallego J, Zamorano J, Aragón-Salamanca A and Rego M 1995 *Astrophys. J.* **455** L1

[18] Gronwall C 1998 in: Thuan T *et al.* (eds), *Proc. 33rd Rencontres de Moriond, Dwarf Galaxies and Cosmology* (Gif-sur-Yvette: Editions Frontières) p 41

[19] Tresse L and Maddox S 1998 *Astrophys. J.* **495** 691

[20] Glazebrook K, Blake C, Economou F, Lilly S and Colless M 1999 *Mon. Not. R. Astron. Soc.* **306** 843

[21] E. N. Archibald, J. S. Dunlop, D. H. Hughes, S. Rawlings, S. A. Eales and R. J. Ivison, Mon. Not. Roy. Astron. Soc. **323**, 417 (2001) arXiv:astro-ph/0002083.

[22] Somerville R S, Primack J R and Faber S M 2001 *Mon. Not. R. Astron. Soc.* **320** 504

[23] L. E. Strigari, J. F. Beacom, T. P. Walker and P. Zhang, JCAP **0504**, 017 (2005) arXiv:astro-ph/0502150.

[24] A. Mirizzi and G. G. Raffelt, Phys. Rev. D **72**, 063001 (2005) arXiv:astro-ph/0508612.

[25] R. Buras, H. -Th. Janka, M. T. Keil, G. G. Raffelt and M. Rampp, Astrophys. J. **587** (2003) 320 arXiv:astro-ph/0205006.

[26] T. Totani, K. Sato, H. E. Dalhed and J. R. Wilson, Astrophys. J. **496** (1998) 216 arXiv:astro-ph/9710203.

[27] R. A. Malaney, Astropart. Phys. **7** (1997) 125 arXiv:astro-ph/9612012.

[28] D. H. Hartmann and S. E. Woosley, Astropart. Phys. **7** (1997) 137.

[29] T. Totani, K. Sato and Y. Yoshii, Astrophys. J. **460** (1996) 303 arXiv:astro-ph/9509130.

[30] M. Kaplinghat, G. Steigman and T. P. Walker, Phys. Rev. D **62** (2000) 043001 arXiv:astro-ph/9912391.

[31] L. E. Strigari, M. Kaplinghat, G. Steigman and T. P. Walker, JCAP **0403** (2004) 007 arXiv:astro-ph/0312346.

[32] M. Fukugita and M. Kawasaki, Mon. Not. Roy. Astron. Soc. **340** (2003) L7 arXiv:astro-ph/0204376.

[33] M. Wurm, F. von Feilitzsch, M. Goeger-Neff, K. A. Hochmuth, T. M. Undagoitia, L. Oberauer and W. Potzel, Phys. Rev. D **75** (2007) 023007 arXiv:astro-ph/0701305.

[34] S. Ando and K. Sato, New J. Phys. **6** (2004) 170 arXiv:astro-ph/0410061.

[35] E. Cappellaro, M. Turatto, D. Y. Tsvetkov, O. S. Bartunov, C. Pollas, R. Evans and M. Hamuy, Astron. Astrophys. **322** (1997) 431 arXiv:astro-ph/9611191.

[36] S. Ando, K. Sato and T. Totani, Astropart. Phys. **18** (2003) 307 arXiv:astro-ph/0202450.

[37] S. Ando and K. Sato, Phys. Lett. B **559** (2003) 113 arXiv:astro-ph/0210502.

[38] C. Lunardini, Astropart. Phys. **26** (2006) 190 arXiv:astro-ph/0509233.

[39] S. Ando, Astrophys. J. **607** (2004) 20 arXiv:astro-ph/0401531.

[40] C. Volpe and J. Welzel, arXiv:0711.3237 [astro-ph].

[41] A. G. Cocco, A. Ereditato, G. Fiorillo, G. Mangano and V. Pettorino, JCAP **0412**, 002 (2004) arXiv:hep-ph/0408031.

[42] J. F. Beacom and L. E. Strigari, Phys. Rev. C **73** (2006) 035807 arXiv:hep-ph/0508202.

[43] C. Lunardini, Phys. Rev. D **73** (2006) 083009 arXiv:hep-ph/0601054.

[44] M. Aglietta *et al.*, Astropart. Phys. **1** (1992) 1.

[45] M. Malek *et al.* [Super-Kamiokande Collaboration], Phys. Rev. Lett. **90** (2003) 061101 arXiv:hep-ex/0209028.

[46] C. Lunardini and O. L. G. Peres, arXiv:0805.4225 [astro-ph].

[47] J. F. Beacom and M. R. Vagins, Phys. Rev. Lett. **93**, 171101 (2004) arXiv:hep-ph/0309300.

[48] J. Dunkley *et al.* [WMAP Collaboration], arXiv:0803.0586 [astro-ph].

[49] I.K. Baldry and K. Glazebrook, Astrophys. J. **593**, 258 (2003).

[50] A.M. Hopkins and J.F. Beacom, Astrophys. J. **651**, 142 (2006).

[51] M.D. Kistler et al, arXiv:0709.0381v2 [astro-ph].

[52] P. Bhattacharjee, S. Chakraborty, S. Das Gupta, K. Kar, Phys. Rev. D **77**, 043008 (2008) arXiv:0710.5922v3 [astro-ph].

[53] M. T. Keil, G. G. Raffelt and H. T. Janka, Astrophys. J. **590**, 971 (2003) arXiv:astro-ph/0208035.

[54] G. G. Raffelt and A. Y. Smirnov, Phys. Rev. D **76**, 081301 (2007) [Erratum-ibid. D **77**, 029903 (2008)] arXiv:0705.1830 [hep-ph].

[55] H. Duan, G. M. Fuller and Y. Z. Qian, arXiv:0801.1363 [hep-ph].

[56] B. Dasgupta, A. Dighe, A. Mirizzi and G. G. Raffelt, arXiv:0801.1660 [hep-ph].

[57] B. Dasgupta, A. Dighe, G. G. Raffelt and A. Y. Smirnov, arXiv:0904.3542 [hep-ph].

[58] G. Fogli, E. Lisi, A. Marrone and I. Tamborra, arXiv:0907.5115 [hep-ph].

[59] S. Chakraborty, S. Choubey, S. Goswami and K. Kar, JCAP **1006**, 007 (2010) [arXiv:0911.1218 [hep-ph]].

[60] http://www.snolab.ca/public/science/index.html

[61] Y. Itow *et al.*, arXiv:hep-ex/0106019.

[62] A. de Bellefon *et al.*, arXiv:hep-ex/0607026.

[63] C. K. Jung, AIP Conf. Proc. **533**, 29 (2000).

[64] S. Abe *et al.* [KamLAND Collaboration], arXiv:0801.4589 [hep-ex].

[65] B. Aharmim *et al.* [SNO Collaboration], Phys. Rev. C **72**, 055502 (2005) arXiv:nucl-ex/0502021.

[66] J. Engel, E. Kolbe, K. Langanke and P. Vogel, Phys. Rev. C **54**, 2740 (1996) arXiv:nucl-th/9606031; E. Kolbe, F. K. Thielemann, K. Langanke and P. Vogel, Phys. Rev. C **52**, 3437 (1995); E. Kolbe, K. Langanke and S. Krewald, Phys. Rev. C **49**, 1122 (1994).

[67] J. F. Beacom, W. M. Farr and P. Vogel, Phys. Rev. D **66**, 033001 (2002) arXiv:hep-ph/0205220.

[68] L. Cadonati, F. P. Calaprice and M. C. Chen, Astropart. Phys. **16**, 361 (2002) arXiv:hep-ph/0012082.

[69] A. Bandyopadhyay, S. Choubey, S. Goswami and K. Kar, arXiv:hep-ph/0312315.

[70] C. Arpesella *et al.* [Borexino Collaboration], Phys. Lett. B **658**, 101 (2008) arXiv:0708.2251 [astro-ph].

[71] J. G. Learned, S. T. Dye and S. Pakvasa, *Prepared for 12th International Workshop on Neutrinos Telescopes: Twenty Years after the Supernova 1987A Neutrino Bursts Discovery, Venice, Italy, 6-9 Mar 2007*

[72] S. Choubey and S. T. Petcov, Phys. Lett. B **594**, 333 (2004) arXiv:hep-ph/0404103.

[73] P. Aprili *et al.* [ICARUS Collaboration], CERN-SPSC-2002-027 (2002).

[74] I. Gil-Botella and A. Rubbia, JCAP **0408**, 001 (2004) arXiv:hep-ph/0404151; A. Bueno, I. Gil-Botella and A. Rubbia, arXiv:hep-ph/0307222.

[75] I. Gil-Botella and A. Rubbia, JCAP **0310**, 009 (2003) arXiv:hep-ph/0307244;

[76] A. Rubbia, arXiv:hep-ph/0402110; http://neutrino.ethz.ch/GLACIER/Welcome.html

[77] B. Baibussinov *et al.*, Astropart. Phys. **29**, 174 (2008) arXiv:0704.1422 [hep-ph].

[78] www-off-axis.fnal.gov/flare/

CHAPTER 7

Variation of Split Pattern and Diffuse Supernova Neutrino Background

In the previous chapters we have seen that the 'collective' nature of simultaneous flavor conversions of both neutrinos and antineutrinos give rise to 'splits' in the spectra of the neutrinos and antineutrinos. These splits occur due to sudden change in the oscillation probability, causing spectral swaps which may end up in observable effects. We also found that the impact of collective oscillations on the spectra are different for the Normal Hierarchy (NH) and the Inverted Hierarchy (IH). This opens up the possibility of identifying the neutrino mass hierarchy via observation of collective effects in the neutrino signal from a future galactic supernova event [1, 2]. Our analysis also described that fact that prospect of finding DSNB in the near future detectors is a promising alternative way of looking at SN neutrinos

As described in the last chapter the two key ingredients in the calculation of DSNB are (i) the SN rate which is proportional to cosmic star formation rate and (ii) the ν and $\bar{\nu}$ energy spectra. Whereas reliable estimates are now available for the star formation rate and the SN rate [3, 4], the prediction for the SN neutrino spectra has gone through an evolution over the years. Earlier considerations of matter induced resonances were followed by incorporating the 'collective' effects due to interaction amongst the neutrinos themselves in the high density central regions of the core. The somewhat simplified study described in the last chapter on the effect of the collective flavor oscillations on DSNB fluxes and the corresponding predicted number of events in terrestrial detectors demonstrated that the event rate gets substantially modified by collective effects. The results also showed that observation of the DSNB fluxes at earth could shed light on the neutrino mass hierarchy. However, that study was based on several assumptions about the collective effects. In particular, in chapter. 4 we described how the neutrino and antineutrino survival probabilities and hence different split patterns depend crucially on the relative luminosities of the initial neutrino fluxes produced inside the exploding star [5, 6, 7]. Therefore, one can predict the final neutrino and antineutrino spectra from a given SN with reasonable accuracy only if one already has access to the initial flux conditions. This complication is further compounded for the DSNB, as the DSNB flux comes from a superposition of the fluxes from all past SNe. Since the initial flux conditions are expected to be sensitive to the properties of the progenitor star and since we have a whole distribution of stars which end up being a SN, it is a complicated business to accurately estimate the DSNB spectra after accounting for the collective effects, which are bound to happen in almost every SN.

In this chapter we incorporate the observation of different split patterns in the spectra for the calculation of DSNB and do not take the relative (anti)neutrino fluxes to have fixed values. The main focus of this analysis is to check the effect of a distribution of supernovae with initial flux on the measurement of the neutrino mass hierarchy via the observation of the DSNB signal. Since the distribution of the initial fluxes over all past SNe are not available to us, we parameterize this by a log-normal distribution. The log-normal distribution has two parameters which define the mean and width of the distribution. Since they are also unknown, we choose various plausible values for them. We calculate the DSNB event rate averaged over these distributions. We study how the hierarchy measurement is affected when one takes the distribution of initial relative fluxes into account and find situations where the hierarchy determination may be possible.

7.1 The Diffuse Supernova Neutrino Background Revisited

As allready described in the previous chapter we briefly recapitulate the calculation of DSNB. The differential number flux of DSNB is

$$F_\nu^{'}(E_\nu) = \frac{c}{H_0}\int_0^{z_{max}} R_{SN}(z)\,F_\nu(E)\frac{dz}{\sqrt{\Omega_m(1+z)^3+\Omega_\Lambda}}\ , \tag{7.1}$$

where $E_\nu = (1+z)^{-1}\,E$ is the redshifted neutrino energy observed at earth while E is the neutrino energy produced at the source, F_ν is the neutrino flux for each core collapse SN, $R_{\rm SN}(z)$ the cosmic SN rate at redshift z, and the Hubble constant taken as $H_0 = 70\ h_{70}\,{\rm km\ s^{-1}\ Mpc^{-1}}$. For the standard Λ-CDM cosmology, we have matter and dark energy density $\Omega_{\rm m} = 0.27$ and $\Omega_\Lambda = 0.73$, respectively [8]. As Eq. (7.1) suggests the DSNB flux at earth depends on two factors: (i) the cosmic SN rate and (ii) the initial SN neutrino spectrum from each SN.

The cosmic SN rate is related to the star formation rate $R_{SF}(z)$, through a suitable choice of Initial Mass Function (IMF) as $R_{SN}(z)$=$0.0132 \times R_{SF}(z) M_\odot^{-1}$[9, 10]. The IMF takes into account that only stars with masses larger than $8M_\odot$ result in supernova explosion. For the cosmic star formation rate we take a conservative estimate of [11] compare to the previously described model [12] in chapter. 6. Thus the results in this chapter would be a conservative limit of DSNB and its neutrino properties resolution capabilities. The R_{SF} considered here in per comoving volume is

$$R_{\rm SF}(z) = 0.32\ f_{SN} h_{70} \frac{e^{3.4z}}{e^{3.8z} + 45} \frac{\sqrt{\Omega_m (1+z)^3 + \Omega_\Lambda}}{(1+z)^{3/2}}\ , \tag{7.2}$$

where f_{SN} is normalization of the order of unity and $R_{\rm SF}(z)$ is in units of $M_\odot {\rm yr^{-1} Mpc^{-3}}$ [11, 13]. The initial SN neutrino spectrum emitted from the neutrinosphere is parameterized in the form [14]

$$\begin{aligned} F_\nu^0(E) &= (\frac{L_\nu^0}{\langle E_\alpha \rangle}) \times (\frac{(1+\zeta_\alpha)^{1+\zeta_\alpha}}{\Gamma(1+\zeta_\alpha)\langle E_\alpha\rangle} \left(\frac{E}{\langle E_\alpha\rangle}\right)^{\zeta_\alpha} e^{-(1+\zeta_\alpha)E/\langle E_\alpha\rangle}) \\ &= \phi_\nu^0 \times \psi(E), \end{aligned} \tag{7.3}$$

where ϕ_ν^0 is the total initial flux estimated for the initial luminosity L_ν^0 and average energy($\langle E_\alpha \rangle$). The spectral shape also depends on the energy distribution $\psi(E)$, which is parameterized by the pinching parameter α. In this study we use $\langle E_{\nu_e}\rangle$= 12 MeV, $\langle E_{\bar\nu_e}\rangle$= 15 MeV, $\langle E_{\nu_x}\rangle$=18 MeV with ζ_{ν_x}=$\zeta_{\bar\nu_x} = 4$ and ζ_{ν_e}=$\zeta_{\bar\nu_e} = 3$. The average energies of the different flux types will also vary from SN to SN. However for simplicity, in this work we choose to keep the average energies fixed. We assume that 3×10^{53} erg of energy is released in (anti)neutrinos by all SNe.

We have already mentioned the fact that the collective and MSW oscillations are widely separated in space and hence they can be considered independent of each other.

Normal hierarchy
$F_{\nu_e} = s_{12}^2 P_c(\phi^r_{\nu_e}, \phi^r_{\bar{\nu}_e}, E)(2P_{13}-1)(F^0_{\nu_e} - F^0_{\nu_x})$ $+s_{12}^2(1-P_{13})(F^0_{\nu_e} - F^0_{\nu_x}) + F^0_{\nu_x}.$
$F_{\bar{\nu}_e} = c_{12}^2 \bar{P}_c(\phi^r_{\nu_e}, \phi^r_{\bar{\nu}_e}, E)(F^0_{\bar{\nu}_e} - F^0_{\nu_x}) + F^0_{\nu_x}.$

Inverted hierarchy
$F_{\nu_e} = s_{12}^2 P_c(\phi^r_{\nu_e}, \phi^r_{\bar{\nu}_e}, E)(F^0_{\nu_e} - F^0_{\nu_x}) + F^0_{\nu_x}.$
$F_{\bar{\nu}_e} = c_{12}^2 \bar{P}_c(\phi^r_{\nu_e}, \phi^r_{\bar{\nu}_e}, E)(2P_{13}-1)(F^0_{\bar{\nu}_e} - F^0_{\nu_x})$ $+c_{12}^2(1-P_{13})(F^0_{\bar{\nu}_e} - F^0_{\nu_x}) + F^0_{\nu_x}.$

Table 7.1: Electron neutrino and antineutrino spectra emerging from a SN.

Thus the flux reaching the MSW resonance region already has the effects of the collective oscillations. It has been seen that collective oscillations can give rise to different split patterns of the neutrino spectra depending on the initial relative flux of ν_e and $\bar{\nu}_e$ with respect to flavor ν_x or ν_y, so we define $\phi^r_{\nu_e}=\frac{\phi^0_{\nu_e}}{\phi^0_{\nu_x}}$ and $\phi^r_{\bar{\nu}_e}=\frac{\phi^0_{\bar{\nu}_e}}{\phi^0_{\nu_x}}$ as measures of the relative fluxes following chapter. 4. The electron antineutrino flux beyond the collective region can swap to x flavor above some energy (single split) or can swap in some energy interval (double split) or even can remain unchanged (no split) depending on the initial relative flux $\phi^r_{\nu_e}$ and $\phi^r_{\bar{\nu}_e}$ [5, 6, 7]. DSNB is affected differently with these different oscillation scenarios. To incorporate the effect of collective oscillations we work in a two flavor scenario [7] as for a shallow neutrino-neutrino interaction potential the three flavor collective evolution effectively involves only two flavors of neutrinos (ν_e, ν_x), while the other flavor (ν_y) does not evolve [15, 16]. The only way ν_y can affect the final neutrino spectrum is by MSW transition. The fluxes after both the collective and MSW oscillation F_{ν_e} and $F_{\bar{\nu}_e}$ are given in Table.7.1.

[7]Recent papers [15, 16] have explored the effect of three flavors on the outcome of the split patterns in collective oscillations. While the three flavor results do differ from that of the two flavors in certain regimes of the initial flux parameter space for IH, the effects are mainly of the nature of a subtle correction when we do the averaging over different distribution. The main conclusions of this chapter – as we later see – therefore remain largely independent of these correction effects.

In Table.7.1, P_{13} is the effective jump probability between the neutrino mass eigenstates due to the atmospheric mass squared driven MSW resonance. It takes a value between 0 and 1 depending on the value of the mixing angle θ_{13}. For θ_{13} large ($\sin^2\theta_{13} \gtrsim 0.01$) $P_{13} \simeq 0$, while for small θ_{13} ($\sin^2\theta_{13} \lesssim 10^{-6}$) $P_{13} \simeq 1$ [17]. The quantities s_{12}^2 and c_{12}^2 stand for $\sin^2\theta_{12}$ (taken to be 0.3 for numerical studies) and $\cos^2\theta_{12}$, respectively. The quantities P_c and $\bar{P}_c$ are the neutrino and antineutrino survival probability after the collective effect, respectively. These collective survival probabilities are calculated numerically taking $\Delta m^2 = 3\times 10^{-3}\ eV^2$ and a small effective mixing angle of 10^{-5}. [8] As discussed before, P_c and/or $\bar{P}_c$, which is a function of the neutrino energy E, show pattern of sudden change between 0 and 1, leading to sudden change in the neutrino and/or antineutrino spectra. Depending on the number of times the value of P_c (and/or $\bar{P}_c$) changes, we can have more than one sudden swap of the neutrino (and/or antineutrino) spectra, referred as multiple split [5, 6, 7]. The split patterns as we have shown, crucially depend on the initial relative flux densities of the neutrino and antineutrino. The initial relative neutrino and antineutrino flux densities are expected to vary among different SN.

This variation in $\phi^r_{\nu_e}$ and $\phi^r_{\bar{\nu}_e}$ in different SNe might have origin in difference of progenitor mass, different luminosity etc. In fact even different simulations allow wide variation of $\phi^r_{\nu_e}$ and $\phi^r_{\bar{\nu}_e}$ within the 2 fold uncertainty around equipartition ($\frac{\langle E_{\nu_x}\rangle}{2\langle E_{\nu_e}\rangle} \le \phi^r_{\nu_e} \le \frac{2\langle E_{\nu_x}\rangle}{\langle E_{\nu_e}\rangle}; \frac{\langle E_{\nu_x}\rangle}{2\langle E_{\bar{\nu}_e}\rangle} \le \phi^r_{\bar{\nu}_e} \le \frac{2\langle E_{\nu_x}\rangle}{\langle E_{\bar{\nu}_e}\rangle}$.) [19]. Most models predict $l_{\nu_e} \simeq l_{\bar{\nu}_e}$, where l_{ν_e} and $l_{\bar{\nu}_e}$ are the relative luminosity ($\frac{L_{\nu_\alpha}}{L_{Total}}$) of ν_e and $\bar{\nu}_e$ respectively [33]. However, the combined luminosity of ν_μ, ν_τ, $\bar{\nu}_\mu$ and ν_τ is seen to be rather disparate between the different model results[9]. The most reliable way to reconstruct the relative luminosity distribution function in principle would be from direct observation of SN events along with their neutrino signal. However, as yet only SN1987A has been observed along with the detection of its neutrinos/antineutrinos. We require to know neutrino fluxes of different flavors from a number of galactic SN with a range of stellar mass and initial conditions before collapse to have information about the possible variation in $\phi^r_{\nu_e}$ and $\phi^r_{\bar{\nu}_e}$. This might take decades and

[8]Note that $P_c = \bar{P}_c = 1$ gives back the SN flux without collective oscillation [18]. P_c=$\bar{P}_c$=1 for NH and P_c=0 above E_c with $\bar{P}_c$=1 for all energies in IH gives back Table.6.2

[9]See for e.g. the compilation of model results in [20].

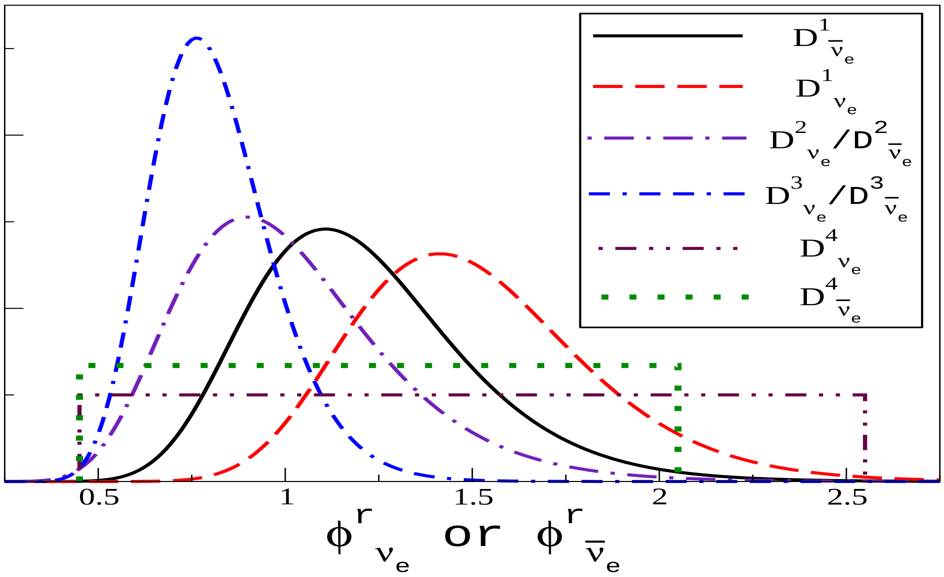

Figure 7.1: The four specimen distributions used in the calculations. The y-axis gives the distribution of supernova in arbitrary units.

is clearly not possible in the near future. So we propose that the SN events contributing to DSNB have various different values of $\phi^r_{\nu_e}$ and $\phi^r_{\bar{\nu}_e}$. For quantitative estimates we assume specific distributions for them. We take $\phi^r_{\nu_e}$ and $\phi^r_{\bar{\nu}_e}$ distributed log-normally, defined by the parameters (μ_1, σ_1) and (μ_2, σ_2) i.e,

$$D_\nu(\mu_1, \sigma_1) = \frac{e^{-(\frac{log(\phi^r_{\nu_e})-\mu_1}{2\pi\sigma_1})^2}}{\sqrt{2\pi}\sigma_1\phi^r_{\nu_e}}; D_{\bar{\nu}}(\mu_2, \sigma_2) = \frac{e^{-(\frac{log(\phi^r_{\bar{\nu}_e})-\mu_2}{2\pi\sigma_2})^2}}{\sqrt{2\pi}\sigma_2\phi^r_{\bar{\nu}_e}}\ . \tag{7.4}$$

We choose a range of values for μ such that the expectation (mean) values of $\phi^r_{\nu_e}$ and $\phi^r_{\bar{\nu}_e}$ are compatible with either Lawrence Livermore (equipartition) or Garching simulations. The parameter σ determines the width of the distribution. Since the variation of $\phi^r_{\nu_e}$ and $\phi^r_{\bar{\nu}_e}$ is expected to be within the 2 fold uncertainty around equipartition [19], the σ's for the distributions are chosen such that the distribution is well within the 2 fold uncertainty of the expectation value. In order to show the effect of the choice of the distribution function we simulate our results for four widely different distributions for $\phi^r_{\nu_e}$ and $\phi^r_{\bar{\nu}_e}$. They are chosen as follows:

1. The expectation is the equipartition value, i.e 1.5 for $\phi^r_{\nu_e}$ and 1.2 for $\phi^r_{\bar{\nu}_e}$ and the variation is within 2 fold uncertainty of 1.5 and 1.2 respectively. The corresponding

values of (μ, σ) turn out to be (0.39,0.21) for neutrinos and (0.16,0.24) for antineutrino We denote this distributions by $D^1_{\nu_e}$ and $D^1_{\bar{\nu}_e}$.

2. The expectation is same for both $\phi^r_{\nu_e}$ and $\phi^r_{\bar{\nu}_e}$ and is taken as 1, the σ is chosen as stated above. Hence the distributions for ν_e and $\bar{\nu}_e$ are identical and is defined by the parameters $(\mu, \sigma) \equiv (-0.03, 0.28)$. We denote this distribution by $D^2_{\nu_e}$ and $D^2_{\bar{\nu}_e}$.

3. The expectation is taken to be the same as the Garching simulations [14], i,e 0.8 for both the ν_e and $\bar{\nu}_e$ and the distributions parameterized by $(\mu, \sigma) \equiv (-0.23, 0.20)$ are the same. We denote this distribution by $D^3_{\nu_e}$ and $D^3_{\bar{\nu}_e}$.

4. We consider the distribution to be constant between 0.45-2.55 for $\phi^r_{\nu_e}$ and 0.45-2.05 for $\phi^r_{\bar{\nu}_e}$, with a normalization factor of $\frac{1}{2.1}$ and $\frac{1}{1.6}$ respectively. We denote this case by $D^4_{\nu_e}$ and $D^4_{\bar{\nu}_e}$.

The four specimen distributions for $\phi^r_{\nu_e}$ and $\phi^r_{\bar{\nu}_e}$ are shown in fig. 7.1. By definition the log-normal distribution functions D^1, D^2 and D^3 are normalized to unity. The choice of our normalization factors for the uniform distribution functions in D^4 ensures that they are normalized to unity as well. We can see from the figure that D^3 has the narrowest spread in the relative flux while the uniform distribution D^4 has the widest. For simplicity we have chosen distribution functions that are independent of the redshift z.

The differential number flux of DSNB with the i^{th} distributions is given by

$$F'^{i}_{\nu}(E_\nu) = \frac{c}{H_0} \int\limits_{\phi^r_{\nu_e min}}^{\phi^r_{\nu_e max}} \int\limits_{\phi^r_{\bar{\nu}_e min}}^{\phi^r_{\bar{\nu}_e max}} \int\limits_{0}^{z_{max}} R_{SN}(z)\, F_\nu(E, \phi^r_{\nu_e}, \phi^r_{\bar{\nu}_e})$$
$$\times D^i_{\nu_e}(\phi^r_{\nu_e})\ D^i_{\bar{\nu}_e}(\phi^r_{\bar{\nu}_e}) \frac{dz\ d\phi^r_{\nu_e} d\phi^r_{\bar{\nu}_e}}{\sqrt{\Omega_m(1+z)^3 + \Omega_\Lambda}}\ , \tag{7.5}$$

where $D^i_{\nu_e}(\phi^r_{\nu_e})$ and $D^i_{\bar{\nu}_e}(\phi^r_{\bar{\nu}_e})$ are the number of supernovae in between the interval $\phi^r_{\nu_e}$ to $\phi^r_{\nu_e} + d\phi^r_{\nu_e}$ and $\phi^r_{\bar{\nu}_e}$ to $\phi^r_{\bar{\nu}_e} + d\phi^r_{\bar{\nu}_e}$, respectively. $F_\nu(E, \phi^r_{\nu_e}, \phi^r_{\bar{\nu}_e})$ is the neutrino flux of each SN with initial relative flux combination $\phi^r_{\nu_e}$ and $\phi^r_{\bar{\nu}_e}$ at a redshift z. z_{max} is taken as 5, whereas $\phi^r_{\alpha min}$ and $\phi^r_{\alpha max}$ are chosen from the 2 fold uncertainty around expectation of the respective distribution. The upper panel in fig. 7.2 shows the antineutrino DSNB flux (in logarithmic scale) for NH and the lower panel shows the flux for IH with P_{13}= 1. In both

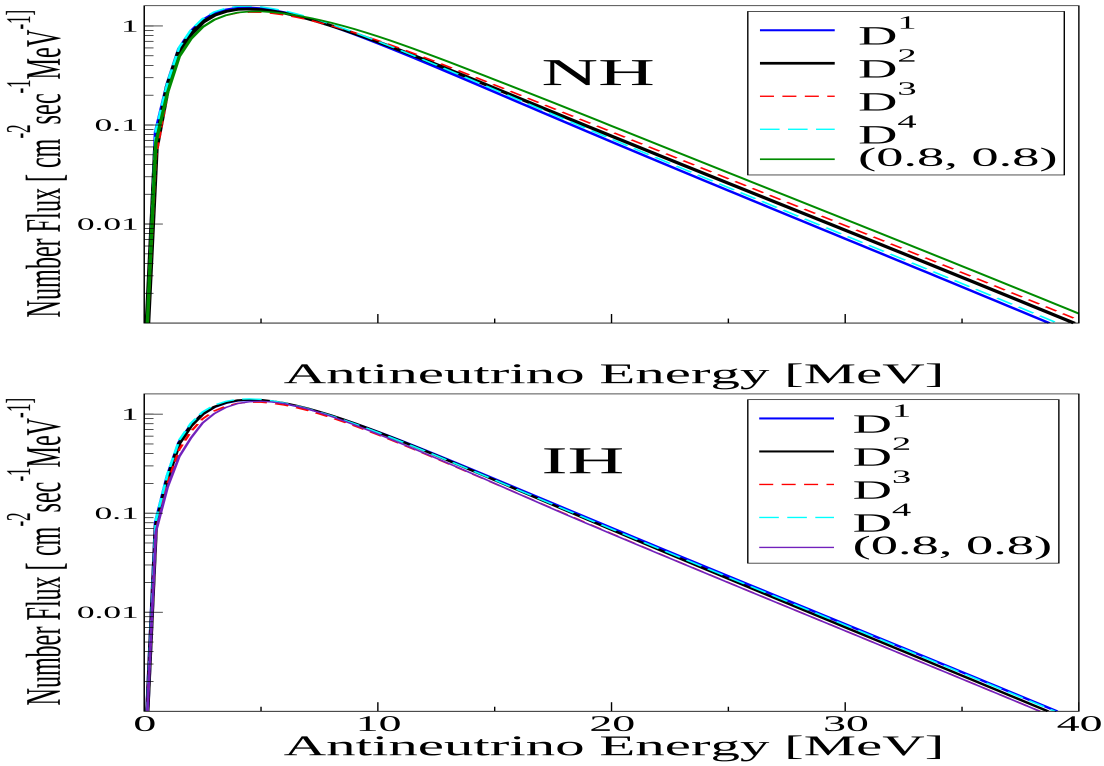

Figure 7.2: $\bar{\nu}_e$ fluxes for NH(upper panel) and IH (lower panel) with small θ_{13} (P_{13}= 1).

panels flux is shown for all of our different distribution (D^1-D^4) of $\phi^r_{\nu_e}$ and $\phi^r_{\bar{\nu}_e}$. In fig. 7.2 we also plotted flux for the case without any distribution of $\phi^r_{\nu_e}$ and $\phi^r_{\bar{\nu}_e}$ but specific value (0.8, 0.8) for the initial relative fluxes ($\phi^r_{\nu_e}$,$\phi^r_{\bar{\nu}_e}$). From the flux figures it is evident that the different distributions give similar DSNB flux. To check whether the small differences in their profile are measurable or not we next calculate the corresponding event rates in different detectors.

7.2 DSNB Event Rates and Hierarchy Measurement

In this section we will very briefly describe the detectors available for DSNB detection as we already had a detailed discussion of detectors in chapter. 6. Since the DSNB fluxes are very small, they are expected to be observed in either very large detectors or in reasonable size detectors with very large exposure times. Our previous analysis in chapter. 6 pointed out the fact that the only reasonable size detector running currently is the Super-Kamiokande (SK) [21] and amongst the proposed large detectors which have

Model	Hierarchy	2.5 Mton-yr (19.3 - 30.0) (MeV)	GD+2.5 Mton-yr (10.0 - 30.0) (MeV)
D^1	NH	76±9	280±17
	IH ($P_{13} = 0$)	92±10	319±18
	IH ($P_{13} = 1$)	80±9	288±17
$(1.5, 1.2)$	NH	75±9	281±17
	IH ($P_{13} = 0$)	98±10	332±19
	IH ($P_{13} = 1$)	75±9	280±17
D^2	NH	88±10	307±18
	IH ($P_{13} = 0$)	103±11	350±19
	IH ($P_{13} = 1$)	76±9	280±17
$(1.0, 1.0)$	NH	102±11	340±19
	IH ($P_{13} = 0$)	103±11	341±19
	IH ($P_{13} = 1$)	77±9	295±18
D^3	NH	98±10	334±19
	IH ($P_{13} = 0$)	113±11	379±20
	IH ($P_{13} = 1$)	70±9	258±16
$(0.8, 0.8)$	NH	112±11	378±20
	IH ($P_{13} = 0$)	113±11	378±20
	IH ($P_{13} = 1$)	70±9	260±17
D^4	NH	82±9	297±18
	IH ($P_{13} = 0$)	97±10	335±19
	IH ($P_{13} = 1$)	79±9	283±17
$(1.5, 1.25)$	NH	77±9	286±18
	IH ($P_{13} = 0$)	97±10	330±19
	IH ($P_{13} = 1$)	76±9	285±17

Table 7.2: Number of expected events per 2.5 Megaton-year of a water Cherenkov with SK like resolution and in a similar detector with Gadolinium loaded.

low energy threshold are the megaton water Cherenkov detectors [22, 23, 24], Gadolinium enriched water Cherenkov detectors [25], very large liquid scintillator detector (LENA) [26] or very large liquid Argon detector [27, 28, 29]. As we have seen that apart from the liquid Argon detector, none of the other detectors hold much promise for the detection of DSNB ν_e, whereas the antineutrino events in Mton water Čerenkov detectors has huge potential compared to these much smaller neutrino ν_e detectors. Even the proposed large liquid scintillator detector (LENA) which mainly detects antineutrino events is also predicted to have substantially smaller number of events compare to the megaton water Čerenkov detectors. Therefore, in rest of this discussion we will focus only on the detection possibilities for the DSNB $\bar{\nu}_e$ fluxes in Mton water Čerenkov detectors. The idea is to look at the highest possible near future detection capabilities and analyse the DSNB and its hierarchy detection sensitivity by including the effect of the proposed distribution of SN over relative fluxes.

All the water Čerenkov detectors use the inverse beta decay $\bar{\nu}_e + p \longrightarrow n + e^+$ interaction for detecting DSNB fluxes. The only difference between them would be in terms of their energy window of sensitivity for the DSNB. Water detectors use the neutrino energy (E_ν) window 19.3 MeV to 30.0 MeV [21], whereas for Gadolinium loaded water detectors the detection window is between 10 MeV and 30 MeV [25]. We show the total number of events for 2.5 Mton-yr exposure in water detectors and 2.5 Mton-yr exposure in Gadolinium loaded water detectors in the third and fourth columns of Table.7.2. The number of events are shown for the four different specimen distributions. Results are shown separately for $P_{13} = 1$ and $P_{13} = 0$ when the neutrino mass hierarchy is inverted (IH) . For the NH, there is no dependence of the $\bar{\nu}_e$ flux on P_{13}, as one can see from Table.7.1 . In each case we also show for comparison the number of events expected when $\phi^r_{\nu_e}$ and $\phi^r_{\bar{\nu}_e}$ are *fixed* at their respective mean values of the distribution [10]. Observing a variation of the number of events changing the $\phi^r_{\nu_e}$ and $\phi^r_{\bar{\nu}_e}$ for these examples without any distribution is an important indicator of how inclusion of distribution can change the DSNB event numbers.

[10]For the uniform distribution D^4 we took the central values of the widths as their representative mean.

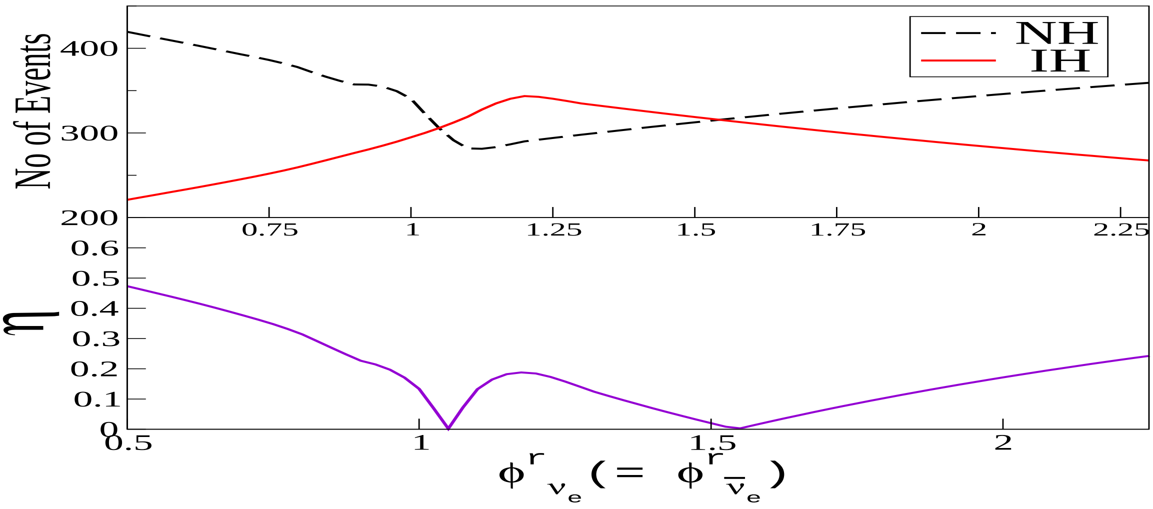

Figure 7.3: Upper panel shows the number of expected DSNB events in 2.5 MtonYr of Gadolinium loaded water detector for normal (NH) and inverted (IH) hierarchies (for IH, $P_{13} = 1$) as a function of $\phi^r_{\nu_e}(= \phi^r_{\bar{\nu}_e})$. The lower panel shows the change of η as a function of $\phi^r_{\nu_e}(= \phi^r_{\bar{\nu}_e})$.

We next turn our attention to the possibility of measuring the neutrino mass hierarchy using DSNB detection. For the distribution examples D^1, D^2 and D^4 the difference of number of events between NH and IH (both $P_{13} = 1$ and $P_{13} = 0$) seems to be within the statistical uncertainty. Whereas for the distribution D^3, though the difference in number of events between NH and IH (with $P_{13} = 1$) decreases significantly compared to the without distribution case, the difference is still greater than the statistical uncertainty. To probe this variation of hierarchy sensitivity with the distribution further let us define the quantity

$$\eta = \frac{|N_{NH} - N_{IH}|}{N_{NH}}, \tag{7.6}$$

which gives a measure of the hierarchy sensitivity of the experiment. The quantities N_{NH} and N_{IH} are the number of expected DSNB events when the hierarchy is normal and inverted, respectively. We note some general features of the quantity η, in Table. 7.2. Firstly, we can see that the relative hierarchy difference η depends on the mean value of $\phi^r_{\nu_e}$ and $\phi^r_{\bar{\nu}_e}$. Secondly, for a given $< \phi^r_{\nu_e} >$ and $< \phi^r_{\bar{\nu}_e} >$ it also depends on the distribution function involved.

For a better understanding of the first issue, we show in the upper panel of fig. 7.3 the variation of the number of events for both the NH and IH cases, as a function of the relative luminosity factor. The analysis is again done for the small mixing angle limit ($P_{13} = 1$) for IH, as it is the more challenging limit from the experimental point of view. We show this for 2.5 MegatonYears of Gadolinium doped water detector[11]. For simplicity we have taken $\phi^r_{\nu_e} = \phi^r_{\bar{\nu}_e}$ in this figure and we do not take any distribution function into account. The lower panel shows the corresponding η as a function of $\phi^r_{\nu_e} = \phi^r_{\bar{\nu}_e}$. We see that η has a very complicated dependence on the relative initial luminosity functions. The variation of η with ϕ^r_νs actually depends on several factors like difference between split pattern of NH and IH, the split/swap energies, the initial relative flux of ν_e, $\bar{\nu}_e$ and ν_x. It is rather high for very low values of $\phi^r_{\nu_e}$ and $\phi^r_{\bar{\nu}_e}$. It starts decreasing as the value of $\phi^r_{\nu_e}$ and $\phi^r_{\bar{\nu}_e}$ increase until it becomes zero around $\phi^r_{\nu_e} = \phi^r_{\bar{\nu}_e} \simeq 1.05$, thereafter it increases for a short while until it reaches a (local) maximum at around $\phi^r_{\nu_e} = \phi^r_{\bar{\nu}_e} \simeq 1.25$. Beyond that the value of η decreases again reaching zero at around $\phi^r_{\nu_e} = \phi^r_{\bar{\nu}_e} \simeq 1.55$, after which it increases again. The most noteworthy thing in the upper panel of this figure is that the number of events for inverted hierarchy has almost linear dependence on $\phi^r_{\nu_e} = \phi^r_{\bar{\nu}_e}$ on both sides of the maximum which comes around $\phi^r_{\nu_e} = \phi^r_{\bar{\nu}_e} \simeq 1.25$. For the normal hierarchy one sees departure from linearity around $\phi^r_{\nu_e} = \phi^r_{\bar{\nu}_e} \simeq 1.1$. This feature is crucial in determining the effect of the distribution function on the hierarchy sensitivity. The effect of taking the distribution function into account boils down to creating a weighted average of the number of events, where the weights are determined by the distribution itself. For the log-normal case the weights are driven by the mean and width of the distribution, which we parameterize in terms of μ and σ. The effect of any distribution can thus be understood with the help of fig. 7.3.

To show the effect of the distribution function we continue to stick to the simplified scenario where $\phi^r_{\nu_e} = \phi^r_{\bar{\nu}_e}$ and show in fig. 7.4 the relative difference η as a function of the

[11] Most of the results shown in this chapter is for megaton class Gadolinium doped water detector to show the impact of the relative initial luminosity and its distribution on the hierarchy measurement using DSNB fluxes. The corresponding sensitivities for smaller scale detectors can be calculated trivially using these numbers.

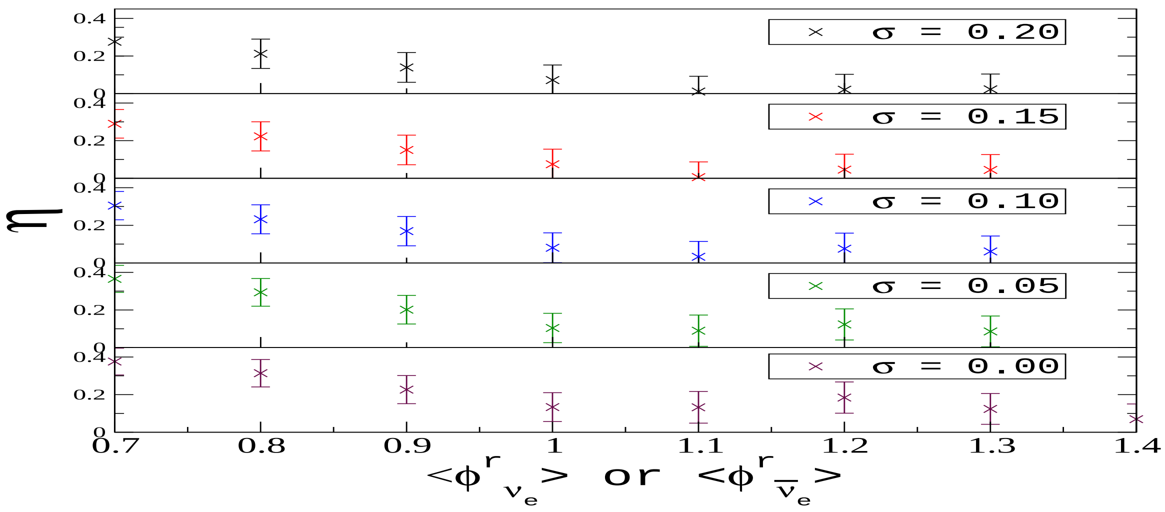

Figure 7.4: Relative difference (η) of number of expected events in normal and inverted hierarchy, per 2.5 Megaton-year in a Gadolinium loaded SK like detector. For the IH case we consider small mixing angle i,e $P_{13} = 1$. The above panels show η for four possible cases with σ being 0.00, 0.05, 0.10, 0.15 and 0.20. The x axis denotes the expectation of $\phi^r_{\nu_e}$ and $\phi^r_{\bar{\nu}_e}$ for the chosen sigma. Here expectation of $\phi^r_{\nu_e}$ and $\phi^r_{\bar{\nu}_e}$ are taken to be same i,e $\mu_1 = \mu_2$. The errors shown are the statistical errors only.

expectation value $\langle\phi^r_{\nu_e}\rangle(= \langle\phi^r_{\bar{\nu}_e}\rangle)$. Here again we take $P_{13} = 1$ for IH. We consider log-normal distribution for the relative luminosities[12] and show η for five different values of σ which controls the width of the distribution. The values and error bars on η correspond to a statistics of 2.5 Megaton-Year data in Gadolinium loaded water detector. The lowest panel with $\sigma = 0$ corresponds to the case where we keep $\phi^r_{\nu_e}(\phi^r_{\bar{\nu}_e})$ fixed and for this case there is no effect of the distribution. This case is similar to that in the lower panel of fig. 7.3. We see that without the effect of the distribution function almost all values of $\phi^r_{\nu_e}(= \phi^r_{\bar{\nu}_e})$ would give hierarchy sensitivity to at least 1σ C.L., while for lower values of the relative luminosity the sensitivity can be seen to be rather good. As we increase σ the sensitivity is seen to go down for all value of the relative luminosity. We find that even for very small values of $\sigma = 0.05$, there is almost no hierarchy sensitivity for $\langle\phi^r_{\nu_e}\rangle(= \langle\phi^r_{\bar{\nu}_e}\rangle) \gtrsim 1$. As σ increases this pattern remains the same, though the sensitivity keeps falling for all values of $\langle\phi^r_{\nu_e}\rangle(= \langle\phi^r_{\bar{\nu}_e}\rangle)$. In the above analysis, σ is considered in a

[12]Our conclusions remain fairly robust against the choice of the distribution function. We have explicitly checked this by repeating fig. 7.4 with uniform distribution and normal distribution. However, we do not present those results as they follow the same pattern that we get for the log-normal distribution.

small range. The idea was to avoid deviating too much from the simulated values of the relative initial luminosities. If the actual variations of ϕ^r_νs for all past supernovae are much larger than the range considered here, then the difference between predicted events for NH and IH would decrease even further, and this could washout the hierarchy sensitivity even for the low ϕ^r_ν cases.

7.3 Discussion

In this chapter we studied the prospects of measuring the neutrino mass hierarchy from observation of the DSNB signal in terrestrial detectors. This study is unique as this is the first time that distribution of the source SN with initial relative neutrino and antineutrino fluxes has been taken into account. It is natural that different SN would emit neutrino and antineutrino fluxes with slightly different initial conditions, depending on the properties of the progenitor star. This is particularly relevant in the context of collective oscillations, where the multiple split patterns depend crucially on the initial relative fluxes. Since the actual distribution function of SN with the initial relative fluxes are unknown, we chose four specimen distribution functions, which have a mean corresponding to the value from SN simulations and a width such that almost all the values are within a factor of two of the mean value. We worked with three log-normal and one uniform distribution. We presented the DSNB fluxes for all the four distributions for both normal and inverted hierarchies. We showed the total predicted number of $\bar{\nu}_e$ events in water detectors, both with and without Gadolinium. The log-normal distribution is characterized by its mean value and its variance. These are parameterized in terms of the variables μ and σ. We studied the dependence of the hierarchy sensitivity to the mean and variance of the log-normal distribution function. We concluded that the hierarchy sensitivity in this experiment had a crucial dependence on the mean value of the relative initial luminosity $\phi^r_{\nu_e}$ and $\phi^r_{\bar{\nu}_e}$. The sensitivity has a predominantly non-linear dependence on $\langle\phi^r_{\nu_e}\rangle$ and $\langle\phi^r_{\bar{\nu}_e}\rangle$, being higher for lower values of these quantities. The effect of the variance parameterized by σ is to reduce the hierarchy sensitivity for all values of the mean $\langle\phi^r_{\nu_e}\rangle$ and $\langle\phi^r_{\bar{\nu}_e}\rangle$. We found that even for very moderate values of $\sigma \simeq 0.05$, there is almost no hierarchy sensitivity in the very small mixing angle limit for $\langle\phi^r_{\nu_e}\rangle = \langle\phi^r_{\bar{\nu}_e}\rangle \gtrsim 1$.

BIBLIOGRAPHY

[1] B. Dasgupta, A. Dighe and A. Mirizzi, Phys. Rev. Lett. **101**, 171801 (2008).

[2] S. Choubey, B. Dasgupta, A. Dighe and A. Mirizzi, arXiv:1008.0308 [hep-ph].

[3] A.M. Hopkins and J.F. Beacom, Astrophys. J.**651**, 142 (2006).

[4] M.D. Kistler et al, arXiv:0709.0381v2 [astro-ph].

[5] B. Dasgupta, A. Dighe, G. G. Raffelt and A. Y. Smirnov, Phys. Rev. Lett. **103**, 051105 (2009)

[6] G. Fogli, E. Lisi, A. Marrone and I. Tamborra, arXiv:0907.5115 [hep-ph].

[7] S. Chakraborty, S. Choubey, S. Goswami and K. Kar, JCAP **1006**, 007 (2010) [arXiv:0911.1218 [hep-ph]].

[8] C. Amsler *et al.* [Particle Data Group], "Review of particle physics," Phys. Lett. B **667**, 1 (2008).

[9] I.K. Baldry and K. Glazebrook, Astrophys. J. **593**, 258 (2003).

[10] P. Bhattacharjee, S. Chakraborty, S. Das Gupta, K. Kar,
Phys. Rev. D **77**, 043008 (2008) arXiv:0710.5922v3 [astro-ph].

[11] Madau P, Pozzetti L and Dickinson M *Astrophys. J.* **498** 106 1998

[12] L. E. Strigari, J. F. Beacom, T. P. Walker and P. Zhang, JCAP **0504**, 017 (2005) arXiv:astro-ph/0502150.

[13] S. Ando and K. Sato, New J. Phys. **6** 170 (2004) arXiv:astro-ph/0410061.

[14] M. T. Keil, G. G. Raffelt and H. T. Janka, Astrophys. J. **590** 971 (2003)

[15] A. Friedland, Phys. Rev. Lett. **104**, 191102 (2010) [arXiv:1001.0996 [hep-ph]].

[16] B. Dasgupta *et al.* [arXiv:1002.2943 [hep-ph]]

[17] A. Bandyopadhyay, S. Choubey, S. Goswami and K. Kar, arXiv:hep-ph/0312315.

[18] A. S. Dighe and A. Y. Smirnov, Phys. Rev. D **62** (2000) 033007 arXiv:hep-ph/9907423.

[19] C. Lunardini and A. Yu. Smirnov, JCAP **0306**, 009 (2003) arXiv:hep-ph/0302033.

[20] M. T. Keil, arXiv:astro-ph/0308228.

[21] M. Malek *et al.* [Super-Kamiokande Collaboration], Phys. Rev. Lett. **90** 061101 (2003) arXiv:hep-ex/0209028.

[22] Y. Itow *et al.*, arXiv:hep-ex/0106019.

[23] A. de Bellefon *et al.*, arXiv:hep-ex/0607026.

[24] C. K. Jung, AIP Conf. Proc. **533**, 29 (2000).

[25] J. F. Beacom and M. R. Vagins, Phys. Rev. Lett. **93**, 171101 (2004)

[26] M. Wurm, F. von Feilitzsch, M. Goeger-Neff, K. A. Hochmuth, T. M. Undagoitia, L. Oberauer and W. Potzel, Phys. Rev. D **75** 023007 (2007) arXiv:astro-ph/0701305.

[27] A.Rubbia, arXiv:hep-ph/0402110;

[28] B. Baibussinov *et al.*, Astropart. Phys. **29**, 174 (2008)

[29] www-off-axis.fnal.gov/flare/

CHAPTER 8

Conclusions

8.1 Summary

In this thesis we have explored the signatures of neutrino mass and mixing in the supernova neutrino spectra and detection. We analyzed different split patterns of SN neutrino spectra and derived the limits on neutrino relative fluxes for a successful heavy element nucleosynthesis inside SN. We have studied the effect of neutrino oscillations on the diffuse supernova neutrino background.

In chapter 2 we have presented the basic ideas of neutrino oscillations, both in vacuum and matter.

In chapter 3 we have discussed the present understanding of stellar core collapse. In this brief discussion we presented the various stages of neutrino emission from the core collapse supernova.

Chapter 4 describes the basic aspects of collective oscillation arising from neutrino-neutrino interaction in a SN environment. Here we have assumed a 2-flavor analysis of collective oscillation where the third flavor is unaffected by this neutrino-neutrino interaction. We have identified the variation of split patterns in final SN neutrino spectra depending on the initial relative flux. We have carried out this analysis for different models of initial SN neutrino spectra for both hierarchies. We have found that the inverted hierarchy(IH) has more interesting split features than normal hierarchy(NH). For NH, other than the very low values almost the whole initial relative flux parameter space shows no split or no effect of collective oscillation. The low values of initial relative flux give rise to only single splits in the spectrum. Whereas for IH we found some six different possible split patterns depending on the values of initial relative flux of different flavors.

Most interestingly in IH one can get double splits in the spectrum which can give distinguishable signature from the NH. However for some range of the the parameter values, IH was also found to give no spectral split like NH.

In chapter 5 we have discussed the possibility of getting allowed regions in the relative flux parameter space for r-process nucleosynthesis. We have considered the impact of the collective oscillations and the spectral splits on the electron fraction Y_e, which determines if the environment is neutron-rich and compatible with r-process nucleosynthesis or not. Since spectral splits modify the electron neutrino and antineutrino spectra in the region where r-process is postulated to happen, and since the pattern of spectral splits depends on the initial conditions of the spectra and the neutrino mass hierarchy, we have showed that the condition $Y_e < 0.5$ required for successful r-process nucleosynthesis will lead to constraints on the initial spectral conditions, for a given neutrino mass hierarchy.

Our analysis has found that the parameter space allowed by r-process was much more constrained in case of IH than that of NH. The part of the parameter space where electron antineutrino flux is much larger than electron neutrino flux seems to be the only region where r-process is allowed in IH. The reason is the abundance of spectral splits in the IH compared to NH. Moreover we also found that stronger constraint on Y_e reduces the allowed parameter space. Thus the exclusion plots for IH and NH for various constraints like electron fraction (Y_e) less than the values 0.35, 0.40, 0.45, 0.50 show that the allowed parameter space shrinks as the allowed Y_e values are decreased.

In chapter 6 we have discussed the Diffuse Supernova Neutrino Background (DSNB) in the context of collective neutrino oscillation. We have calculated the neutrino fluxes including the effect of collective and MSW oscillation. Earlier considerations of matter induced resonances are followed by incorporating the 'collective' effects in the high density central regions of the core.

The whole analysis has been done for the simplistic scenario of collective effects, where for antineutrinos in NH there is no swap and the whole spectrum is swapped for IH. In contrast for neutrinos the swap in IH is taken to occur at the critical energy ($E_c = 7MeV$) and the NH spectrum is kept unaltered. We have showed that for the situations with different SNe having the same neutrino spectral split patterns the hierarchy distinction may be possible with future megaton water Cherenkov detectors. In this collective conversion picture we have calculated that the event rate as a function of θ_{13} and find that they could be different from previous estimates by upto 50%, for small values of θ_{13}.

In chapter 7 we have proposed the idea of probing the variation of DSNB with the initial relative neutrino flux. DSNB flux comes from a superposition of the fluxes from all past SNe. Since the initial flux conditions are expected to be sensitive to the properties of the progenitor star and since we have a whole distribution of stars which end as SN, realistically one should not take all supernovae to have the same relative neutrino and antineutrino flux. So we have considered the distribution of SN as functions of the relative fluxes and calculated the event numbers averaged over the distributions. Thus the observation of different split patterns in the spectra are incorporated in the calculation of DSNB. The main focus have been on checking the effect of the distribution of supernovae with initial flux on the possibility of distinguishing neutrino mass hierarchies via the observation of the DSNB signal. As the actual distribution of SNe with the initial fluxes are not available to us, we have parameterized this by different distributions like log normal, uniform. We have calculated the DSNB event rate averaged over these distributions mainly for antineutrinos in both hierarchies with very small mixing angle ($\theta_{13} < 10^{-5}$).

Our analysis in chapter 6 with simpler collective picture has shown that if all past SNe were to produce identical $\bar{\nu}_e$ fluxes, then it would be possible to distinguish the normal from the inverted hierarchy using the DSNB signal even for very small θ_{13} with megaton-class water Cherenkov detectors. However the calculations in chapter 7 have demonstrated that once the distribution of the fluxes from all SNe are taken into account, the situation becomes more complicated. In the scenario of low mean values of the initial flux ratio distribution, the mass hierarchy determinability through DSNB has been found to survive the averaging, though the difference decreases significantly with respect to the one without the distribution. However for larger values of initial flux ratio it becomes impossible to distinguish hierarchy through DSNB once the distribution is taken into account.

8.2 Future Outlook

In the last few years the whole subject of supernovae neutrinos has evolved a lot. The understanding of MSW oscillation in SN early in this decade has been followed by the new developments of collective oscillation. In fact the studies involving collective oscillations have seen a huge evolution in last two-three years. The analytic understanding of all the related processes still need a lot of clarifications. Topics like multi angle analysis, effect of solar mass squared difference on collective oscillation and effect of non standard interaction need more analysis. In fact success of the widely used simpler single angle approximation compared to the realistic but very involved multiangle angle analysis is yet to be properly explained. In future these problems on the general structure of the collective oscillations need to be addressed.

Another problem that needs attention is the analysis of the r-process nucleosynthesis in a more detailed way. Details like neutrino interaction on heavy nuclei and α-particle during r-process are needed to be incorporated. Analysing this r-process problem in light of sterile neutrinos and collective oscillation seems really important.

In future one also needs to investigate DSNB, as one realizes that there are several areas that need improvement in the DSNB estimation. For example, instead of considering the collective oscillations driven by only atmospheric mass squared difference one can also consider solar mass squared difference. Basically the complete three flavor analysis of the problem may give interesting results. Again adding multiangle analysis to the collective effect solutions would make the results more precise. So the area of collective oscillations of supernova neutrinos and its connection to issues of neutrino physics and supernova explosions alongwith r-process nucleosynthesis will continue to be an exciting field of research.

LIST OF PUBLICATIONS

Papers marked with a star ($\star$) are included in this thesis.

1. $\star$**On the Observability of Collective Flavor Oscillations in Diffuse Supernova Neutrino Background**.
   Sovan Chakraborty, Sandhya Choubey and Kamales Kar.
   Preprint arXiv:1006.3756 [hep-ph].(submitted to journal).

2. **Constraining Scalar Singlet Dark Matter with CDMS, XENON and DAMA and Prediction for Direct Detection Rates** .
   Abhijit Bandyopadhyay, Sovan Chakraborty, Ambar Ghosal, Debasish Majumdar.
   Preprint arXiv:1003.0809 [hep-ph]. (To appear in JHEP)

3. **Interpreting the bounds on Dark Matter induced muons at Super-Kamiokande in the light of CDMS data** .
   Abhijit Bandyopadhyay, Sovan Chakraborty, Debasish Majumdar.
   Preprint arXiv:1002.0753 [hep-ph].
   Int. J. Mod. Phys. **A.25** :3741-3747, 2010.

4. $\star$**Collective Flavor Oscillations Of Supernova Neutrinos and r-Process Nucleosynthesis**.
   Sovan Chakraborty, Sandhya Choubey, Srubabati Goswami, Kamales Kar
   Preprint arXiv:0911.1218 [hep-ph].
   Journal of Cosmology and Astroparticle Physics (JCAP) 1006:007, 2010.

5. $\star$**Effect of Collective Flavor Oscillations on the Diffuse Supernova Neutrino Background**.

   Sovan Chakraborty, Sandhya Choubey, Basudeb Dasgupta, Kamales Kar.

   Preprint arXiv:0805.3131 [hep-ph].

   Journal of Cosmology and Astroparticle Physics (JCAP) **0809:013, 2008**.

6. **Upper Limit on the Cosmic Gamma-Ray Burst Rate from High Energy Diffuse Neutrino Background** .

   Pijushpani Bhattacharjee, Sovan Chakraborty, Srirupa Das Gupta, Kamales Kar.

   Preprint arXiv:0710.5922 [astro-ph].

   Phys. Rev. **D77** :043008, 2008.